UNIVERSITY OF CALIFORNIA, SAN DIEGO

The Effects of Cytoskeletal Disruption and Mechanical Load on Cardiac Conduction

A dissertation submitted in partial satisfaction of the requirements for the degree Doctor of Philosophy

in

Bioengineering

by

Adam Thomas Wright

Committee in charge:

Professor Andrew McCulloch, Chair
Professor Wayne Giles
Professor Sanjiv Narayan
Professor Jeffrey Omens
Professor Robert Ross
Professor Gabriel Silva

2010

The dissertation of Adam Thomas Wright is approved, and it is acceptable in quality and form for publication on microfilm and electronically:

_____

_____

_____

_____

_____

_____

Chair

University of California, San Diego

2010

TABLE OF CONTENTS

LIST OF FIGURES

ACKNOWLEDGEMENTS

The work presented in this dissertation represents some of the research I have conducted during my time with the Cardiac Mechanics Research Group in the Department of Bioengineering at the University of California, San Diego. I would like to thank all of the people who have helped me throughout my experience in graduate school.

First, I would like to thank my advisor, Dr. Andrew McCulloch, for his advice and support. He could always be counted on for fresh insights into problem solving. He and Dr. Jeff Omens have created a great research group studying a wide range of fields in cardiovascular research, and I am thankful to have spent my time as a member of the CMRG team. Dr. Omens has a strong background in instrumentation and experimental techniques and he has been a great resource for me. I would also like to thank the rest of my committee for their input and insights into my research.

I especially thank Bob Mills for his help in training me and guiding me through my early years in the lab. Bob was a graduate student a couple of years older than me who developed many of the experimental and analytical techniques I used through my research. He trained me in many of my experimental techniques and was a great (and thankfully, patient) mentor to a young, clueless incoming grad student. Hunaid Gurji was another graduate student who helped to train me and learn along side with me. I thank them both for not only their help in the lab, but also their friendship during their time in San Diego.

A number of other members of CMRG have been instrumental during my time with the group. Eleanore Hewitt, our lab manager, has kept the lab running for years … far longer than I have been with the group. She seems to know everyone at UCSD to help get things done in the lab, and can help find any lab supplies you can possibly need. Zhuangjie Li was an expert in experimental techniques and was very helpful during my early years. Thanks also to the other members of the group who have come and gone through my time for providing insight and ideas during my time in the lab.

Finally, and most importantly, thanks to my friends and family. My parents have always been there to provide their support and encouragement, without which I never would have made it this far. Thanks to the friends I've made during my time in San Diego, especially Jennifer Marciniak for her help editing and giving input towards my dissertation.

The text and figures of Chapter 1 Mechanoelectric Coupling in the Heart, in part, are a reprint of the material as it appears in: Mills RW, Wright AT, Narayan SM, McCulloch, AD. The effects of wall stretch on ventricular conduction and refractoriness in the whole heart. In: Kohl P, Sachs F, Franz MR, eds. *Cardiac Mechano-Electric Coupling & Arrhythmias*. Oxford University Press; to be published in 2011: Chapter 25. Reprinted with permission from Oxford University Press. The dissertation author was a primary researcher and author of this book chapter.

The data and figures in Chapter 3 Cardiac-Specific Vinculin Knockout Model are, in part, from the following published work: A. E. Zemljic-Harpf, J. C. Miller, S. A. Henderson, A. T. Wright, A. M. Manso, L. Elsherif, N. D. Dalton, A. K. Thor, G. A. Perkins, A. D. McCulloch, and R. S. Ross, Cardiac-myocyte-specific excision of the

vinculin gene disrupts cellular junctions, causing sudden death or dilated cardiomyopathy, *Mol Cell Biol*, vol. 27, pp. 7522-37, 2007. Printed with permission from the American Society of Microbiology and Copyright Clearance Center. The dissertation author was the primary researcher and author of the work presented here, and the co-authors listed in this publication directed and supervised the research that forms the basis of this chapter, or were primary researchers of material not presented here.

The data and figures in Chapter 3 Cardiac-Specific CAR Knockout Model are, in part, from the following published work: B. K. Lim, D. Xiong, A. Dorner, T. J. Youn, A. Yung, T. I. Liu, Y. Gu, N. D. Dalton, A. T. Wright, S. M. Evans, J. Chen, K. L. Peterson, A. D. McCulloch, T. Yajima, and K. U. Knowlton, "Coxsackievirus and adenovirus receptor (CAR) mediates atrioventricular-node function and connexin 45 localization in the murine heart," *J Clin Invest*, vol. 118, pp. 2758-70, 2008. Printed with permission from the American Society for Clinical Investigation and Copyright Clearance Center. The dissertation author was the primary researcher and author of the work presented here, and the co-authors listed in this publication directed and supervised the research that forms the basis of this chapter, or were primary researchers of material not presented here.

The text and figures of Chapter 4 in part, will be submitted for publication. The dissertation author was the primary researcher and author of the work presented here, and any co-authors of this publication directed and supervised the research that forms the basis for this chapter.

VITA

1980	Born, Newport Beach, California
2003	B.S., University of California, Davis
2005	M.S., University of California, San Diego
2010	Ph.D., University of California, San Diego

PUBLICATIONS

A. E. Zemljic-Harpf, J. C. Miller, S. A. Henderson, **A. T. Wright**, A. M. Manso, L. Elsherif, N. D. Dalton, A. K. Thor, G. A. Perkins, A. D. McCulloch, and R. S. Ross, "Cardiac-myocyte-specific excision of the vinculin gene disrupts cellular junctions, causing sudden death or dilated cardiomyopathy," *Mol Cell Biol*, vol. 27, pp. 7522-37, 2007.

B. K. Lim, D. Xiong, A. Dorner, T. J. Youn, A. Yung, T. I. Liu, Y. Gu, N. D. Dalton, **A. T. Wright**, S. M. Evans, J. Chen, K. L. Peterson, A. D. McCulloch, T. Yajima, and K. U. Knowlton, "Coxsackievirus and adenovirus receptor (CAR) mediates atrioventricular-node function and connexin 45 localization in the murine heart," *J Clin Invest*, vol. 118, pp. 2758-70, 2008.

R. W. Mills, **A. T. Wright**, S. M. Narayan, A. D. McCulloch. The effects of wall stretch on ventricular conduction and refractoriness in the whole heart. In: P. Kohl, F. Sachs, M. R. Franz, eds. *Cardiac mechano-electric coupling and arrhythmias*: 2nd ed. Oxford University Press; 2011: Chapter 25

ABSTRACT OF THE DISSERTATION

The Effects of Cytoskeletal Disruption and Mechanical Load on Cardiac Conduction

by

Adam Thomas Wright

Doctor of Philosophy in Bioengineering

University of California, San Diego, 2010

Professor Andrew D. McCulloch, Chair

Myocardial disease is often associated with altered cardiac conduction and increased incidence of arrhythmia. Underlying mechanisms responsible for changes in conduction include altered calcium handling, myocardial remodeling, and mechanically induced changes in electrophysiology. The goal of this work was to utilize optical mapping experimental techniques and genetically modified mouse models to investigate

two of these mechanisms: myocardial remodeling associated with disruption of the cytoskeleton, and increased mechanical load.

Optical mapping was used to image electrical conduction in the isolated mouse heart. A multi-functional tandem lens optical setup was designed and built for use with a large chip, high-speed CMOS camera. Experimental and analytical techniques were developed to image conduction in the freely beating isolated mouse heart and in cardiomyocyte monolayers.

Genetically modified mice provide useful experimental models of cardiac diseases. Four murine models with targeted ablation of cytoskeletal proteins each displayed altered myocardial remodeling and impaired cardiac conduction. Ablation of vinculin and desmoplakin in the heart each resulted in disruption of intercalated disc structure, disrupted myocardial conduction, and increased incidence of arrhythmias. Ablation of enigma homolog protein (ENH) and coxsackievirus and adenovirus receptor (CAR) each resulted in disruption of conduction through the specialized cardiac conduction system, without affecting myocardial conduction.

An acute increase in ventricular load has previously been shown to slow conduction in the isolated rabbit heart. In the freely beating, isolated mouse heart, we observed a similar conduction slowing with pressure loading of the left ventricle. Preliminary experiments indicate that membrane unfolding, specifically caveolae opening, may play a role in this conduction slowing by altering passive membrane electrical properties.

Chapter 1: General Introduction

The heart is an electro-mechanical organ that pumps blood through the circulatory system by rhythmic contraction and relaxation. Efficiency of cardiac function is dependent on a steady, controlled rhythm and coordinated myocardial contraction. The specialized conduction system controls rhythm and regulates timing of atrial and ventricular contraction. Rapid impulse propagation through the ventricular myocardium is regulated by cardiomyocyte excitability and passive tissue electrical properties. Disruption of action potential conduction in the heart can lead to deadly arrhythmias. Changes in cardiac structure and mechanical forces in the ventricles have been associated with development of cardiomyopathies. These changes can alter conduction through disruption of cardiomyocyte or myocardial structure, or direct mechanically induced changes in electrical properties.

The objectives of this work are to investigate the effect of cardiomyocyte structural abnormalities and increased mechanical stretch on cardiac conduction. This chapter will describe cardiomyocyte structure and the importance of cytoskeletal structural integrity on cardiac function. It will also introduce the phenomenon of mechanoelectric coupling and the effects of myocardial stretch on cardiac conduction.

Cardiomyocyte Structure and Cardiac Function

Cardiomyocyte Ultrastructure

Cardiomyocytes are the muscle cells in the heart wall that contract in a coordinated manner to effectively pump blood through the circulatory system. These cells are highly specialized and display a complex subcellular architecture to generate strong contractile forces and transmit forces from cell to cell, and from cell to the surrounding extracellular matrix.

Sarcomeres and Z lines

Sarcomeres are the subcellular contractile structures composed of overlapping actin and myosin filaments. Force is generated by crossbridge formation between myosin heads and the actin filaments during contraction. These units are highly organized end to end and are aligned to generate force along the long axis of the cell. These end-to-end junctions are called Z lines (or Z discs) and are the subcellular features that give cardiac muscle fibers their characteristic striated appearance (Figure 1.1).[1] α-Actinin is the primary structural protein at the Z line linking adjacent sarcomeres, but there are also a number of other proteins located at the Z lines that act as stretch sensors, including titin, muscle-specific LIM protein (MLP), and several PDZ-LIM domain containing proteins, including cypher, enigma, and enigma homolog protein (ENH). External forces applied to a cardiomyocyte are "felt" by these proteins, and they induce signaling cascades that alter gene expression and cellular processes. In order to effectively couple sarcomeric force from cell to extracellular matrix (ECM) and

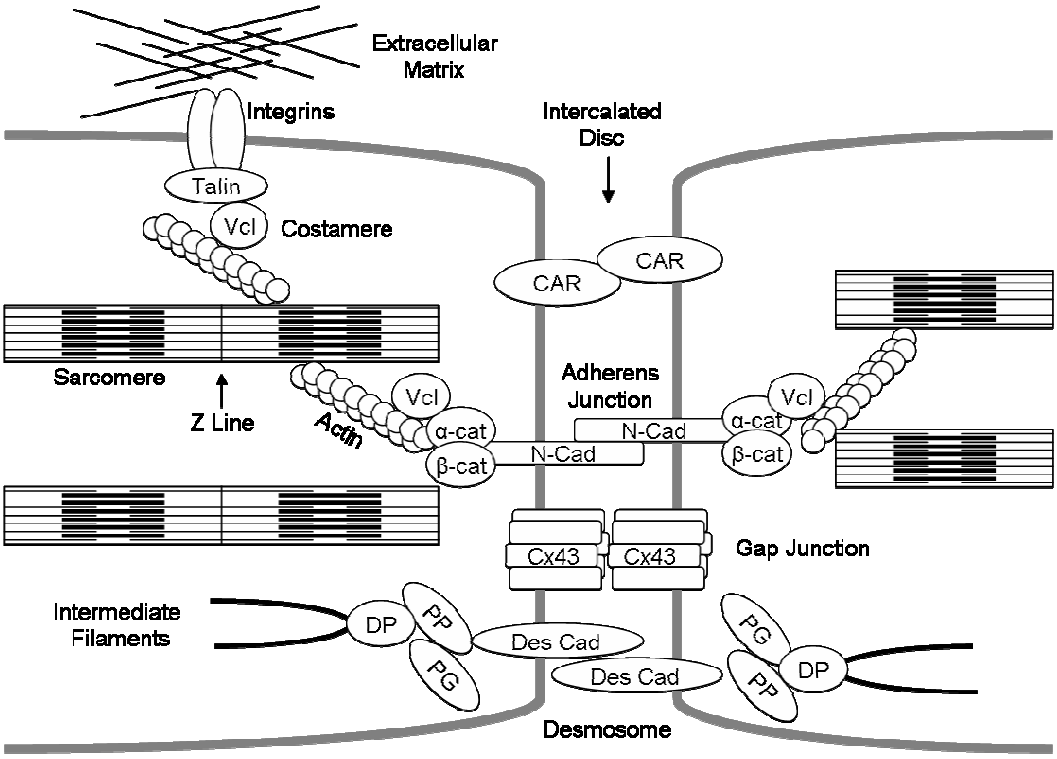

Figure 1.1: Cardiomyocyte junctions. Costameres are specialized structures aligned along the Z discs bridging the actin cytoskeleton to the surrounding extracellular matrix. This protein bridge consists of membrane-spanning integrins, talin, and vinculin (Vcl), which binds directly to actin. Intercalated discs form end-to-end cellular plaques that contain three prominent types of junctions. Desmosomes and adherens junctions are structural junctions that transmit intercellular forces. Gap junctions are specialized channels that link the cytoplasm of one cell to another. Gap junctions are important for efficient impulse propagation through the myocardium. Abbreviations: Vcl – vinculin, α-cat – α-catenin, β-cat – β-catenin, N-Cad – N-cadherin, Cx-43 – connexin-43, DP – desmoplakin, PP – plakophilin, PG – plakoglobin, and Des Cad – desmoplakin cadherins, CAR – coxsackievirus and adenovirus receptor.

from cell to cell, the sarcomeres must be tethered to the sarcolemma. The specialized sarcolemmal structures at these junctions are costameres at cell-matrix junctions, and intercalated discs at cell-cell junctions.

Costameres

Costameres are structures that align in bands around the cardiomyocyte along the Z lines and link the actin cytoskeleton to the surrounding ECM (Figure 1.1). The primary proteins that form this structural bridge are integrins, talin, and vinculin (Vcl). Integrins span the sarcolemma and directly bind to ECM molecules outside of the cell and talin inside of the cell. Vinculin binds directly to both actin and talin to complete this bridge.[2] Costameres transmit externally applied forces to induce changes in cellular processes through mechanotransduction, and transmit stresses from the cytoskeleton to the extracellular matrix during myocyte contraction. Expression and organization of vinculin and integrins at costameres is dependent on the mechanical environment, and important to maintain cell adhesion and structural integrity. In isolated cardiomyocytes, expression of these proteins is upregulated with applied stretch and downregulated when the cells are arrested.[3]

Intercalated Discs

Intercalated discs (ICDs) are complexes that form cell-cell junctions at the longitudinal ends of cardiomyocytes. There are three primary types of junctions found in ICDs: adherens junctions, desmosomes, and gap junctions (Figure 1.1). Adherens junctions are strong structural junctions that mechanically link the actin filaments of the

cytoskeleton from cell to cell. These junctions directly couple sarcomeric contractile forces between cells. N-cadherin is the transmembrane protein that binds cell to cell in the extracellular space. N-cadherin is bound to actin through a protein complex containing alpha- and beta- catenins and vinculin.[4] Desmosomes are junctions that link the intermediate filaments of one cell to another. These junctions also provide structural support to maintain a tight coupling between two cells. Desmosomal cadherins are the transmembrane proteins that bind in the extracellular space. Plakoglobin and plakophilin bind cadherins to the intermediate filaments through the protein desmoplakin. The third structures are gap junctions which are responsible for direct intercellular coupling. Gap junctions consist of connexons in the sarcolemmae of the two adjacent cardiomyocytes. Connexons are hemichannels that align with each other to form a functional pore from the cytoplasm of one cell to the next. Connexons consist of six connexin proteins, of which connexin-43 is the most common type in the working ventricular myocardium, and connexins-45 and -30.2 are the predominant isoforms in the specialized conduction system.[5] These specialized junctions allow the flow of small molecules, including metabolites and ions, from the cytoplasm of one cell to the next.[6] Intercellular ion flow through gap junctions is necessary for rapid impulse propagation through the myocardium and efficient cardiac contraction. Finally, coxsackievirus and adenovirus receptor (CAR) is another transmembrane protein localized at the intercalated discs in the adult myocardium.[7] This protein was first discovered as a receptor for the viruses for which it was named, but its physiological role is not fully understood.[8] It has been discovered that the extracellular domains of CAR form homodimers and is thought to serve as a cell-cell adhesion molecule.[9]

Cytoskeletal Proteins and Cardiac Dysfunction

The complex cellular ultrastructure is important in maintaining cardiomyocyte function and the pumping efficiency of the heart. Mutations in sarcomeric proteins can alter crossbridge cycling and affect contractility of the subunits. Transmission of contractile force to the sarcolemma, and thus to surrounding ECM and adjacent cells, can be impeded with alterations in costameric and ICD structure and protein localization. This change in force transmission can decrease myocardial contractility, as well as alter stresses "felt" by mechanotransducing sensor proteins at the Z lines. Mutations in these mechanotransducing proteins can also change cellular processes by changing gene expression and protein phosphorylation. Finally, disruption of ICD structure may alter gap junction conductivity, impeding the rapid action potential propagation required for efficient pumping and presenting a proarrhythmic phenotype. Disruption of these structures has been linked to several forms of arrhythmia and cardiomyopathy both clinically and *in vivo* in genetically modified mouse models.

Costameric Proteins

Several studies have investigated the effect of ablation of costameric proteins on cardiac function and development. In the mouse model, global knockout of β-integrins[10] results in embryonic death, as does knockout of the associated proteins vinculin[11] and talin[12]. Death is associated with defects in cellular adhesion and disorganized cytoskeletal structure. Mice with a heterozygous global knockout of vinculin are viable and do not have any obvious abnormalities. However, they display abnormal intercalated discs and disorganized Z-lines. Electrocardiogram (ECG)

analysis revealed a prolonged QRS complex, indicating delayed myocardial activation. Additionally, these mice are predisposed to cardiac failure when challenged with increased hemodynamic load.[13] Cardiac specific ablation of β-integrins results in mice that live to adulthood, but display decreased hemodynamic function, increased fibrosis, disruption of the cytoskeleton, and development of dilated cardiomyopathy by 6 months of age. Additionally, these mice are less tolerant to increased hemodynamic load.[14]

Z Line Proteins

There are many proteins that make up the mechanotransducing complexes at the Z lines of cardiomyocytes that have been associated with cardiomyopathies. Titin is a very large protein that is integral in sarcomere structure. Screenings of conditional mutations in titin result in mice with varying cardiac phenotypes, from embryonic death, to early onset of severe cardiomyocytes and death by 5 weeks of age.[15] These phenotypes are all associated with severe disruption of sarcomere structure. MLP deficiency results in development of a dilated cardiomyopathy. These hearts display severe chamber dilation and impaired contractility, associated with fibrosis and disruption of cardiomyocyte cytocarchitecture.[16] Global knockout of cypher results in death by 5 days of age associated with skeletal muscle failure and disrupted Z lines.[17] Mice with cardiac-specific ablation of cypher develop a dilated cardiomyopathy with decreased contractility and development of disrupted Z lines. Induced ablation at adulthood resulted in a similar phenotype, indicating that cypher plays a critical role in maintaining Z line structure.[18]

Intercalated Disc Associated Proteins

Intercalated discs contain both structural and electrical junctions and are thus important to maintain mechanical stability and rapid action potential propagation. Therefore, disruption of these structures is often associated with slowed impulse conduction and an increased incidence of arrhythmias, as well development of severe functional cardiomyopathies.

Direct knockout of gap junction proteins alters action potential propagation and increases incidence of arrhythmias and sudden death. Global knockout of connexin-43 results in cardiac developmental abnormalities and neonatal death.[19] Mice heterozygous for connexin-43 live to adulthood, but analysis of ventricular conduction has demonstrated varying results. Guerrero, *et. al.* observed slowed ventricular conduction and prolonged QRS complex in heterozygous mice compared to wild-type mice.[20] However, Morley, *et. al.* observed normal QRS complex duration and no difference in conduction velocity in these heterozygotes using optical mapping techniques.[21] Cardiac specific ablation of connexin-43 results in normal cardiac structure and hemodynamic function, but the mice die suddenly by 2 months of age. These deaths were associated with spontaneous ventricular tachycardia and slowed ventricular conduction.[22] However, lack of connexin-43 does not affect formation and organization of adherens junctions and desmosomes at the ICD.[23]

Disruption of adherens junctions and desmosomes can disrupt ICD assembly and mechanical stability. Murine models of global knockout of vinculin,[11] N-cadherin,[24] and plakoglobin[25, 26] all die at the embryonic stage with disruption in cardiac development. As mentioned, mice heterozygous for vinculin display normal

cardiac function, but have disrupted intercalated disc organization and a prolonged QRS complex.[13] An inducible model of cardiac specific knockout of N-cadherin displayed dissolution of ICD structure, loss of cardiac contractile function, and sudden cardiac death due to spontaneous ventricular tachycardia.[27] Loss of N-cadherin also resulted in lowered levels of connexin-43 and slowed action potential propagation as assessed by ECG analysis and optical mapping.[28] Murine hearts with heterozygous expression of plakoglobin develop dilation of the right ventricle, reduced right ventricular function, and spontaneous tachycardia *in vivo* and in an isolated heart preparation. However, these heterozygotes do not have any differences in intercalated disc structure or connexin-43 distribution and density.[29]

Mechanoelectric Coupling in the Heart

Many studies have linked volume overload or increased myocardial strain (wall stretch) with atrial and ventricular arrhythmias.[30] Although the mechanisms for these mechanical load-induced rhythm disturbances remain unclear, they generally involve either triggered activity or reentrant conduction.[31] Though both of these mechanisms may contribute, reentry is the predominant mechanism underlying ventricular arrhythmias associated with mechanical dysfunction.[32] Stability of a reentrant circuit depends on the constant presence of excitable tissue ahead of the activation wavefront. Slowed conduction and decreased refractoriness can therefore promote and sustain reentry, while increased dispersion of conduction velocity and refractoriness can provide a substrate for its initiation.[33] Observations on the acute effects of

myocardial strain on conduction velocity have varied widely with experimental preparation, mechanical loading conditions and measurement techniques. Given the inherent difficulties in measuring regional myocardial mechanics and conduction velocity in the whole heart without disturbing mechanical or electrical properties, many of the discrepancies between experimental reports are probably attributable to differences in experimental methods or definitions.

Factors Influencing Speed and Path of Conduction

Intracellular conduction is determined by passive membrane capacitance, longitudinal resistances, and voltage-dependent membrane conductances.[34] Membrane capacitance is a function of the dielectric properties of the membrane and the membrane surface area to cell volume ratio. Increasing membrane capacitance slows the initial depolarization from resting potential to threshold, and reduces conduction velocity. Intracellular and extracellular longitudinal resistances determine how rapidly ions travel in the direction of conduction and are affected by the effective internal and external cross-sectional areas available for ion transport.

The voltage-gated fast sodium current usually determines how rapidly the local membrane depolarizes (action potential phase 0), creating the electrochemical gradient that drives longitudinal ion diffusion. The conductance of these channels is influenced by channel kinetics and other regulatory processes, such as ligand gating and autonomic stimulation.[35] Altering resting membrane potential influences conduction speed in a biphasic manner.[36] Model studies suggest that this effect acts through membrane excitability,[37] as depolarization of the resting membrane potential decreases the

charge required to reach threshold, but increases sodium channel inactivation, decreasing conduction velocity.

Intercellular conduction is primarily regulated by the conductance of gap junctions, which is sensitive to ischemia, pH, intracellular cation concentrations, and transjunctional voltage.[6] Activation wavefront curvature also affects propagation speed; a convex wavefront must stimulate an expanding volume of resting tissue, imposing a greater electrical load and slowing conduction.[38]

The path of conduction through the myocardium is a function of gap junction distributions, myocyte branching, fiber angle dispersion, the laminar sheet organization of the myofibers, and the presence of connective tissue septa within the interstitium. The direction of fastest propagation follows the myocardial fiber direction due to the distribution of gap junctions within the cell,[6] with fiber conduction speed typically being two- to ten-fold faster than the cross-fiber direction. Within the ventricle, fiber angles follow a left-handed helix in the epicardium and smoothly transition to a right-handed helix in the endocardium. Therefore, as activation spreads transmurally, the principal axis of fastest in-plane propagation rotates and the wave front changes shape. Transverse to the fiber direction, cardiomyocytes are stacked into branching laminar sheets about 4-6 cells thick surrounded by a perimysial collagen fascia. A model reconstruction of tissue microarchitecture showed that this organization results in conduction across the sheet planes being slowed by 40% compared with cross-fiber conduction within the sheets.[39]

Measuring Conduction Velocity During Myocardial Stretch

Conduction velocity in one direction is usually calculated as the distance between recording electrodes aligned perpendicular to the wavepath divided by the interelectrode conduction time. In this case, the distance between recording sites and the number of myocytes per unit physical length can change during loading. Therefore, conduction velocity has been defined with both a spatial and material reference. Spatial conduction velocity is defined with a constant interelectrode distance before and during stretch. Material conduction velocity is defined between the same two physical points on the myocardium, thus material conduction velocity describes mechano-electric coupling effects over a constant segment of tissue.

However, to account for potential changes in conduction path with stretch in studies of two or three-dimensional conduction, a highly resolved spatial description is most appropriate. In practice, to determine the two-dimensional conduction direction, the conduction time is sampled from an array of positions, and the gradients of activation time are used to calculate local conduction velocities.[40] High spatial resolution sampling is achieved using contact electrode arrays or high speed optical mapping of action potential propagation with a fluorescent voltage-sensitive dye. One advantage of optical mapping is that it is non-contact, diminishing the chance of mechanical artifacts during measurement. Experimental methodologies and optical mapping techniques are further described in Chapter 2.

Effects of Stretch on Conduction Velocity in the Heart

Early investigations into the effects of myocardial stretch on conduction speed were limited to one-dimensional propagation. In studies of ventricular and atrial strips of myocardium from various species, stretching from slack length to the length of maximal developed tension caused a proportionate increase in spatial conduction velocity while material conduction velocity remained nearly unchanged, but additional stretch caused slowing of both measures.[41] A similar biphasic relationship between spatial conduction velocity and stretch has been observed in more recent studies in isolated rabbit papillary muscle.[42] Faster spatial conduction during stretch was also observed in sheep Purkinje fibers.[43, 44] In canine Purkinje fibers, both spatial and material conduction velocity initially increased with stretch and then decreased, but conduction in cat trabeculae was not similarly affected.[45] Conversely, spatial conduction velocity in rat papillary muscle decreased with stretch, while papillary muscle from several other species showed no effect.[46] Despite the varied effects of stretch across different structures, tissue types, and species, most of these studies imply that conduction velocity may increase with stretch. However, these studies mostly concentrated on specialized structures, and after being excised, these tissues were not subject to the same multiaxial constraints as *in vivo*.

Other studies have focused on the effect of physiological loading on whole chamber activation times. In the dog heart *in vivo*, QRS duration correlated with acute increases in left ventricular pressure,[47] while left atrial dilation increased atrial activation time,[48] and ventricular volume inflation in isolated rabbit hearts increased maximal activation times.[49] In contrast, one study of volume load in canine ventricle

in vivo reported no change in spatial conduction time,[50] while cellular conduction velocity increased during volume load of rat atrium.[51] These whole chamber studies indicate that stretch slows material conduction; however, they do not directly compare measures of conduction speed or path.

More recent studies have investigated the effects of stretch on two-dimensional epicardial surface conduction using electrode arrays, in order to directly study the path of propagation. In volume-loaded left ventricles of isolated rabbit hearts after ventricular cryoablation of all but a thin epicardial layer, neither graded load nor changes in pacing cycle length significantly alter fiber or cross-fiber conduction velocities.[52] The authors acknowledged that the cryoablation procedure stiffened the ventricle, possibly protecting the viable layer from mechanical stimulus. Conversely, studies in the isolated rabbit atria displayed decreased spatial conduction velocity[53, 54] as well as increased dispersion of conduction velocity, altered direction of propagation, and increased occurrence of local conduction block[54] during myocardial stretch.

Sung *et al*.[55] used non-contact optical mapping during left ventricular volume loading in isolated rabbit heart, and employed a model-based analysis technique[56] that accounted for epicardial curvature and changes in conduction path, and allowed comparison of conduction velocity with local fiber direction. An increase of intraventricular pressure from 0 to 30 mmHg resulted in heterogeneous epicardial fiber and cross-fiber strains on the order of 3% and 1.5%, respectively, and a 16% decrease in transverse spatial conduction velocity.[55] Figure 1.2 shows an example of the increase in activation times due to ventricular volume loading and the resulting velocity vector

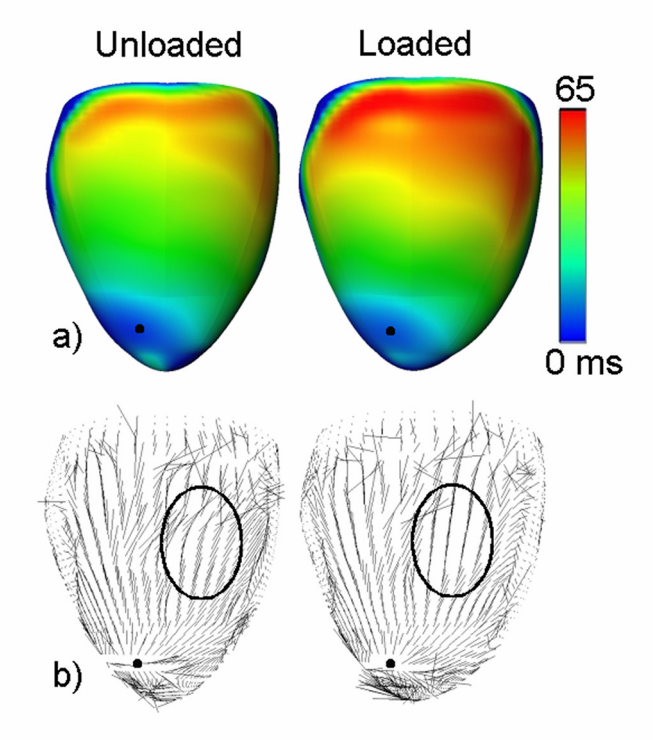

Figure 1.2: Activation time fields (a) and conduction velocity vector fields (b) before and during application of 30 mmHg ventricular volume load in isolated rabbit heart, using methods from Sung and colleagues.[56] The small solid circle indicates the approximate position of pacing. The ellipses outline a region in which the apparent direction of conduction has been changed by application of load.

field. It also illustrates that application of stretch can alter the path of conduction. Conduction velocity returned to baseline when load was removed. Similar results were obtained by our group in a more recent study in the isolated rabbit ventricle.[57] In an alternative preparation, optical mapping revealed a 7.5% slowing of conduction velocity in monolayers of neonatal rat ventricular cardiomyocytes cultured on an elastic membrane during stretch.[58] These two dimensional studies that also include changes in conduction path more consistently show conduction slowing due to stretch.

Potential Stretch-Induced Factors that Influence Conduction Velocity

Myocardial stretch may affect conduction speed in a number of ways. Stretch has been reported to depolarize the resting membrane potential,[59] and this may be sufficient to slow conduction through fast sodium channel inactivation. Inward current through cation non-selective stretch-activated channels (SACs) may depolarize the resting membrane during stretch. Several of the effects of mechano-electric coupling in myocardial preparations have been seen to be blocked by non-specific inhibitors of SACs, including gadolinium inhibition of increased cellular conduction velocity during stretch in rat atria,[51] and reduction of peak conduction velocity increase in stretched papillary muscle by streptomycin.[60] However, Mills and colleagues found conduction slowing during ventricular filling was likely not due to changes in excitability and not attenuated in the presence of gadolinium[57] or streptomycin.[55] Sustained stretch may also increase resting membrane potential through altered cellular calcium handling.[61] Myofilament binding sensitivity to calcium increases with stretch, and prolonged stretch results in a slow increase in the calcium transient, which

subsequently interacts with other currents. However, increased resting potential should lower pacing threshold, but ventricular filling has been reported to have no effect on,[49, 62] or to increase threshold.[52] SACs, altered calcium handling, or stretch-sensitive cellular signaling could also regulate the conductances associated with phase 0 of the action potential, thus decreasing the maximum rate of rise of membrane potential.[35]

Alternatively, stretch may result in changes in tissue and cell geometry, changing path of conduction or altering distributed electrical properties of the myocardium. Penefsky and Hoffman[41] postulated that increased one-dimensional spatial conduction velocity was the result of increased fiber alignment during stretch. Rosen *et al.*[45] observed that stretch caused significant membrane unfolding, decreased cell diameter, and slightly increased packing of the extracellular space. Unfolding of 'slack' membrane and integration of caveolae to the surface sarcolemma has also been observed in the loaded intact rabbit ventricle in a more recent study.[63] Cell stretch would result in an increased surface area to volume ratio and a reduced cell cross-sectional area, increasing the effective longitudinal intracellular resistance. Others suggested stretch might result in a decrease in specific membrane capacitance (capacitance/area),[43, 44] possibly due to membrane unfolding, accounting for increased spatial conduction velocity during moderate stretch. However, recent data indicate that increased membrane tension results in an increase in capacitance.[64]

Myocardial stretch might also alter conduction through changes in intercellular coupling. Gap junction permeability is regulated by several factors that might be regulated by stretch, including intracellular cation concentrations and cell signaling pathways (primarily through connexin phosphorylation).[6] Additionally, it has been

demonstrated that connexin hemichannel permeability is sensitive to both shear strain[65] and membrane stretch,[66] so mechanical forces at cell-cell junctions might directly affect gap junction conductance. However, it has been shown that rate of propagation is not very sensitive to changes in intercellular conductance at normal levels of cellular coupling.[67]

Mills *et al.* implemented a bidomain model analysis of the membrane potential response to a non-excitatory stimulus to investigate changes in these myocardial electrical properties during ventricular volume loading.[57] The results suggested that wall stretch resulted in a 21% increase of the cross-fiber space constant, indicating reduced intercellular resistance that would increase conduction velocity, and a 56% increase in membrane capacitance, which would slow conduction (Figure 1.3). Computational simulations implementing these counteracting changes were consistent with experimental findings of a ~15% slowing of conduction during ventricular loading. This explanation of stretch-induced changes in conduction velocity might account for the varying results obtained in different experimental preparations if the interaction between these two changes in tissue electrical properties varies in different tissue preparations and loading conditions. Further studies are required to investigate the cellular mechanisms behind these changes in passive electrical properties of the myocardium and the resulting change in conduction velocity. Development of similar experimental techniques in the isolated mouse heart provides a platform to conduct such studies, taking advantage of the availability of genetically modified murine models.

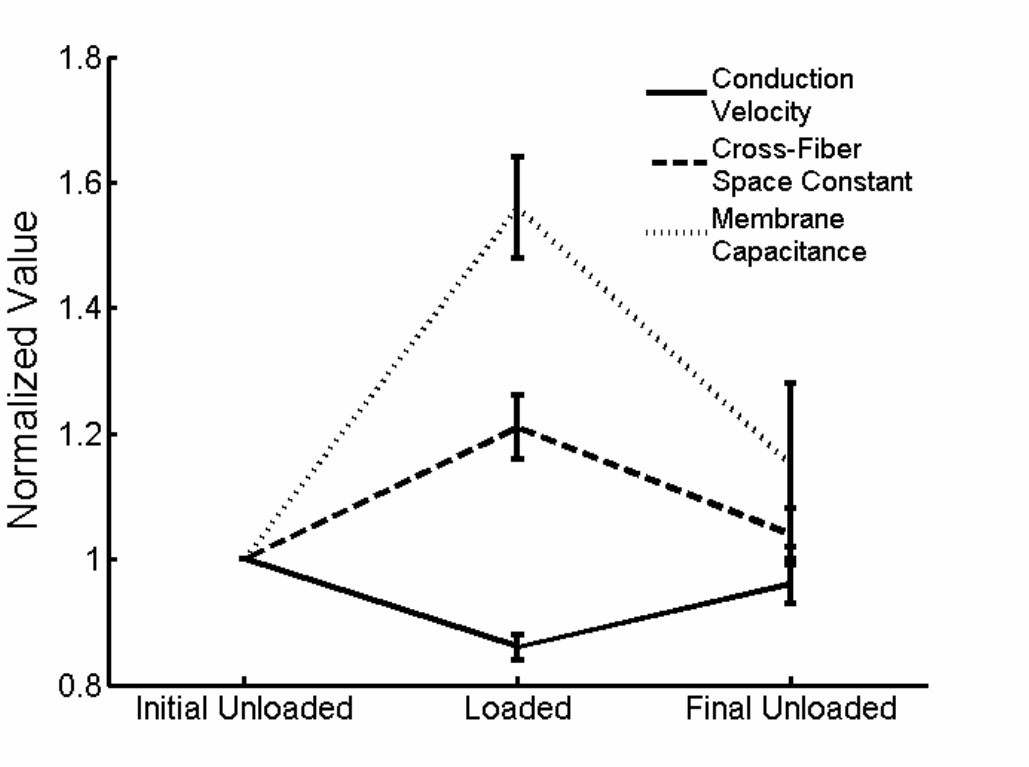

Figure 1.3: Conduction velocity slowing in the volume loaded rabbit left ventricle is associated with an increase in space constant and an increase in membrane capacitance, as observed by Mills and colleagues.[57] Space constant and capacitance were measure with a bidomain model analysis of the potential response to a non-excitatory point stimulus. Values returned to baseline when load was removed. All values are normalized by initial unloaded values.

Research Objectives

The primary objectives of this research are: 1) develop an experimental platform to study the electrical function of the murine heart, 2) study the effects of cytoskeletal disruption on cardiac conduction, and 3) investigate conduction slowing associated with increased ventricular load and potential cellular mechanisms of this phenomenon.

In chapter 2, development of a new experimental platform and analytical methods is described. This system implements optical mapping techniques with a new camera system and optical setup. This system was designed for use in various experimental models, including the isolated murine heart and cardiomyocyte monolayers.

In chapter 3, this experimental platform was used to investigate the electrophysiological phenotype of four knockout models of cytoskeletal proteins: vinculin, desmoplakin, coxsackievirus and adenovirus receptor, and enigma homolog protein. These four proteins are involved in maintaining cellular structure and junctions. Ablation of these proteins in the heart results in different electrical abnormalities through various cellular mechanisms.

Finally, in chapter 4, conduction changes associated with stretch were observed in the murine heart and cardiomyocyte monolayers. Conduction slowing has been associated with changes in membrane capacitance. During stretch, the role of membrane unfolding was analyzed in caveolae deficient mouse models.

The text and figures of this chapter, in part, are a reprint of the material as it appears in: Mills RW, Wright AT, Narayan SM, McCulloch, AD. The effects of wall

stretch on ventricular conduction and refractoriness in the whole heart. In: Kohl P, Sachs F, Franz MR, eds. *Cardiac Mechano-Electric Coupling & Arrhythmias*. Oxford University Press; to be published in 2011: Chapter 25. Reprinted with permission from Oxford University Press. The dissertation author was a primary researcher and author of this book chapter.

Chapter 2: Development of Optical Mapping System and Analysis Methods

Introduction

Optical recording of action potential propagation is a relatively new experimental technique which provides many benefits over traditional electrophysiological measurement techniques. Contact electrode recording has been performed for decades, but each of the recording modalities has limitations. Direct measurements of the transmembrane voltage transients can be obtained using an intracellular electrode. This provides an accurate recording with high temporal resolution from a single cell and is considered the "gold standard" in electrical recording of the cardiac action potential, but it is difficult to implement in intact myocardium and only samples from a single location.

Monophasic action potential (MAP) electrodes are contact electrodes that do not penetrate the cell membrane. Although the cellular basis for the monophasic action potential is still under debate, MAP electrodes provide transient recordings that closely match intracellular recordings with high a temporal resolution.[68] These electrodes are useful for analysis of depolarization and repolarization in intact myocardium from a single location. Some groups have created arrays of MAP electrodes to simultaneously

record from several locations,[69] but these are still limited in spatial resolution compared with other recording techniques.

Extracellular potential recordings reveal a biphasic deflection during membrane depolarization. Extracellular electrode arrays can provide simultaneous recordings of these potential transients from multiple locations with high temporal resolution. These can be used to identify activation patterns in a network of electrically active cells *in vivo* or *in vitro*. The spatial density of these arrays has traditionally been limited to, at most, hundreds of locations. However, new microfabrication techniques and data acquisition hardware allow for simultaneous recording from thousands of locations.[70] While these arrays can provide high spatial and temporal resolution recordings of depolarization, they do not provide information about repolarization and require physical contact.

More than 30 years ago, molecular probes were found to bind to the sarcolemma of cardiac tissue and exhibit a change in fluorescence correlated with changes in transmembrane potential.[71] High speed optical recording of fluorescence from these probes provides an optical representation of the transmembrane potential transients. New camera systems are now capable of high speed recording from many pixels, and implementation of different optics enables measurement on many scales, from subcellular resolution to whole heart imaging. Our lab has used high speed charge-coupled device (CCD) cameras to image action potential propagation in the isolated rabbit heart. This preparation displays bright fluorescence and relatively large signals. The goal of this work was to develop an imaging system capable of recording electrical activity in a variety of cardiac preparations, including the freely beating isolated mouse

heart and cardiomyocyte monolayers. This setup includes a new camera system and optics. Additionally, analysis software has been developed for new experimental applications of this system.

Experimental Platform

Imaging Sensor

The optical sensor is the pivotal component of an optical mapping system. The three commonly used sensors used for multiple site recording are photodiode arrays (PDAs), charge-coupled device (CCD) cameras, and complementary metal-oxide-semiconductor (CMOS) cameras. Each of these sensor types has its advantages and disadvantages. The primary parameters considered when selecting a sensor for optical mapping are sensitivity, spatial resolution, and temporal resolution. Sensitivity is dependent on the intrinsic noise of the sensor, the light collecting capability of a pixel (termed well depth, a function of the pixel area collecting light), and the dynamic range of the sensor. Spatial resolution refers to the number of pixels collecting a signal, and temporal resolution is the frame rate of the system.

Photodiode arrays are most commonly used in low-light experimental preparations, such as *in vitro* cell imaging. They are the most sensitive type of sensor to produce an excellent signal-to-noise ratio due to their large pixel area (on the order of 1 mm x 1 mm), and they can record with very high temporal resolution. However, these systems are spatially limited. Most PDAs are on the order of tens to, at most, a couple

hundred pixels. These systems become expensive and difficult to build at higher spatial resolutions.

CCD cameras are commonly used to image whole heart preparations that emit relatively high-intensity fluorescence. These cameras have a much higher spatial resolution with tens of thousands of sampling pixels. However, these pixels are significantly smaller (10 – 25 μm), resulting in lower sensitivity. Additionally, the readout method CCDs employ limits their temporal resolution. In order to compensate for these limitations, binning of pixels (averaging over neighboring pixels) can increase the effective well depth and temporal resolution of the system. The cameras previously used by our group were the Dalsa D1-256A and D1-128T. Binned, these cameras could image at 128 x 128 pixels and 400 frames per second with an 8-bit output dynamic range, and 64 x 64 pixels at 950 frames per second with a 10-bit output dynamic range, respectively. These cameras were adequate to image impulse propagation in the intact myocardium of isolated rabbit, rat, and mouse hearts.

New advances in CMOS cameras have brought these sensors to use in cardiac optical mapping. CMOS technology implements individual pixel readout allowing for high temporal resolution (up to 10,000 frames per second) at high spatial resolution. However, the circuitry for this takes up some of the pixel area, limiting the light collecting area. Traditionally, CMOS cameras have relatively small pixels as well, limiting their sensitivity. Recently, large-pixel CMOS cameras have been developed to increase well depth. The SciMedia MiCAM Ultima camera has 100 x 100 pixels, a large chip (10 mm x 10 mm), and large well depth. This camera can image at an adjustable frame rate as fast as 10,000 frames per second. Additionally, this camera

system can record with two cameras simultaneously, which is useful for imaging multiple fields of view or dual wavelength imaging. Due to its high temporal and spatial resolutions, high sensitivity, and functional flexibility, this camera system was selected for development of a new imaging system.

Optics Configuration

There are several optical configurations implemented in optical mapping. For single cell or high-magnification imaging, a microscope system with a high numerical aperture (NA, the capacity of a lens to collect light) objective has been used. However, for macroscopic imaging at a low magnification or when a longer working distance (distance from the sample to the lens) is required, there are fewer objectives available with adequate NAs, so alternative optical configurations have been implemented.

For macroscopic imaging of cardiomyocyte monolayers, some groups have developed contact recording systems. These systems do not require a lens, rather fluorescence is transferred from the sample to the photodiodes through an optical fiber bundle.[72] In previous studies, our group has used a single fast (high NA) 50 mm lens (Navitar) to focus the image on the CCD chip (Figure 2.1A). Using the small chip Dalsa CCD cameras, these lenses are adequate to image an adequate field of view to image a rabbit heart (around 5 cm x 5 cm). Inserting extension tubes between the lens and the sensor changed the working distance of the lens to allow imaging of a smaller field of view more appropriate for imaging mouse hearts (1 cm x 1 cm). However, these extension tubes decrease the effective NA of the optics system. The chip of the MiCAM Ultima is much larger, and use of a single lens system with a chip of this size

results in a very large field of view. For example, when imaging a mouse heart, the ventricles were imaged by only a small fraction of the pixels, effectively decreasing spatial resolution. Additionally, a single lens optical setup is not adequate for imaging very low light level preparations, such as cardiomyocyte monolayers.

A tandem lens system implements two high NA, infinity-focused lenses to collect fluorescence, collimate the light rays, and focus the image onto the sensor chip. In this system the magnification of the image is determined by the ratio of the focal lengths of the two lenses. Implemented with the MiCAM Ultima camera, such a system can provide the desired field of view for imaging of the mouse heart (10 mm x 10 mm) using two identical lenses. Swapping out one of the lenses for another of a different focal length can provide different magnifications of the system. Additionally, the light collected from the imaged object can be split once it is collimated to image with multiple sensors or simultaneously viewed with an eyepiece. This can be used to image the same field of view at two wavelengths for ratiometric imaging. A tandem lens system also drastically improves the overall light collecting ability compared with low magnification objectives (as much as a 300 fold increase in light collecting efficiency).[73] This makes the tandem lens optical configuration much better for imaging preparations with low fluorescence emission intensity.

Because of these advantages, a custom tandem lens system was designed and constructed to be used with the MiCAM Ultima. This system implements low magnification planapo stereoscope lenses (Leica, 0.5x, 1x, 2x, and 5x), which, used in different combinations, can result in a number of magnification levels for imaging cardiac preparations at different scales. Two filter boxes were built to hold filters and

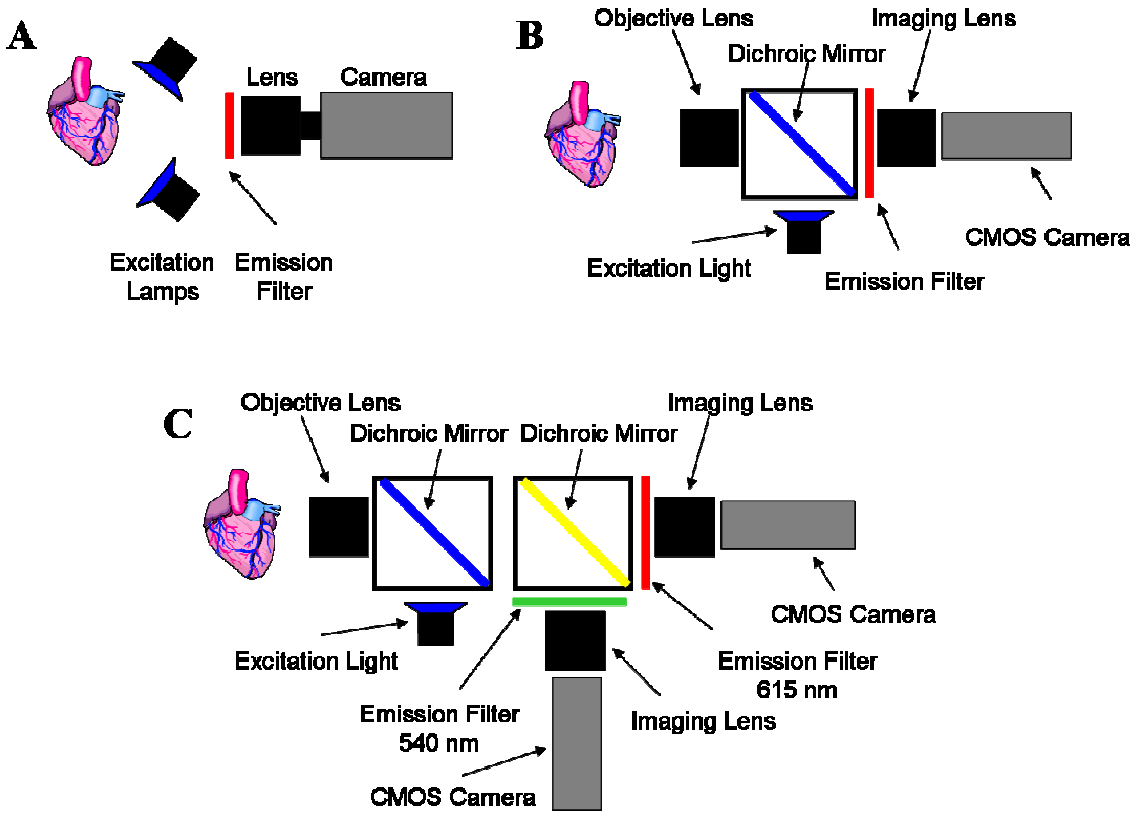

Figure 2.1: Optics Configurations. (A) Single fast lens focuses image onto camera sensor. (B) Tandem lens configuration implements an objective lens that collimates light rays, and an imaging lens to focus the image onto the camera system. (C) Dual wavelength imaging configuration. Light is collimated, split with a dichroic mirror, and imaged with two cameras at two different wavelengths.

dichroic mirrors. Adapter pieces were built to attach and align the lenses and camera (Figure 2.1B). It can also be adapted to split fluorescence emission for dual wavelength imaging (Figure 2.1C). Finally, the filter box can be mounted on a vertical or horizontal stage for fine focus control in different experimental configurations.

Excitation Light Source

Traditionally, xenon arc lamps or quartz-tungsten lamps have been used as an excitation light source. These lamps provide a wide spectrum illumination light source that is filtered to the excitation wavelength of the potentiometric probe. Recent advances in semiconductor technology have resulted in high intensity light emitting diodes (LEDs). These LEDs provide a steady and bright light source at a variety of wavelengths depending on what material is used in the semiconductor. Previously our group has used a 300 Watt xenon arc lamp as an excitation light source. In order to improve light source intensity and reduce noise, two blue LED light sources were tested: a 40-LED array bulb (LEDtronics) and a high intensity LED (Luxeon). Each of these LEDs emitted light in a narrow band of wavelengths around 470 nm, eliminating the need for an excitation filter. Additionally, both of these LEDs are far less expensive and provided steadier and brighter excitation light than the xenon arc lamp. Use of these LEDs has diminished noise due to fluctuations in excitation intensity and brighter excitation improves signal to noise ratio. However, tissue stained with a fluorescent voltage sensitive dye is subject to photobleaching and phototoxicity, so care must be taken to avoid over exposure to these brighter light sources.

Data Acquisition System

During isolated heart experiments, a number of physiological and experimental signals are observed and recorded, including the electrocardiogram, intraventricular pressure, coronary flow rate, temperature, and stimulus pulse. A data acquisition system was constructed to record these signals and control the light source, stimulator, and camera trigger during optical mapping experiments. This system consists of an analog data acquisition system (NI DAQPad 6015, National Instruments) and signal conditioning unit (NI SC 2345, National Instruments) with voltage isolation units (SCC-AI03) and a thermocouple module (SCC-TC01), and is controlled by custom software written in LabView.

Analysis Software

Analysis of optical recordings is performed using custom written MATLAB scripts. Many of these analysis scripts have been preserved from older studies as described previously.[55, 57, 74, 75] The following is a brief overview of signal conditioning and analysis, including new analyses used in this work.

Signal Conditioning and Analysis

Signal Conditioning

Optical mapping data from the MiCAM Ultima is stored in a proprietary file format, and image stacks are imported into MATLAB with a custom script. Recorded fluorescence intensity decreases with an increase in transmembrane voltage, so signals

are normalized with respect to baseline intensity (ΔF/F) and inverted to better represent action potentials (Figure 2.2A). Spatial phase-shift and temporal median filtering are implemented to reduce noise in the signal as previously described.[74]

Action Potential Analysis

Each action potential at each pixel is analyzed to identify activation and repolarization times (Figure 2.2B). Activation time is determined as the time of maximum slope (dF/dt) during the action potential upstroke and activation map over the ventricular epicardium are created, showing the rate and path of action potential propagation (Figure 2.2C).

The baseline and peak of the action potential are identified. Repolarization time is found at a specified level of repolarization (Figure 2.2B, 50% and 80%), and action potential duration at these levels of repolarization are calculated.

Conduction Velocity and Wavefront Curvature

Spatial gradients of activation time are used to calculate local apparent conduction velocity vectors at each pixel.[40] Vector components are used to quantify the apparent epicardial conduction velocity magnitude.

The path of action potential propagation during point stimulation of the ventricles is dependent on local conductivities. The shape of the activation wavefront can give insights into the heterogeneity of these local conductivities. Wavefront curvature is a quantitative measure of the path of propagation. During point stimulation, activation should expand in a convex shape. This would result in a positive wavefront

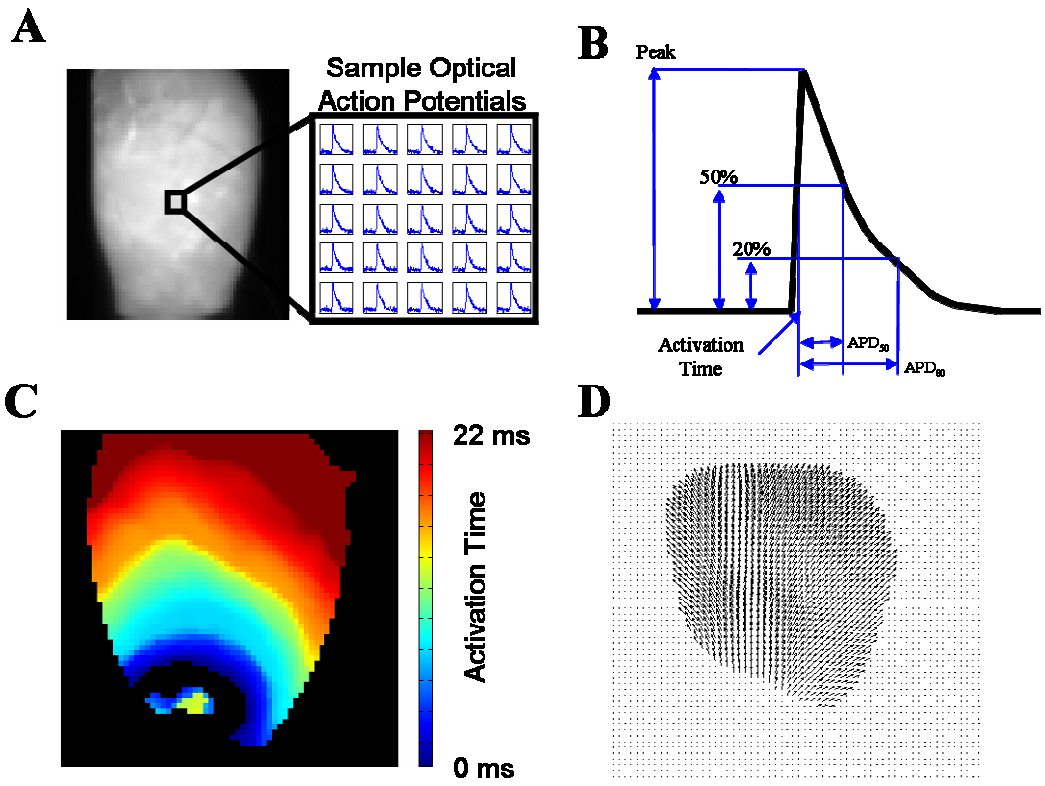

Figure 2.2: Optical mapping signal analysis. (A) Stacks of fluorescent images were imported into MATLAB and signals were normalized and filtered. (B) Each action potential at every pixel is identified. Activation time was identified at max dF/dt. The baseline and AP peak were determined and APD was calculated at different levels of repolarization. (C) Activation maps display timing and path of wavefront propagation. (D) Local conduction velocity vectors were calculated as local gradients in activation time.

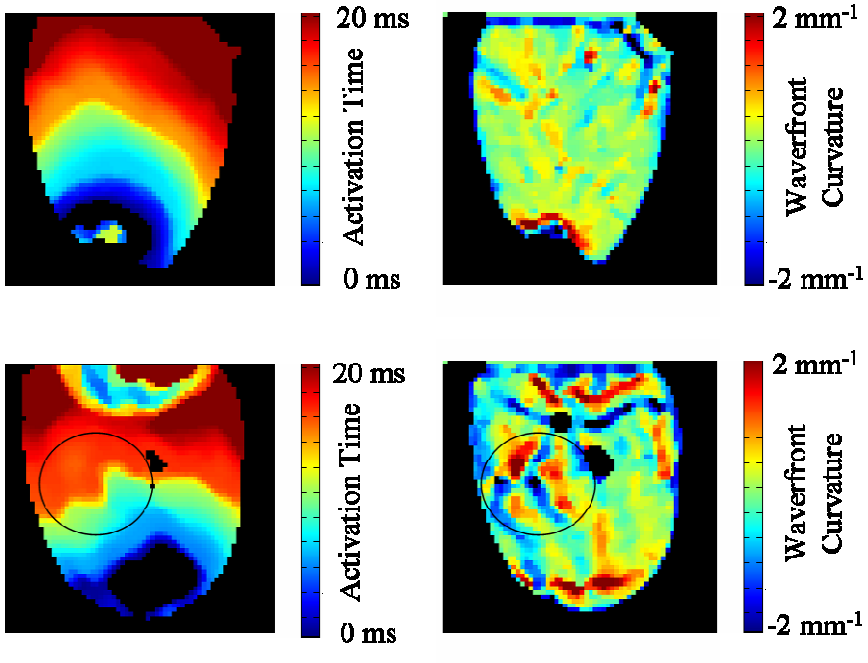

Figure 2.3: Wavefront curvature was calculated from the normalized conduction velocity vector field. In the upper panel, conduction propagates in an organized, convex path. Local calculated wavefront curvature was uniform and mostly positive in value. In the lower panel, the activation wavefront was disturbed (circled area). The correlating wavefront curvature was very heterogeneous and contained areas of high negative values.

curvature. Local conduction delays would result in local concave conduction paths (negative curvature). To calculate wavefront curvature, the conduction velocity vectors are normalized and decomposed into their x and y components (V_x, V_y). The spatial derivatives of these components are calculated to find the local curvature using the formula: $\kappa = \partial V_x / \partial x + \partial V_y / \partial y$ (Figure 2.3)

Motion Artifact Removal

One of the primary issues encountered during analysis of optical mapping data is motion artifact. During contraction, the tissue imaged by a pixel moves from one area to another. This introduces a large artifact in the recorded signal, limiting analysis of the action potential. Depolarization results in a rapid shift in fluorescence that is faster than any change due to motion. Therefore, activation time can still be calculated in the freely beating heart with careful analysis. However, motion artifact makes it difficult to measure repolarization. To account for this, most researchers use mechanical restraint of the tissue or chemical intervention with a mechano-electric uncoupler. Unfortunately, mechanical restraint can lead to tissue ischemia and can introduce mechanical artifact in studies of mechano-electric coupling, and chemical uncouplers have been shown to alter conduction velocity and action potential morphology.[76, 77]

Alternatively, post experiment analysis methods have been investigated to remove motion artifact. For example, ratiometric approaches have been implemented in the isolated heart.[78, 79] The fluorescence spectrum of the potentiometric probe di-4-ANEPPS emission shifts to a lower wavelength as the transmembrane voltage increases. The largest change in intensity is at higher wavelengths (around 610 nm), so this is

typically the spectrum recorded, explaining the inverted optical action potential recorded. Recording in the green spectrum (540 nm) displays an upright action potential. Some of the motion artifact can be removed by taking the ratio of the recorded signals at these wavelengths. However, there is still a shift of tissue during contraction so the same tissue is not recorded by a single pixel throughout the action potential. Therefore, researchers have implemented motion tracking algorithms to track tissue movement and correct for the resulting artifact.[80] Using the new camera and optics setup, dual wavelength imaging of the isolated mouse heart has been implemented to correct for motion artifacts in conjunction with a Lucas-Kanade optical flow motion tracking algorithm (Figure 2.4).

Optical Mapping of Cardiomyocyte Monolayers

Most optical mapping studies are conducted on whole heart, or perfused myocardial sections. Cardiomyocyte monolayers represent an alternative experimental model for study of action potential propagation with several advantages.[81, 82] Cultures are in a well-defined two dimensional structure of purified cardiomyocytes. Their orientation can be manipulated with physical cues or controlled matrix deposition. Additionally, viral gene transfection can be implemented to alter gene expression. This new optical mapping system can been used to map cardiomyocyte monolayers *in vitro.*

Cardiomyocytes are isolated from 1 to 2 day old Sprague-Dawley rats and plated on a fibronectin coated tissue culture dish. Cells are cultured for 5 to 6 days prior to optical mapping. Cultures are stained with 30 μM of the potentiometric dye di-8-

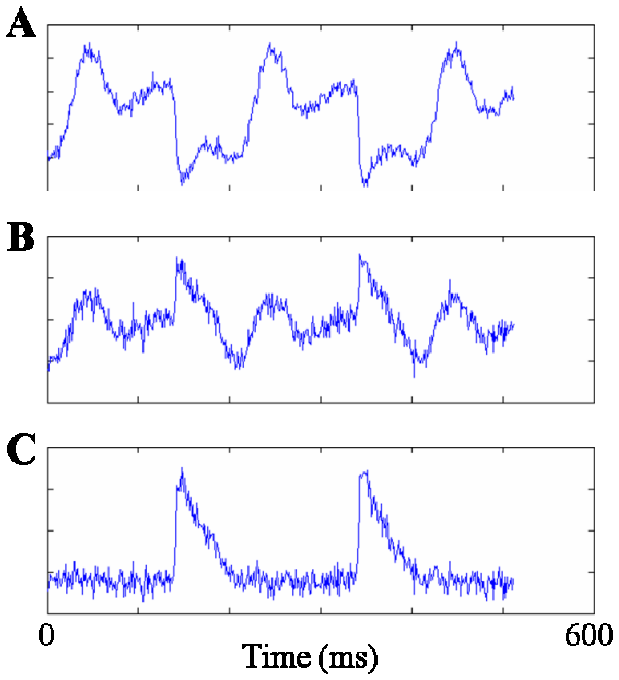

Figure 2.4: Fluorescence recordings in the freely beating mouse heart at 615 nm (A) and 540 nm (B) display large motion artifact. Motion artifact can be removed with ratiometry and motion tracking (C).

ANEPPS mixed with 20% Pluronic F-127 in Tyrode's solution. The culture is gently shaken for 15 minutes, and then maintained at room temperature for an additional 25 minutes. The staining solution is removed and replaced by dye-free medium before imaging the cardiomyocyte monolayer. The camera is configured in a vertical position on a focus drive to image the culture from above. Two 1x lenses are implemented to image a field of view of 10 mm x 10 mm. The cells are excited with a high intensity LED (Luxeon, Star/O) and fluorescence is collected with the tandem lens optical system, filtered at >610 nm, and focused onto the sensor of the CMOS camera recording 500 frames per second.

The system is capable of recording action potential propagation through the cardiomyocyte monolayer (Figure 2.5A). Acquired signals can be processed and analyzed using the same analysis software used in whole heart imaging data. Signal to noise ratio of the acquired data is sufficient for action potential duration analysis and identification of upstroke. Activation maps display smooth propagation through the monolayer (Figure 2.5B). The ability to optically map cardiomyocyte monolayers provides another unique experimental platform for future experiments.

Discussion

Optical mapping of action potential propagation through myocardium is a technique that has been used for over two decades. This technique provides the advantage of non-contact mapping with high spatial and temporal resolutions, compared with traditional extracellular and MAP electrode recording techniques. Here, an optical

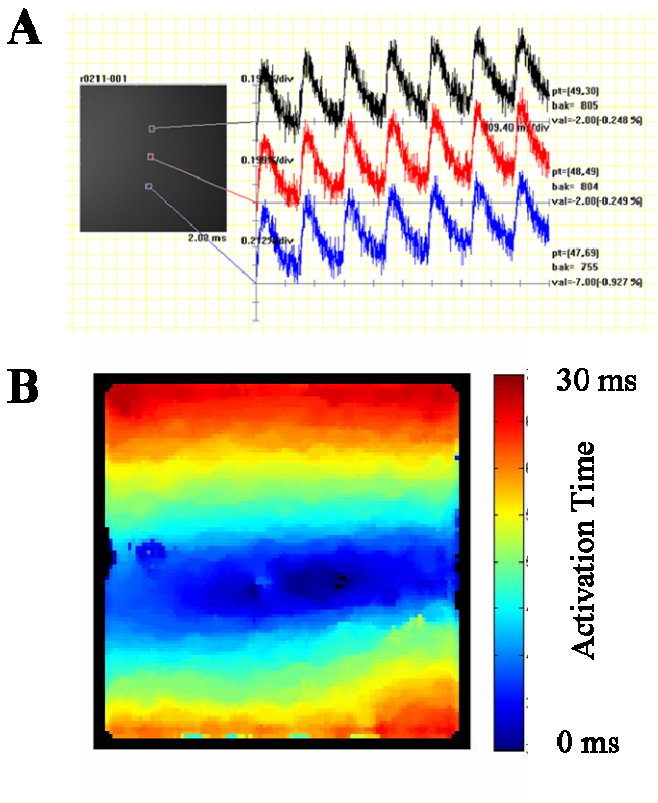

Figure 2.5: Optical mapping of cardiomyocyte monolayers. (A) Sample action potentials recorded during intrinsic rhythm. (B) Activation map of action potential propagation through the monolayer.

mapping system capable of recording electrical activity in a wide range of preparations, from cardiomyocyte monolayers to isolated intact hearts, has been developed. The tandem lens configuration provides optimal light collecting ability of the system and allows for easy change in magnification. Additionally, this design can be set up in a number of arrangements for single or dual camera imaging. Dual wavelength imaging, in conjunction with motion tracking algorithms, can be implemented to eliminate motion artifact in the freely beating heart. Fluorescent images acquired with this system are imported into MATLAB and analyzed using custom software. Signals are filtered, and action potential features are identified to create activation maps and measure action potential duration. Activation maps are used to observe conduction path, calculate conduction velocity, and calculate wavefront curvature as a measure of wavefront organization. The imaging system and the analysis methods described provide a useful platform for recording action potential propagation in a number of experimental models. In the following chapters, these methods will be implemented to investigate several electrophysiological phenotypes and phenomenoa.

Chapter 3: Cytoskeletal Proteins and Cardiac Conduction

Introduction

Cardiomyocytes are specialized striated muscle cells of the heart. Their cellular ultrastructure is arranged to generate strong contractile forces and transmit these forces to the surrounding tissue. The cytoskeleton of cardiomyocytes is composed of a network of proteins that are involved in mechanical stability of the cell and cellular signaling pathways (Figure 1.1). Disruption of the cytoskeletal structure can lead to structural and electrical remodeling. Mutations in cytoskeletal proteins have been linked to the development of progressive heart diseases associated with cardiac dysfunction, altered electrical function, and increased incidence of arrhythmia. Recently, the use of transgenic murine models has allowed researchers to investigate the role of individual proteins on cardiac development and function. The objective of this work was to use optical mapping techniques to investigate the electrophysiological phenotype of murine models with targeted disruption of four cytoskeletal proteins: vinculin, desmoplakin, coxsackievirus and adenovirus receptor, and enigma homolog protein.

Cardiac-Specific Vinculin Knockout Model

Background

Vinculin is a ubiquitously expressed cytoskeletal protein localized at the cell membrane. It is part of protein complexes linking the actin cytoskeleton to the cell membrane at specialized structures.[83] Vinculin is found at both cell-cell and cell-matrix junctions and has been shown to bind with many proteins, including integrin-associated proteins alpha-actinin, talin, and paxillin, and the adherens junction associated protein alpha-catenin.[4, 84]

In cardiomyocytes, costameres are sarcolemmal structures that link the actin cytoskeleton to the extracellular matrix (ECM) through integrins, proteins that span the membrane, and adhere to ECM molecules. Vinculin binds to actin and serves as a link in this protein bridge. In these structures, vinculin is bound to integrins indirectly through talin.[2] Costameres serve to mechanically couple the extracellular matrix to the cytoskeletal frame of the myocyte. These structures transmit externally applied forces to induce changes in cellular processes through mechanotransduction, and transmit stresses from the cytoskeleton to the extracellular matrix during myocyte contraction. Expression and organization of vinculin and integrins at costameres is dependent on the mechanical environment, and important to maintain cell adhesion and structural integrity. In isolated cardiomyocytes, expression of these proteins was upregulated with applied stretch and downregulated when the cells were arrested.[3]

Intercalated discs (ICDs) are complexes that form cell-cell junctions at the longitudinal ends of cardiomyocytes that are composed of three primary types of

junctions. Desmosomes and adherens junctions are structures that mechanically couple the cytoskeleton of one cell to another. These junctions transmit mechanical forces from cell to cell. Vinculin is localized at the adherens junctions, along with catenins and N-cadherin, to link the actin cytoskeleton to the sarcolemma.[4] The third structures are gap junctions which are responsible for cell-cell electrical coupling through specialized transmembrane pores composed of connexin proteins.[6]

A few studies have been performed to investigate the role of vinculin in maintaining cardiac structure and function. Clinically, vinculin levels are increased in the failing heart, and have been shown to decrease after recovery with an assist device.[85] Additionally, mutations of the muscle-specific vinculin splice isoform metavinculin have been associated with development of dilated cardiomyopathy clinically.[86] Global knockout of vinculin in the mouse results in death by embryonic day 10.5. Death was associated with defects in neural development and a structurally undeveloped heart with rhythm disturbances.[11] Mice with a heterozygous global knockout of vinculin are viable and do not have any obvious abnormalities; however, they display a prolonged QRS, abnormal intercalated discs, and disorganized Z-lines. Additionally, these mice are predisposed to cardiac failure when challenged with increased hemodynamic load.[13]

Cardiac-Specific Vinculin Knockout Model

To further understand the role of vinculin in cardiac structure and function, a murine model has been developed with cardiac specific knockout of vinculin (cVclKO).[87] Using Cre-loxP technology, functional vinculin was knocked out in the

ventricular cardiomyocytes with a ventricular myosin light chain-2 (MLC2v) driven Cre-recombinase. This system efficiently knocked out vinculin specifically in cardiomyocytes.

These mice are viable through early development and appeared healthy and had normal hemodynamic function, but there was an increase in sudden death in the cVclKO mice compared with control littermates. Those that survived later developed hypertrophy, mild fibrosis, and eventually a dilated cardiomyopathy. Because the young, healthy-looking cVclKO mice were dying suddenly, further work was done to study any electrophysiological abnormalities in these mice. Conscious electrocardiogram (ECG) recordings were taken using telemetry, and they revealed conduction block, premature ventricular contractions (PVCs), and runs of polymorphic ventricular tachycardias. Additionally, vinculin deficient hearts showed dissolution of intercalated discs and redistribution of connexin-43, the primary protein forming electrically coupling gap junctions between cardiomyocytes, in young mice prior to the onset of cardiac failure. To further investigate these arrhythmias and the effects of the observed remodeling on action potential propagation, we implemented optical mapping techniques to analyze ventricular activation patterns and impulse propagation through the myocardium.

Experimental Methods

Isolated Heart Preparation

Cardiac specific vinculin knockout mice (cVclKO) and control littermates at 8 weeks of age (n=7 for each group) were used for optical mapping studies. All animal

protocols were approved by the UCSD Institutional Animal Care and Use Committee. The mice were administered an intraperitoneal injection of heparin (100 USP Units), anesthetized with isoflurane and sacrificed by cervical dislocation. The heart was rapidly excised, washed in cold arrest solution, and the aorta cannulated on a 20-gauge stainless steel cannula.

The coronaries were perfused with an oxygenated modified Krebs-Henseleit solution: 24.9 mM $NaHCO_3$, 1.2 mM KH_2PO_4, 11.1 mM dextrose, 1.2 mM $MgSO_4$, 4.7 mM KCl, 118 mM NaCl, and 2.55 mM $CaCl_2$. The perfusate was maintained at 35-37 °C and a coronary flow rate of 1 to 2 mL/min was achieved by applying a constant pressure of 70 mmHg. The coronaries were cleared and the heart was allowed to beat freely and equilibrate for 15 minutes. Surface ECG electrodes were set in place and recordings were taken throughout the experiment. A 0.8 mL bolus of 25 μM of the voltage-sensitive dye di-4-ANEPPS (Molecular Probes) was injected into the perfusion line. The heart was paced with a digital stimulator (DS8000, World Precision Instruments) epicardially from the left ventricular apex with a bipolar platinum electrode at a constant current two times threshold.

Optical Mapping

The left ventricular epicardium was illuminated by two 470nm wavelength, 3.6W 40-LED cluster bulbs (Ledtronics, Inc.). Fluorescence emission was passed through a >610 nm high-pass filter, focused with a fast 50 mm lens (1:0.95, Navitar) and recorded by a 12-bit charge-coupled-device (CCD) camera (CA-D1-0128T, Dalsa). Images of a 9 mm x 9 mm field of view were acquired at 950 frames per second and at

spatial resolution of 64 x 64 pixels. During image acquisition, motion artifact was attenuated with perfusion of 15 mM 2,3-butanedione monoxime (Sigma). Data was acquired during intrinsic rhythm to observe epicardial activation patterns during intrinsic atrio-ventricular impulse propagation and observe the occurrence of any spontaneous arrhythmias, and during epicardial pacing at the apex of the left ventricle at a cycle length of 200 ms to measure epicardial conduction velocity and wavefront curvature.

Data Analysis

The time series of fluorescent images provides temporal intensity signals at each pixel. Each signal was normalized with respect to baseline intensity ($\Delta F/F$) and inverted to better represent a cardiac action potential. Spatial phase-shift and temporal median filtering were implemented to reduce noise in the signal.[74] Activation time was determined as the time of maximum slope (dF/dt) during the action potential upstroke and activation map over the ventricular epicardium were created, showing the rate and path of action potential propagation.

During ventricular pacing, spatial gradients of activation time were used to calculate local apparent conduction velocity vectors at each pixel and quantify apparent epicardial conduction velocity.[40] The path of action potential propagation during point stimulation of the ventricles is dependent on local conductivities. The shape of the activation wavefront can give insights into the heterogeneity of these local conductivities. Wave-front curvature was quantified by calculating the gradient of the normalized conduction velocity vector field. The pixels with negative curvature were

binned and a quantifiable value of curvature was defined as the 95 percentile of these binned negative curvature values.[88] Positive curvatures are expected from a wavefront originating from a point source. A disorganized wavefront can be quantified by a greater negative curvature, indicating heterogeneous areas of local conduction block.

Effect of Increased Ventricular Load

Application of mechanical load to the myocardium alters conduction velocity (See Chapter 4). Because vinculin plays a critical role in transmitting stress at cell-cell and cell-matrix junctions, a pilot study was conducted to observe the effects of volume loading of the left ventricle (LV) on conduction velocity in the cVclKO and control heart. An additional two cVclKO and two control hearts were isolated and mapped as described. A fluid filled balloon attached to a syringe and an in-line pressure transducer was inserted into the LV through the mitral valve. The unloaded state was defined when the end diastolic pressure (EDP) of the LV was 0 mmHg, and loaded state was defined when the balloon was inflated to increase EDP to 30 mmHg. The myocardium was preconditioned with repeated loading and unloading of the ventricle and the electrophysiological effects were observed with a recorded ECG. Di-4-ANEPPS was loaded and the heart was paced at the midwall epicardium of the LV. Optical recordings were taken in the unloaded state. The ventricle was loaded and recordings were taken after one minute of equilibration. Finally, the EDP was returned to 0 mmHg and optical recordings were taken in the final unloaded state. Conduction velocity was analyzed in the maximum and minimum directions of conduction.

Results

Intrinsic Rhythm and Ventricular Activation

After the heart was hung and allowed to equilibrate, ECG recordings were taken to observe intrinsic rhythm prior to perfusion of di-4-ANEPPS. In this state, six of seven cVclKO hearts displayed spontaneous PVCs (Figure 3.1D), while none of the seven control hearts displayed arrhythmic events ($P < 0.005$). Optical mapping of ventricular activation during intrinsic rhythm revealed no difference in activation sequence or timing during normal atrio-ventricular conduction between cVclKO and control hearts (Figure 3.1A and 3.1B). Activation maps of these beats displayed a clear LV breakthrough site and relatively short global epicardial activation times on the order of 5 msec. However, ectopic events were optically recorded in several of the cVclKO hearts (Figure 3.1C) while none were observed in control hearts. These ectopic beats were clearly identifiable due to a change in activation sequence and a delay in epicardial activation.

Epicardial Conduction During Ventricular Pacing

Action potential propagation was recorded during epicardial pacing from the LV apex. Local apparent epicardial conduction velocity vectors were calculated using the spatial gradient of activation time over the surface of the LV. Conduction velocity was slightly faster, but not significantly different in the cVclKO hearts compared with control littermates (262.5 ± 22.2 mm/sec in cVclKO vs. 216.7 ± 13.6 mm/sec in control hearts; mean ± S.E.). However, activation wavefronts were disturbed in the cVclKO hearts (Figure 3.2), which was quantified by calculating wavefront curvature. There

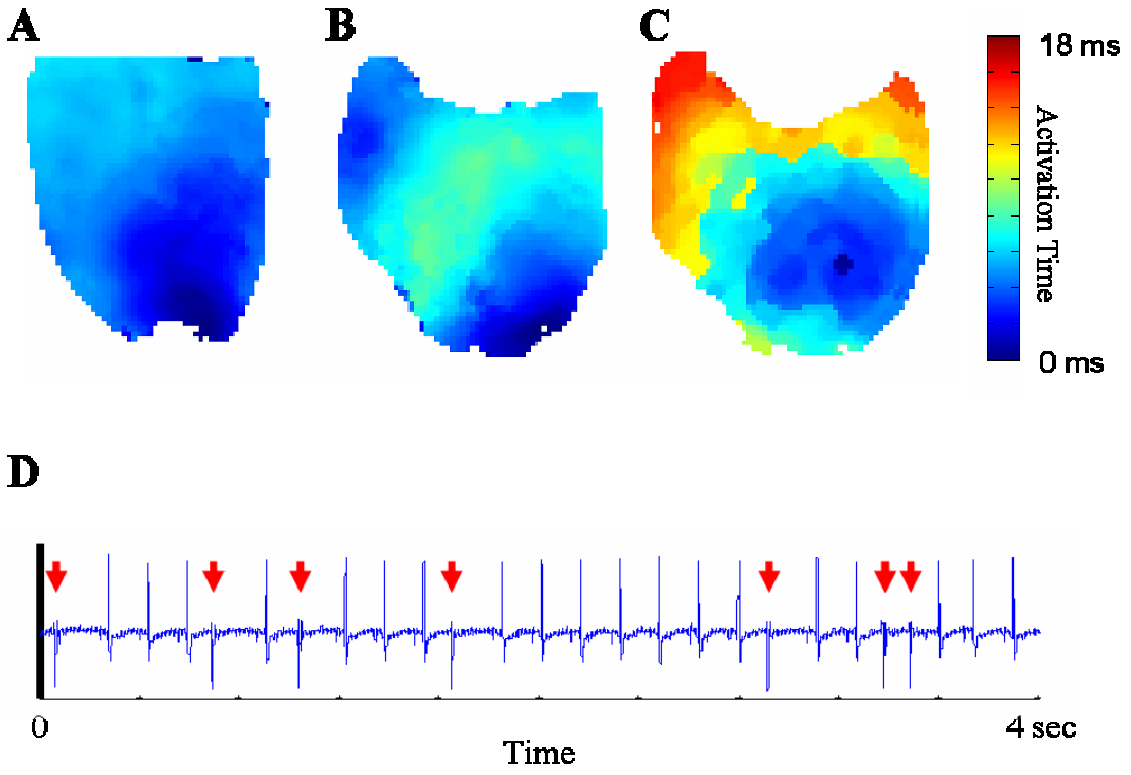

Figure 3.1: Sample activation maps of ventricular epicardium during intrinsic atrioventricular rhythm in a control (A) and cVclKO (B) hearts display similar activation patterns and global epicardial activation time. Following isolation and prior to dye loading, 6 of 7 cVclKO and 0 of 7 control hearts displayed ventricular arrhythmias observed by surface electrocardiogram ($P<0.005$). (D) An ECG recording of a cVclKO heart displaying several ventricular ectopic events (marked with red arrows). Ventricular ectopic events were observed optically in cVclKO hearts as beats with abnormal breakthrough sites and delayed activation. (C) A sample activation map of an ectopic event in the same cVclKO heart as in (B).

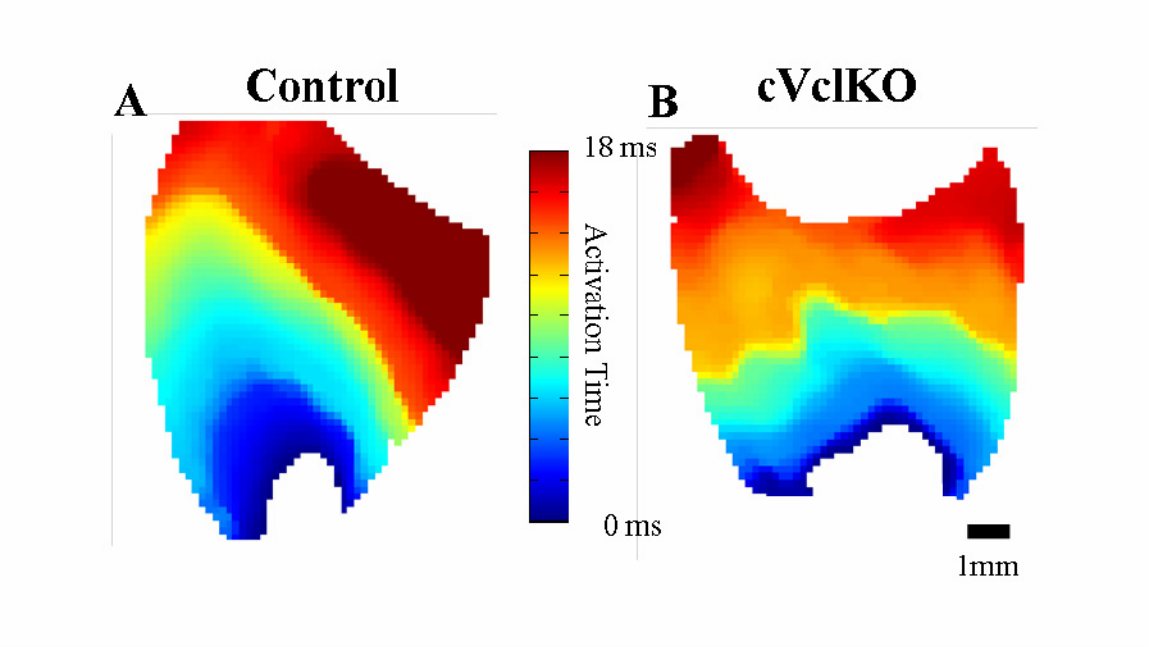

Figure 3.2: Representative activation maps of control (A) and cVclKO (B) hearts during epicardial pacing of the LV apex. Apparent conduction velocity was not significantly different in the knockout hearts, but cVclKO hearts displayed irregular conduction wavefronts with regions of greater negative curvature (-1.284 ± 0.435 mm^{-1} in cVclKO vs -0.751 ± 0.333 mm^{-1} in control; $P < 0.05$; n=7 each).

was a significantly greater negative wavefront curvature in cVclKO hearts compared to control hearts (-1.284 ± 0.435 mm^{-1} in cVclKO hearts vs. -0.751 ± 0.333 mm^{-1} in control hearts, $P < 0.05$). Greater negative wavefront curvatures indicate the presence of local conduction blocks in the myocardium. This provides a proarrhythmic substrate in the myocardium during action potential propagation.

Effect of Increased Ventricular Load

Because vinculin plays a role in transmitting externally applied forces to the actin cytoskeleton of cardiomyocytes and induce cellular response, an intraventricular fluid-filled balloon was implemented to observe the effects of increased ventricular pressure on myocardial conduction velocity. An acute increase in LV EDP from 0 to 30 mmHg resulted in premature ventricular contractions observed by surface ECG. However, non-sustained ventricular tachycardia (VT) was induced in two of two cVclKO hearts (Figure 3.3A), but not in either of two control hearts. The effect of ventricular load on conduction velocity was measured using optical mapping techniques. Conduction slowed slightly in both fiber and cross-fiber directions in both the cVclKO and control hearts with increased load, and increased with a return to the unloaded state (Figure 3.3B). cVclKO hearts are more prone to induction and maintenance of ventricular tachycardias than control hearts when an external mechanical load is applied, but this does not appear to be due to a difference in load-induced conduction changes in the myocardium.

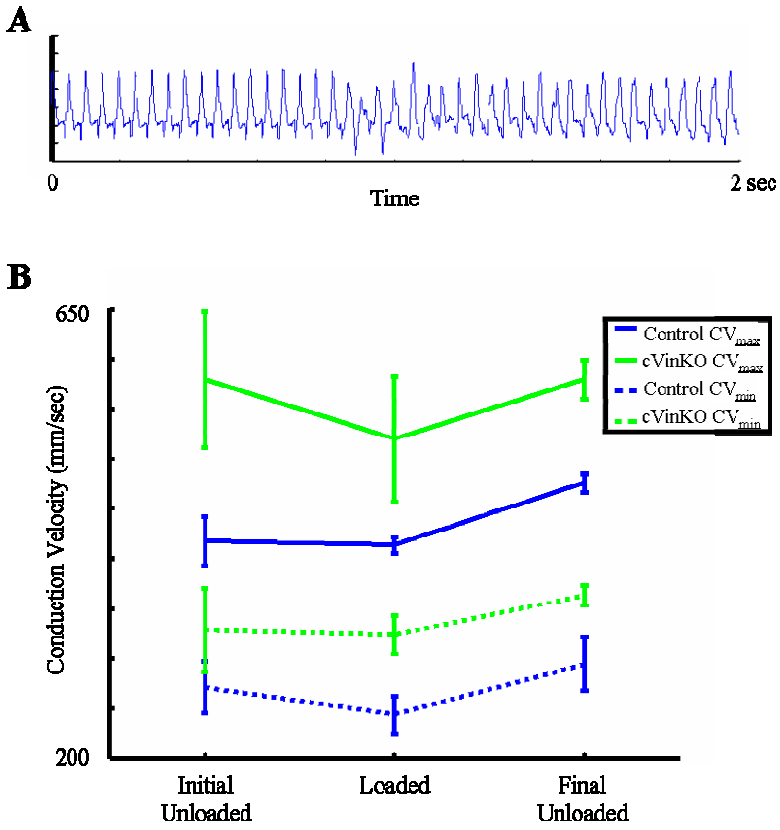

Figure 3.3: Acute volume loading resulted in ventricular ectopic events in both control and cVclKO hearts, but resulted in non-sustained VT in 2 of 2 cVclKO hearts and 0 of 2 control hearts. (A) Example of VT observed in one of the cVclKO hearts. At the basal state, conduction velocity was faster in the cVclKO hearts than in the wild type litter mates in both the CVmax and Cvmin directions. (B) Volume loading of the LV resulted in slight conduction slowing in both cVclKO hearts and control littermates, and a subsequent increase when the EDP was returned to 0 mmHg. Despite the absence of vinculin to aid in the transmission of externally applied mechanical forces to the actin cytoskeleton of the cardiomyocytes, mechanical loading still resulted in a slowing of conduction similar to that seen in wild-type hearts. (see Chapter 4)

Discussion

Vinculin plays an important role in maintaining the structural integrity of cardiomyocytes and their cell-cell and cell-matrix junctions as it acts as a bridge between the actin cytoskeleton and the sarcolemma at costameres and intercalated discs. In this cardiac specific vinculin knockout model, vinculin ablation results in development of a dilated cardiomyopathy in older mice, but no obvious functional abnormalities at earlier stages. However, prior to evidence of cardiac failure, hearts display structurally disrupted intercalated discs and altered expression and localization of costameric and intercalated disc associated proteins.[87] Additionally, these mice experience pronounced ventricular arrhythmias and an increased incidence of sudden cardiac death. Direct observation of action potential propagation using optical mapping techniques has provided further insight into the incidence and underlying mechanisms of these deadly arrhythmias.

Observation of the intrinsic rhythm of the isolated heart with a surface ECG revealed ventricular rhythm disturbances, both ectopic events and non-sustained ventricular tachycardias, in the cVclKO hearts, while none of the control hearts demonstrated a propensity towards such arrhythmic events. Ventricular ectopic events were also observed optically in several cVclKO hearts, signified by slower global epicardial activation and an altered activation sequence on the LV epicardium. The fact that intrinsic beats originating in the atria do not appear different in the cVclKO heart seems to indicate that there is no gross abnormality in the specialized conduction system of the cVclKO hearts, or a significant delay in wavefront propagation through the wall of the myocardium during intrinsic atrio-ventricular rhythm.

During ventricular pacing, there was no significant difference in conduction velocity magnitude through the myocardium in the cVclKO hearts compared with controls. In fact, conduction velocity was slightly higher in the knockout hearts despite disruption of intercalated discs. N-cadherin is the transmembrane protein that forms homodimers in the extracellular space of adherens junctions at the ICD.[4] An inducible model of cardiac specific knockout of N-cadherin display a similar, but more severe, pathological phenotype as the cVclKO hearts. N-cadherin knockout hearts displayed dissolution of ICD structure, loss of cardiac contractile function, and sudden cardiac death due to spontaneous ventricular tachycardia,[27] as well as lowered levels of connexin-43 and a prolonged QRS complex.[28] Optical mapping revealed a significant slowing of ventricular conduction velocity in the N-cadherin knockout heart similar to that seen in cardiac specific knockout of connexin-43 itself.[22] The cVclKO heart does not exhibit reduction in connexin-43 protein, but there is a reorganization of gap junctions to the lateral walls of the cardiomyocytes.[87] Most of the measurements of epicardial conduction velocity in this cVclKO study were made during apical pacing, so the principle direction of propagation on the epicardium is in the cross-fiber direction. If there is a redistribution of gap junctions to these side-to-side cell junctions, this may account for the slight increase in conduction velocity observed.

During ventricular pacing, propagating wavefronts were significantly more disorganized in cVclKO hearts compared to control hearts, indicating areas of local block. This disorganization indicates the presence of heterogeneities of electrical properties throughout the myocardium. Regions of decreased conductivities could slow propagation as the rest of the wavefront continues to propagate, leading to the

observation of greater negative curvature. Large heterogeneities can present a severe proarrhythmic substrate. Similar wavefront disorganization has been observed in a chimeric mouse model with heterogeneous distribution of connexin-43 in the myocardium.[88] As is commonly observed with Cre-lox models, there was not uniform knockout of vinculin in the myocardium in the cVclKO heart. Vinculin knockout resulted in connexin-43 redistribution to produce a heterogeneous distribution of gap junctions in the myocardium.

Vinculin is one of the primary linking proteins in the costameres as well as the ICD. Knockout of other proteins in the costameres has been shown to result in cardiac dysfunction. Cardiac specific ablation of β-integrins results in mice that live to adulthood, but display decreased hemodynamic function, fibrosis, disruption of the cytoskeleton, and development of dilated cardiomyopathy by 6 months of age. Additionally, these mice are less tolerant to increased hemodynamic load.[14] cVclKO hearts develop a similar dilated cardiomyopathy at 3 months of age. These structural defects can lead to myocardial and cellular remodeling that can alter cardiomyocyte electrophysiology as a secondary effect. These optical mapping studies were performed on mice at 8 weeks of age, prior to development of these pathological conditions, so it appears that vinculin is necessary for the formation and maintenance of intercalated disc and normal distribution of gap junctions in the myocardium.

Acute ventricular loading has been shown to slow conduction velocity in isolated rabbit[55] and mouse hearts (see Chapter 4). In the pilot study described in this section, increased load resulted in a comparable decrease in conduction velocity in both cVclKO and control hearts. This would indicate that the cellular mechanisms

responsible for this conduction slowing are not dependent on the presence of vinculin in the costameres or ICDs. Acute increase of mechanical load has been shown to induce triggered events (premature ventricular contractions, PVCs) in the isolated rabbit heart.[89] PVCs were also observed during ventricular load in the current study in both control and cVclKO hearts. However, these triggered events induced non-sustained tachycardia in both of the knockout hearts, but not in either of the control hearts. These are very preliminary results, but they would indicate that the myocardium of the cVclKO hearts is more susceptible to initiation and maintenance of reentrant arrhythmias. The observed heterogeneity of gap junction distribution and intercellular conductivities could explain this susceptibility to these sustained and deadly arrhythmias.

In conclusion, vinculin ablation in the heart has been shown to result in development of dilated cardiomyopathy after several months. However, these cVclKO mice are more susceptible to sudden cardiac death prior to development of severe pathological symptoms. Isolated cVclKO hearts display normal intrinsic activation patterns during atrioventricular conduction, but also display ventricular ectopic beats and non-sustained ventricular tachycardia. Vinculin deficiency results in disruption of ICDs and heterogeneities in connexin-43 density in the myocardium that result in disorganized wavefronts during impulse propagation. This may provide the arrhythmogenic substrate responsible for the increased incidence of deadly arrhythmias.

Cardiac-Specific Desmoplakin Knockout Model

Background

Desmosomes are intercellular junctions that link the intermediate filaments of the cytoskeleton to the sarcolemma at cell-cell junctions. Desmosomes are tight structural junctions that transmit stresses from cell to cell. They are abundant in tissues that are exposed to large stresses such as the skin and cardiac muscle.[90] In cardiomyocytes, desmosomes are primarily located in the intercalated discs at the longitudinal ends of the cell. Desmosomes provide structural support to maintain a tight coupling between two cells. There are four primary proteins that make up desmosomes. Desmosomal cadherins are the transmembrane proteins that bind in the extracellular space. Plakoglobin and plakophilin bind to the intracellular part of the desmosomal cadherins. Finally, desmoplakin binds to the plakoglobin/plakophilin complex and directly to the intermediate filaments.[91]

Mutations of desmosomal proteins have been linked to disease of the skin and cardiac tissue clinically.[92] In particular, arrhythmogenic right ventricular cardimyopathy (ARVC) is a particular type of heart disease that is primarily associated with mutations of these proteins.[91] ARVC is associated with myocyte loss, primarily in the right ventricle, and replacement with fibrofatty tissue, as well as increased incidence of ventricular arrhythmia.[93] Mutations of desmosomal proteins have also been linked to remodeling of other intercalated disc proteins, including other desmosomal proteins and gap junctions.[94] In fact, remodeling of gap junctions appears to be diffusive and is not limited to the right ventricle. These heterogeneous

changes in connexin distribution might be responsible for the increased arrhythmogenicity. Murine models have been used to investigate the importance of desmosome in cardiac structure and function as well. Global knockout of plakoglobin[25, 26] and plakophilin[95] has been shown to be embryonic lethal, and a model with reduced expression of plakoglobin demonstrates symptoms similar to those observed clinically in ARVC.[29]

Cardiac-Specific Desmoplakin Knockout Model

To further understand the role of desmosomes, and particularly desmoplakin, in cardiac structure and function, a murine model has been developed with cardiac specific knockout of desmoplakin (cDpKO). Using Cre-loxP technology, functional desmoplakin was knocked out in the ventricular cardiomyocytes with a ventricular myosin light chain-2 (MLC2v) driven Cre-recombinase. This system efficiently knocked out desmoplakin specifically in cardiomyocytes.

Homozygous knockout mice are viable and survive until adulthood, but develop a progressive cardiomyopathy with many characteristics similar to clinical ARVC. They display disruption of desmosomes and disorganized intercalated discs. The right ventricular wall is thin, and the right ventricle contractility is reduced. These hearts exhibit myocyte loss and replacement with fibrotic and fatty tissue in right and left ventricular walls and diminished cardiac function. Additionally, these mice displayed ventricular arrhythmias and a widened QRS complex, indicating delayed ventricular conduction, during ECG analysis. It was hypothesized that lack of desmoplakin impairs ICD structural integrity and disrupt cardiac conduction. To further investigate the effect

of desmoplakin deficiency on impulse propagation in the myocardium, optical mapping techniques were implemented to directly observe ventricular activation sequences and action potential propagation through the myocardium.

Experimental Methods

Isolated Heart Preparation

Cardiac specific desmoplakin knockout mice (DpKO) and control littermates (n=6 for each group) were used for optical mapping studies. All animal protocols were approved by the UCSD Institutional Animal Care and Use Committee. The mice were administered an intraperitoneal injection of heparin (100 USP Units), anesthetized with isoflurane and sacrificed by cervical dislocation. The heart was rapidly excised, washed in cold arrest solution, and the aorta cannulated on a 20-gauge stainless steel cannula.

The coronaries were perfused with an oxygenated modified Krebs-Henseleit solution: 24.9 mM $NaHCO_3$, 1.2 mM KH_2PO_4, 11.1 mM dextrose, 1.2 mM $MgSO_4$, 4.7 mM KCl, 118 mM NaCl, and 2.55 mM $CaCl_2$. The perfusate was maintained at 35-37 °C and a coronary flow rate of 1 to 2 mL/min was achieved by applying a constant pressure of 70 mmHg. The coronaries were cleared and the heart was allowed to beat freely and equilibrate for 15 minutes. Surface ECG electrodes were set in place and recordings were taken throughout the experiment. A 0.8 mL bolus of 25 μM of the voltage-sensitive dye di-4-ANEPPS (Molecular Probes) was injected into the perfusion line. The heart was paced with a digital stimulator (DS8000, World Precision Instruments) epicardially from the posterior base of the right ventricle with a bipolar platinum electrode at a constant current two times threshold.

Optical Mapping

The ventricular epicardium was illuminated by two 470 nm wavelength, 3.6W 40-LED cluster bulbs (Ledtronics, Inc.). Fluorescence emission was passed through a >610 nm high-pass filter, focused with a fast 50 mm lens (1:0.95, Navitar) and recorded by a 12-bit charge-coupled-device (CCD) camera (CA-D1-0128T, Dalsa). Images of a 9 mm x 9 mm field of view were acquired at 950 frames per second and at spatial resolution of 64 x 64 pixels. During image acquisition, motion artifact was attenuated with perfusion of 15 mM 2,3-butanedione monoxime (Sigma). Data was acquired during intrinsic rhythm, imaging the anterior ventricular epicardium to observe epicardial activation patterns during intrinsic atrio-ventricular impulse propagation and observe the occurrence of any spontaneous arrhythmias. The right ventricular epicardium was imaged during epicardial pacing at the posterior base of the right ventricle at a cycle length of 200 ms to measure epicardial conduction velocity and wavefront curvature.

Data Analysis

The time series of fluorescent images provides temporal intensity signals at each pixel. Each signal was normalized with respect to baseline intensity ($\Delta F/F$) and inverted to better represent a cardiac action potential. Spatial phase-shift and temporal median filtering were implemented to reduce noise in the signal.[74] Activation time was determined as the time of maximum slope (dF/dt) during the action potential upstroke and activation map over the ventricular epicardium were created, showing the

rate and path of action potential propagation. A measure of epicardial activation time was calculated during intrinsic rhythm by binning activation times of all pixels over the anterior epicardial surface and defining activation time as the 95th percentile minus the 5th percentile.

During ventricular pacing, spatial gradients of activation time were used to calculate local apparent conduction velocity vectors at each pixel and quantify apparent epicardial conduction velocity.[40] The path of action potential propagation during point stimulation of the ventricles is dependent on local conductivities. The shape of the activation wavefront can give insights into the heterogeneity of these local conductivities. Wave-front curvature was quantified by calculating the gradient of the normalized conduction velocity vector field. The pixels with negative curvature were binned and a quantifiable value of curvature was defined as the 95th percentile of these binned negative curvature values.[88] Positive curvatures are expected from a wavefront originating from a point source. A disorganized wavefront can be quantified by a greater negative curvature, indicating heterogeneous areas of local conduction block.

Results

Intrinsic Rhythm and Ventricular Activation

After the heart was hung and allowed to equilibrate, ECG recordings were taken to observe intrinsic rhythm prior to perfusion of di-4-ANEPPS. During this equilibration, 4 of 6 cDpKO hearts displayed premature ventricular contractions (PVC) while none of the six control hearts displayed arrhythmic events (Figure 3.4E). PVCs

were also optically recorded in all of the cDpKO hearts (Figure 3.4C and 3.4D) while none were observed in control hearts. Visual observation of activation maps and corresponding ECG recordings were used to distinguish between PVCs and beats originating from intrinsic atrio-ventricular conduction. Activation maps of PVCs displayed a change in activation sequence and a delay in epicardial activation.

Optical mapping of the anterior ventricular epicardium during intrinsic beats with impulse originating in the atria revealed delayed and irregular epicardial activation sequences in cDpKO hearts compared to control hearts. Anterior epicardial activation time was significantly greater in the cDpKO hearts compared to control hearts (5.24 ± 0.64 ms in cDpKO hearts vs. 2.19 ± 0.20 ms in control hearts, $P < 0.002$; mean ± S.E.; Figure 3.4A and 3.4B). Activation patterns in the control hearts displayed clear breakthrough sites towards the apex of both the right and left ventricles (Figure 3.5A-D). cDpKO activation patterns were diverse from heart to heart, but most displayed multiple and/or irregular breakthrough sites (Figure 3.5E-H). Some hearts demonstrated breakthrough only on the epicardium of one ventricle, indicating a functional block of the His bundles (Figure 3.5G and 3.5H).

Epicardial Conduction During Ventricular Pacing

Action potential propagation was recorded during epicardial pacing from the posterior right ventricular base. Local apparent epicardial conduction velocity vectors were calculated using the spatial gradient of activation time over the surface of the right ventricle. Conduction velocity was not different in the cDpKO hearts compared with control littermates (375.9 ± 53.8 mm/sec in cDpKO vs. 382.2 ± 34.0

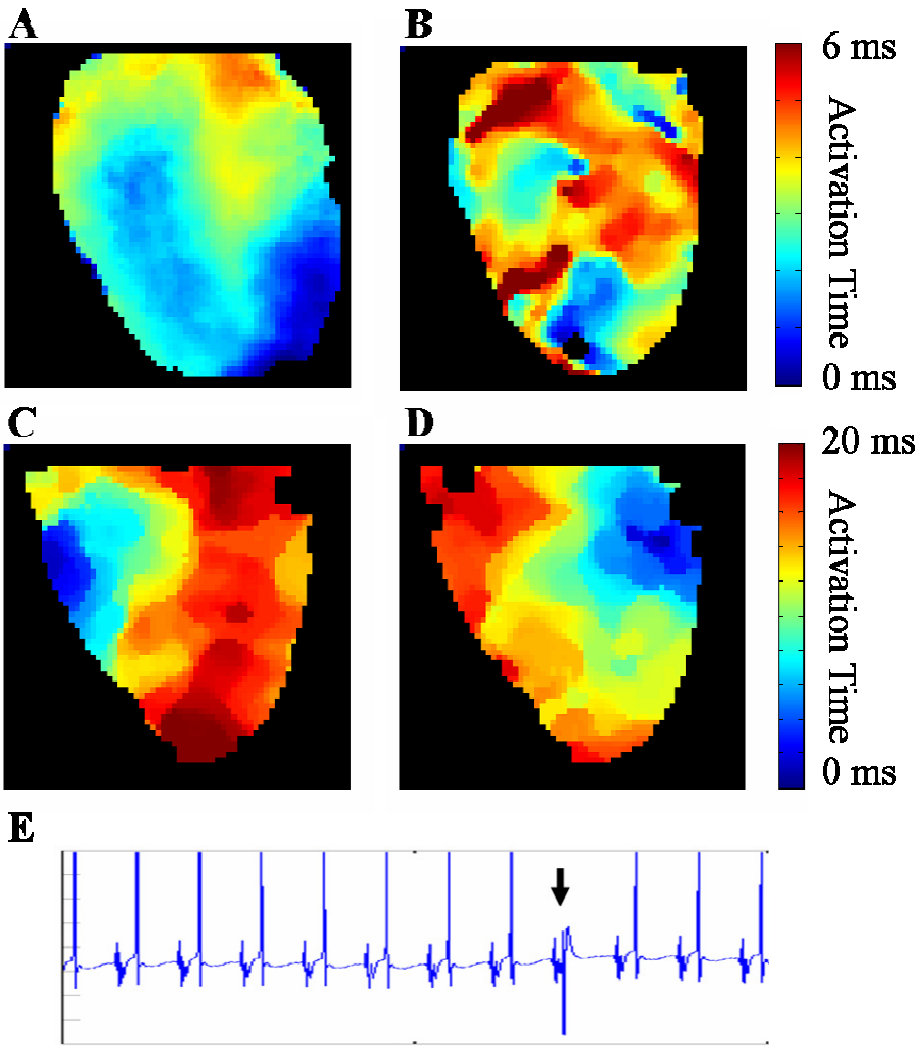

Figure 3.4: Anterior epicardial activation is significantly delayed in the cDpKO hearts (B) compared to control hearts (A) during intrinsic rhythm. Prior to dye loading, premature ventricular contractions (PVC) were observed by ECG in cDpKO hearts prior to dye loading (E, PVC marked with arrow), but not in control hearts. PVCs were also optically observed. C and D are two recorded PVCs from the same heart, demonstrating significantly delayed epicardial activation and different loci of impulse initiation. These arrhythmic events originated from both the right (C) and left (D) ventricular base.

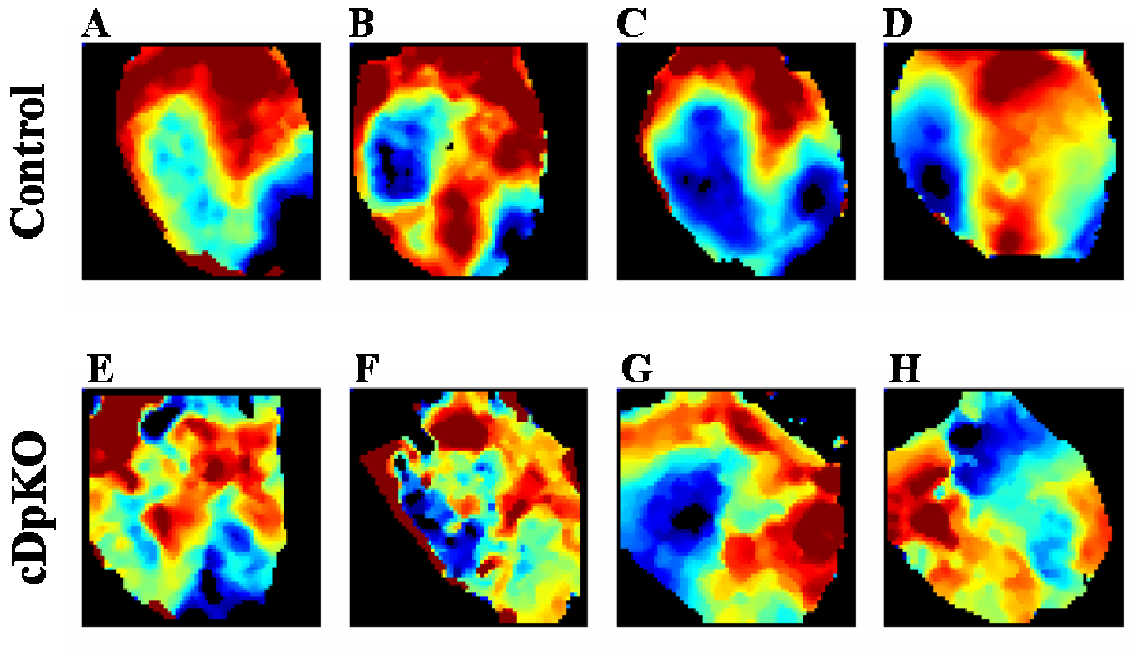

Figure 3.5: Sample activation maps of the anterior epicardium during intrinsic rhythm. Control hearts (A-D) clearly display two distinct breakthrough sites, areas of early activation, towards the apex of the left and right ventricles. cDpKO hearts (E-H) display irregular epicardial activation sequences. The pattern of activation was not consistent from heart to heart, but most lacked distinct breakthrough sites on both the left and right ventricles. Some hearts (H) displayed early activation in the left ventricles and delayed propagation to the right ventricle, consistent with right bundle branch block which has been associated with ARVC clinically. Note: Activation time color scales are not consistent from heart to heart to better show activation pattern and location of impulse breakthrough.

mm/sec in control hearts). However, activation wavefronts were highly disorganized in the cDpKO hearts (Figure 3.6), which was quantified by calculating wavefront curvature. There was a significantly greater negative wavefront curvature in cDpKO hearts compared to control hearts (-1.570 ± 0.293 mm^{-1} in cDpKO hearts vs. -0.852 ± 0.080 mm^{-1} in control hearts, $P < 0.05$). Greater negative wavefront curvatures indicate the presence of local conduction blocks in the myocardium. This provides a proarrhythmic substrate in the myocardium during action potential propagation.

Discussion

Desmosomes are structural intercellular junctions that link the intermediate filaments of the cytoskeleton to the sarcolemma at the intercalated disc in cardiomyocytes.[90] As described, mutations of desmosomal proteins have been clinically linked to a progressive arrhythmogenic cardiomyopathy, ARVC.[91] Cardiac-specific ablation of desmoplakin in the mouse provides a murine model that develops a similar cardiomyopathy that can be used to study the development and characteristics of this disease.

Desmoplakin deficient hearts develop dilation and loss of function of the right ventricle. Heterozygous expression of the associated desmosomal protein plakoglobin, results in a similar phenotype.[29] These mice develop right ventricular dilation and loss of contractility. However, unlike cDpKO hearts, plakoglobin heterozygous hearts do not display any change in intercalated disc structure or connexin-43 distribution. Alternatively, siRNA silencing of the desmosomal protein plakophilin in cultured

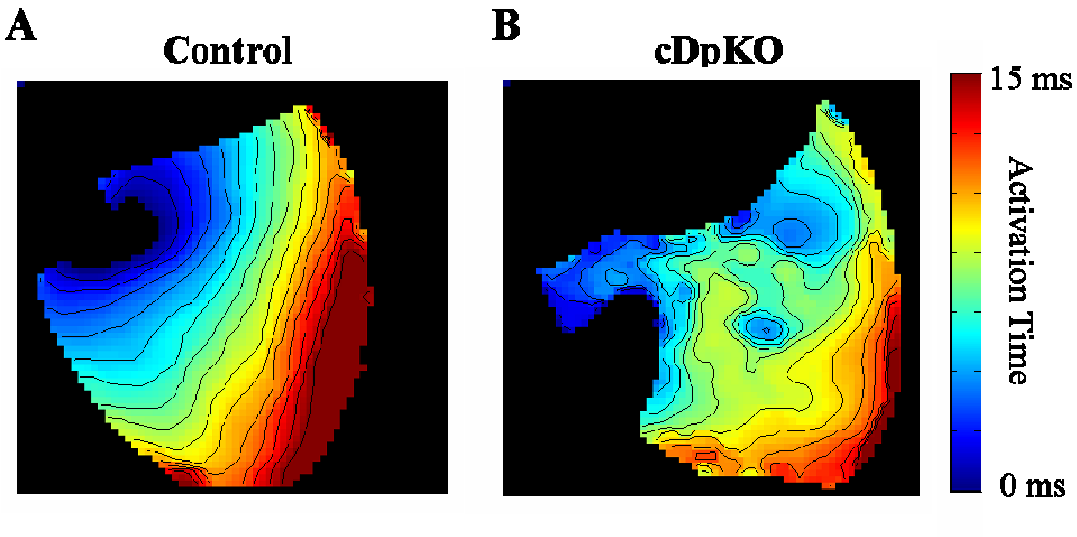

Figure 3.6: Activation map of action potential propagation during epicardial pacing of the posterior base of the right ventricle. Activation wavefront is disrupted in cDpKO hearts compared with control hearts. This disorganization was quantitatively assessed by measuring wavefront curvature. Negative wavefront curvatures were significantly greater in cDpKO hearts compared to control hearts.

neonatal rat cardiomyocytes results in loss of desmosome structure and redistribution of connexin-43 from the intercalated discs.[96]

Structural remodeling in the cDpKO hearts may account for the electrophysiological abnormalities observed using optical mapping. During epicardial pacing of the ventricle, cDpKO hearts display abnormal impulse propagation with a greater negative curvature of the propagating wavefront. This indicates the presence of local conduction block caused by heterogeneous myocardial conductivities. Similar wavefront disorganization has been observed in a chimeric mouse model with heterogeneous distribution of connexin-43 in the myocardium[88] as well as in vinculin deficient hearts.[87] cDpKO hearts develop heterogeneous myocyte loss, fibrosis, and fatty deposits, as well as disruption of the intercalated discs. These distributed changes in myocardial architecture are likely responsible for the local conduction delays responsible for the disorganized wavefronts observed.

Despite disorganization of intercalated discs and the observed wavefront abnormalities, there was no difference in apparent epicardial conduction velocity in the cDpKO hearts. A similar phenotype was observed in hearts deficient in vinculin, an adherens junction protein also located at the intercalated disc.[87] However, cardiac specific knockout of the adherens junction protein N-cadherin resulted in dissolution of the intercalated discs and delayed conduction velocity.[27, 28] Direct knockout of connexin-43 in the heart results in slowed conduction[22], with no change in the structure of adherens junctions and desmosomes at the intercalated discs.[23]

Ventricular ectopic beats were observed *in vivo* and in the isolated heart by ECG, as well as optically, in the cDpKO hearts. Similarly, plakoglobin heterozygous hearts

displayed spontaneous ventricular arrhythmias, which originate from the right ventricle.[29] Anterior epicardial activation was also severely disrupted and significantly prolonged in the cDpKO hearts during atrio-ventricular conduction. Some activation maps indicate the presence of a functional block in the conduction system. Clinically, ARVC has been associated with right bundle branch block.[97] Some of the hearts display a single breakthrough site with severely delayed activation time. Bundle branch block would also be consistent with the observed prolonged QRS complex recorded *in vivo*, despite no change in impulse conduction velocity through the myocardium.

In conclusion, cardiac specific knockout of desmoplakin results in a murine model that exhibits a cardiac phenotype similar to the clinical symptoms of ARVC. Structural remodeling of the myocardium results in heterogeneous changes in electrical properties and, thus, a proarrhythmic substrate that manifests ventricular ectopic events and tachycardia. Myocardial conduction is disorganized but, surprisingly, not slowed during ventricular pacing due to this heterogeneous remodeling. The unusual activation patterns observed during intrinsic rhythm might also be due to these heterogeneities that disrupt impulse propagation from the conduction system to the epicardium. Additionally, activation sequences of some hearts indicate a functional block in the cardiac conduction system itself.

Cardiac-Specific CAR Knockout Model

Background

Coxsackievirus and adenovirus receptor (CAR) is a transmembrane protein which was first identified as a common receptor for the two viruses for which it was named.[8] It is highly expressed in the brain[98] and heart[99] at the embryonic and neonatal stages and is required for cardiac development.[100-102] During development, CAR expression decreases in the heart and is localized at the intercalated discs in adult cardiomyocytes.[7, 103] Many studies have been conducted investigating the role of CAR on viral transfection and the pathogenesis of viral myocarditis, but the physiological role of CAR is still not fully understood.

The extracellular domains of CAR are thought to homodimerize between two cells.[9] In *in vitro* studies, CAR was shown to co-localize and bind with tight junction protein ZO-1 at cell-cell junctions and regulate cell adhesion.[104] In cardiomyocytes, the intercalated disc (ICD) is a specialized structure at the longitudinal end cell-cell junctional complex. The primary junctions at the ICD are desmosomes and adherens junctions, which are structural junctions mechanically linking the cytoskeleton of one cell to another, and gap junctions, which are intercellular channels responsible for ion flow driving action potential propagation. CAR is found at the ICD in both the functional myocardium and in the specialized conduction system. CAR might play a role in maintaining the structural and functional integrity of these junctions.

The cardiac conduction system is a specialized network of cells that regulate the timing and organization of cardiac contraction. Impulse propagation from the atria to

the ventricles travels through the atrioventricular (AV) node, a specialized structure that delays activation of the ventricles to allow ventricular filling. AV block is a clinical arrhythmia of impaired conduction through the AV node. Impulse conduction through the AV nodal cells is highly dependent on gap junction conductivities at the intercalated discs. Connexin-45 and connexin-30.2 are the primary connexins that form gap junctions at the intercalated discs of the cells in AV node.[5]

Cardiac-Specific CAR Knockout Model

To investigate the role of CAR on cardiac structure and function, particularly intercalated disc structure and gap junction distribution and function, a murine model with cardiac-specific excision of CAR (CAR-cKO) was created.[105] Using Cre-loxP technology, CAR was knocked out specifically in cardiomyocytes with an α-myosin heavy chain (α-MHC) driven Cre-recombinase. These mice were viable through adulthood and did not display any apparent cardiac dysfunction at a young age. They developed a cardiomyopathy with increased fibrosis and loss of contractility beginning at 21 weeks of age. However, ECG analysis revealed AV block and complete AV dissociation *in vivo* in the CAR-cKO hearts in young mice. Optical mapping techniques were implemented to further investigate the activation patterns associated with this AV dysfunction and directly observe the effect of CAR knockout of myocardial action potential propagation.

Experimental Methods

Isolated heart preparation

Cardiac specific CAR knockout mice (CAR-cKO) and control littermates at 4 to 6 weeks of age (control n=7, CAR-cKO n=6) were used for optical mapping studies. All animal protocols were approved by the UCSD Institutional Animal Care and Use Committee. The mice were administered an intraperitoneal injection of heparin (100 USP Units), anesthetized with isoflurane and sacrificed by cervical dislocation. The heart was rapidly excised, washed in cold arrest solution, and the aorta cannulated on a 20-gauge stainless steel cannula.

The coronaries were perfused with an oxygenated modified Krebs-Henseleit solution: 24.9 mM $NaHCO_3$, 1.2 mM KH_2PO_4, 11.1 mM dextrose, 1.2 mM $MgSO_4$, 4.7 mM KCl, 118 mM NaCl, and 2.55 mM $CaCl_2$. The perfusate was maintained at 35-37 °C and a coronary flow rate of 1 to 2 mL/min was achieved by applying a constant pressure of 70 mmHg. The coronaries were cleared and the heart was allowed to beat freely and equilibrate for 15 minutes. The heart was submersed in heated perfusate in an optical bath chamber, and a volume-conducted ECG was monitored and recorded throughout the experiment. Following equilibration, the ECG was recorded to observe baseline rhythm. A 1 mL bolus of 26 μM of the voltage-sensitive dye di-4-ANEPPS (Molecular Probes) was injected into the perfusion line. During recording of paced beats, the ventricular epicardium was paced with a digital stimulator (DS8000, World Precision Instruments) and a platinum unipolar electrode at a constant current 1.5-times threshold.

Optical Mapping

The atrial or ventricular epicardium was illuminated by two 470 nm wavelength, 3.6W 40-LED cluster bulbs (Ledtronics, Inc.). Fluorescence emission was passed through a >610 nm high-pass filter, focused with a fast 50 mm lens (1:0.95, Navitar) and recorded by a 12-bit charge-coupled-device (CCD) camera (CA-D1-0128T, Dalsa). Images of a 9 mm x 9 mm field of view were acquired at 950 frames per second and at a spatial resolution of 64 x 64 pixels.

To analyze the whole heart activation sequence, imaging of the anterior and posterior surfaces of the atria and ventricles was performed in the freely beating heart during intrinsic rhythm. Midwall pacing of the left ventricular epicardium at a cycle length of 150 ms was implemented to observe the rate of action potential propagation through the myocardium. Activation and conduction velocity recordings were taken in the freely beating heart, while motion artifact was attenuated with perfusion of 15 mM 2,3-butanedione monoxime (Sigma) during action potential duration measurements.

Data Analysis

The time series of fluorescent images provides temporal intensity signals at each pixel. Each signal was normalized with respect to baseline intensity ($\Delta F/F$) and inverted to better represent a cardiac action potential. Spatial phase-shift and temporal median filtering were implemented to reduce noise in the signal.[74] Activation time was determined as the time of maximum slope (dF/dt) during the action potential upstroke and activation map over the ventricular epicardium were created, showing the rate and path of action potential propagation. During ventricular pacing, spatial

gradients of activation time were used to calculate local apparent conduction velocity vectors at each pixel and quantify apparent epicardial conduction velocity.[40] To measure action potential duration, the baseline signal and peak of the action potential were calculated. Repolarization at 20%, 50%, and 80% levels was identified at the corresponding return of signal from peak to base, and the action potential duration at these levels of repolarization was calculated from the time of activation.

Results

Intrinsic Rhythm and Epicardial Activation Pattern

After the heart was cannulated and allowed to equilibrate, ECG recordings were taken to evaluate intrinsic rhythm in the isolated heart. Analysis of these recordings revealed severe AV node dysfunction in the CAR-cKO hearts compared with control hearts (Figure 3.7). Most CAR-cKO hearts demonstrated complete AV block with independent atrial and ventricular rhythms. In these hearts, recordings revealed consistent PP intervals and RR intervals of different cycle lengths with no apparent relationship. Atrial rhythms were observed both faster (Figure 3.7B) and slower (Figure 3.7C) than ventricular rhythms. These ECGs indicate that there were independent pacemakers for the atria and ventricles which both demonstrate rhythmic automaticity. Some hearts displayed consistent atrial rhythms, with inconsistent RR intervals (Figure 3.7D). In this recording, it appears there is inconsistent AV conduction with some junctional escape rhythm.

Optical mapping of the epicardium revealed normal activation patterns of the atria and ventricles during intrinsic rhythm in both the CAR-cKO and control hearts.

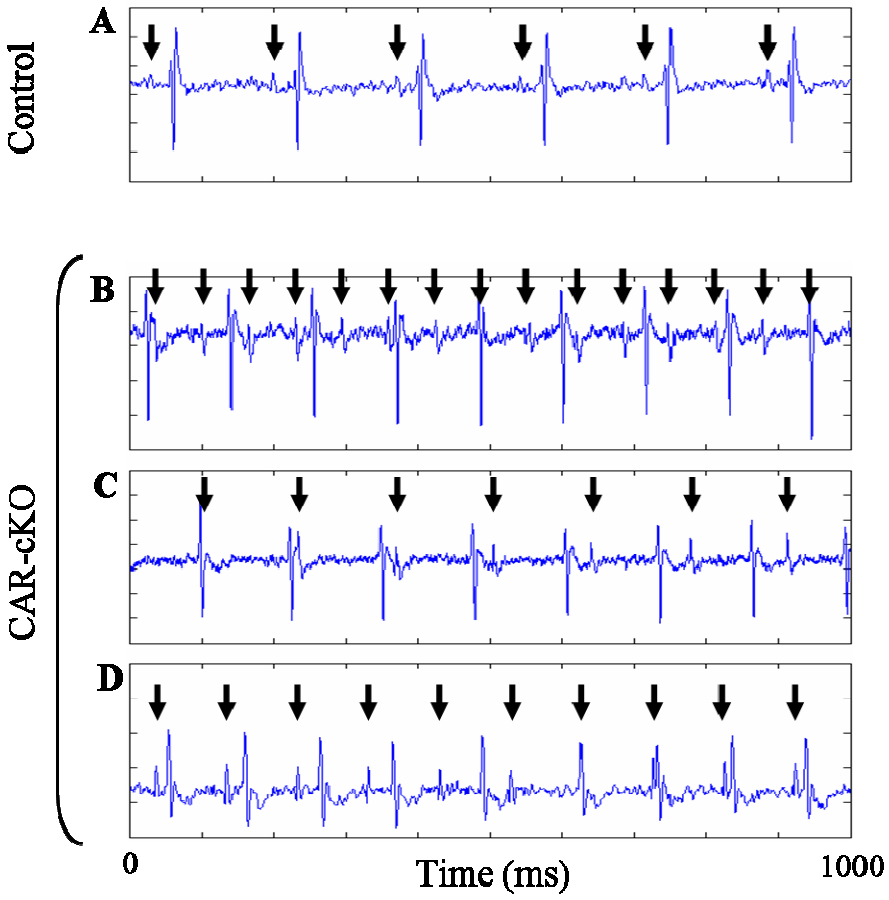

Figure 3.7: ECG recordings of the isolated heart prior to dye loading. (A) Control hearts demonstrated steady rhythm with regular P-waves (denoting atrial depolarization, marked with arrows) and a consistent PQ interval. (B-D) CAR-cKO hearts display AV node dysfunction. PP interval was consistent in a single recording, indicating normal sinus function, but varied greatly from heart to heart. Some hearts demonstrated regular RR intervals, but a complete AV dissociation, with PP interval shorter (B) or longer (C) than the than the RR interval. Others displayed inconsistent RR intervals, which might indicate some AV conduction with a milder degree of block (D).

(Figure 3.8). In the atria, the site of earliest activation is near the sinoatrial (SA) node at the posterior right atrium, indicating that the SA node is serving as the autorhythmic atrial pacemaker (Figure 3.8A). Activation maps of the anterior surface of the ventricles displayed breakthrough sites at both the left and right ventricles and short ventricular activation times (Figure 3.8B). This indicates that ventricular impulse propagation originates from somewhere in the specialized conduction system and propagates to the epicardium through the functional myocardium. There was no difference between control and CAR-cKO hearts in epicardial activation time of the anterior atria (control, 6.3 ± 1.1 ms; CAR-cKO, 7.7 ± 1.7 ms; P = n.s.; mean ± S.E.), posterior atria (control, 7.3 ± 2.1 ms; CAR-cKO, 8.6 ± 2.5 ms; P = n.s.), and the anterior ventricular surface (control, 2.7 ± 0.2 ms; CAR-cKO, 3.0 ± 0.3 ms; P = n.s.) (Figure 3.9A). To accurately compare activation times, it would be ideal to maintain a constant cycle length from heart to heart because conduction velocity is dependent on cycle length due to fast sodium channel kinetics. However, it was impossible to pace atrially to assess ventricular epicardial activation time due to the AV node dysfunction.

Conduction Velocity and Action Potential Morphology

To observe myocardial conduction velocity, the hearts were paced epicardially from the left ventricular midwall and apparent conduction velocity was measured in the directions fastest and slowest conduction, CVmax and CVmin respectively. There was no difference in apparent conduction velocity in the CAR-cKO hearts compared with control hearts (CVmin: control, 290 ± 20 mm/s vs. CAR-cKO, 301 ± 20 mm/s; CVmax: control, 637 ± 33 mm/s vs. CAR-cKO, 603 ± 56 mm/s) (Figure 3.9B). This indicates

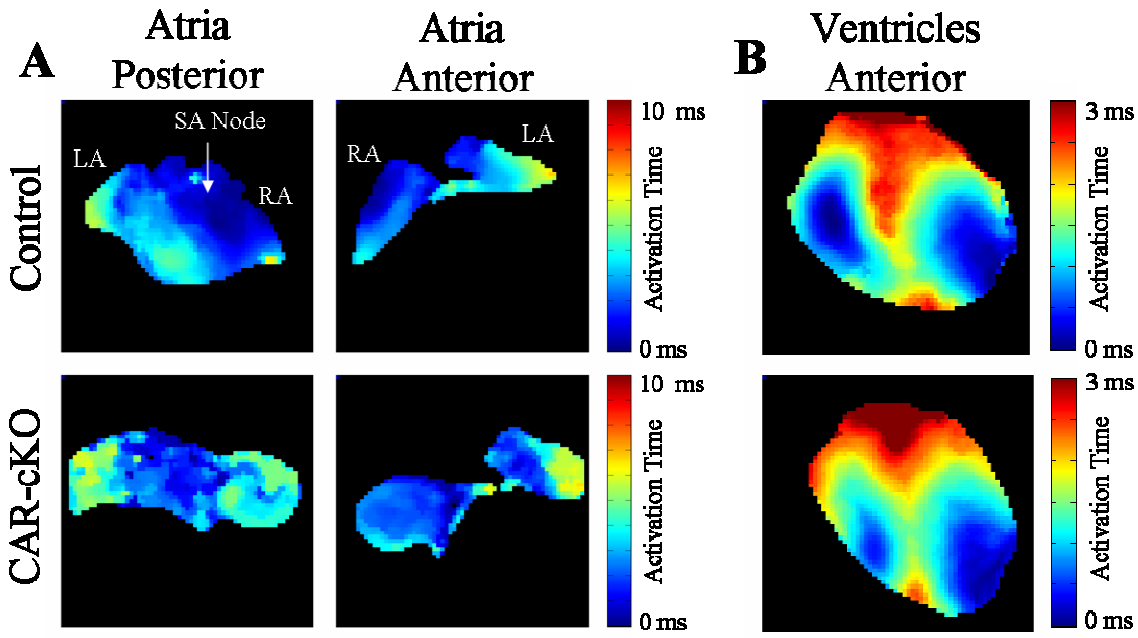

Figure 3.8: Atrial (A) and ventricular (B) activation patterns during intrinsic rhythm. CAR-cKO hearts display normal activation patterns on the atrial and ventricular epicardial surfaces. In the atria (A) earliest activation occurs near the SA node and propagates to the rest of the atrial myocardium. In the ventricles (B) there are clear breakthrough (earliest epicardial activation) sites towards the apex of the left and right ventricles. These patterns indicate that the SA node is the source of automaticity in the ventricles and, despite AV conduction dysfunction in the CAR-cKO hearts, impulse propagation in the ventricles originates in the specialized conduction system and propagates through the functional myocardium.

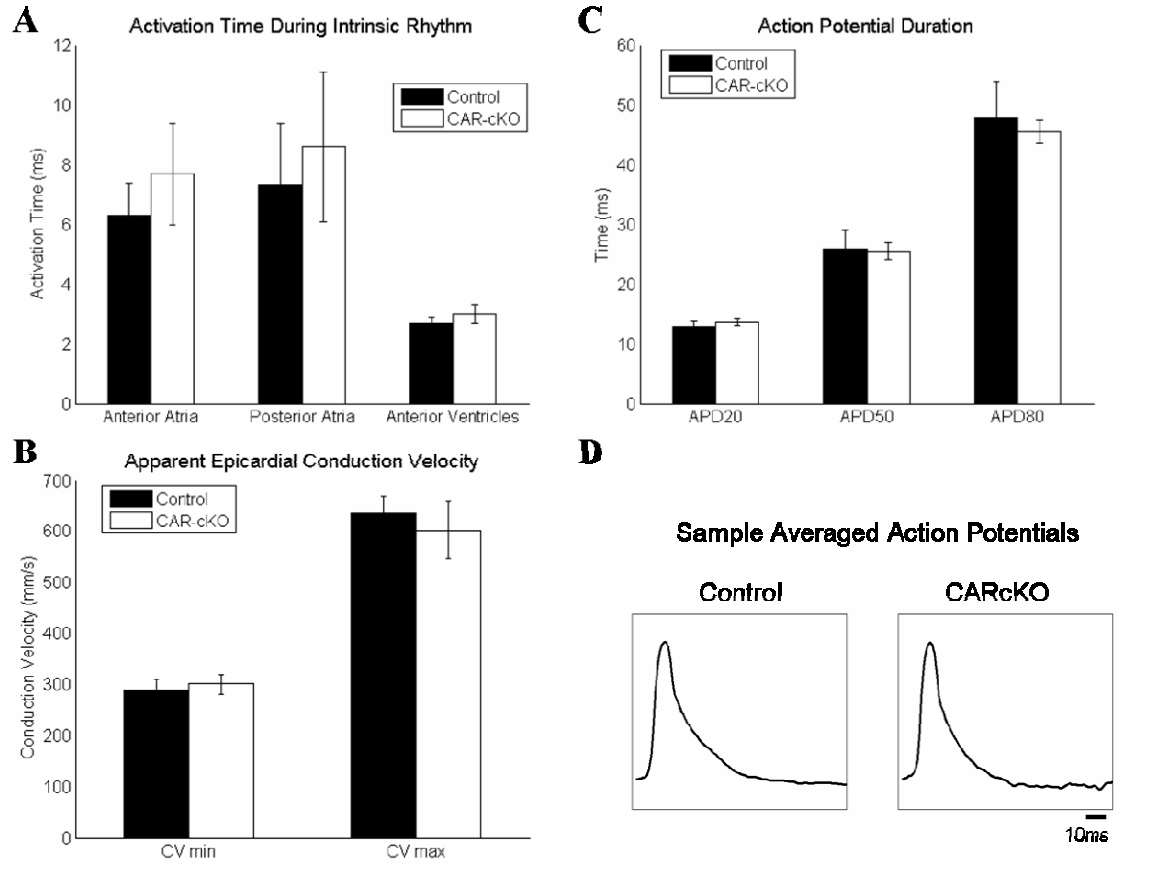

Figure 3.9: (A) Atrial and ventricular epicardial activation times are no different in CAR-cKO hearts compared with control hearts during intrinsic rhythm. (B) During ventricular pacing, there is no difference in apparent conduction velocity of myocardial action potential propagation. (C, D) At a constant cycle length of 150 ms, there was no difference in action potential morphology. APD at the 20%, 50%, and 80% levels of repolarization (C). (D) Sample action potentials recorded from a CAR-cKO and control heart.

that loss of CAR does not affect conduction velocity through the left ventricular myocardium. Action potential was also recorded during ventricular pacing and no difference was observed in action potential morphology and duration (Figure 3.9C and 3.9D).

Discussion

Coxsackievirus and adenovirus receptor (CAR) is a transmembrane protein which plays an important role in cardiac development. Global knockout of CAR results in embryonic death at E11.5.[100-102, 105] These mice display disorganized myofibrils and hyperplasia of the left ventricular myocardium.[101, 102] In the adult myocardium, CAR is still highly expressed and localized to the intercalated discs, but the physiologic role of CAR in the adult myocardium is not fully understood. It has been shown that the extracellular domains of CAR homodimerize,[9] and CAR co-localizes with ZO-1 at cell-cell junctions and regulate cell adhesion.[104] The cardiac-specific CAR knockout model (CAR-cKO) was studied to investigate the role of CAR in intercalated disc structure and its importance in maintaining efficient action potential propagation.

CAR-cKO mice display severe defects in atrioventricular (AV) node conduction as assessed by ECG *in vivo* and in the isolated heart preparation. Despite rhythm disturbances and lack of coordination in ventricular and atrial contraction, activation sequence and timing are no different in the ventricles or atria of the CAR-cKO hearts than in control hearts. This implies that atrial rhythm is still coordinated by and originates at the SA node, and ventricular impulse propagation is conducted through the

specialized conduction system. This corresponds with the absence of any difference in QRS complex observed in *in vivo* ECG recordings. Atrial rhythm was observed to be both faster and slower than ventricular rhythm in hearts displaying complete AV dissociation. The RR interval in isolated CAR-cKO hearts was observed to be shorter than in control hearts, as observed *in vivo*.[105] A similar AV node dysfunction was also observed in an inducible cardiac-specific CAR knockout model.[106] In this model, tamoxifen injection induced knockout of CAR in the adult heart and resulted in progressive prolongation of the PR interval, ultimately resulting in complete AV block. Investigation of AV node function was also observed in global CAR knockout embryos using Doppler analysis of mitral and aortic blood flow at E10.5.[105] This analysis revealed a prolonged PR interval in CAR-cKO mice compared with wild-type and heterozygous littermates.

Due to the observed AV node dysfunction, CAR localization in the AV node, and the effect of CAR ablation on AV node structure and protein localization was assessed.[105] CAR was localized at the intercalated discs of the AV nodal cells in wild-type hearts,[102, 105] but CAR-cKO hearts displayed no difference in AV node structure.[105] Connexins- 45, 30.2, and 40 are the predominant connexin isoforms found in the AV node. It was found that CAR forms a complex with connexin-45 and CAR-cKO hearts contained lower levels of connexin-45 and loss of localization to AV node ICDs.[105] This loss of connexin-45 might account for the disruption of conduction through the AV node. A similar loss of connexin-45 was observed in the inducible cardiac-specific CAR knockout.[102]

In the ventricular myocardium, CAR-cKO hearts displayed a slight disruption of the intercalated disc associated with small areas of increased space between the cells at the adherens junctions and disorganized myofilament attachment.[105] However, there was no difference of connexin-43 expression and localization to the intercalated discs. Therefore, it is not necessarily surprising that there was no delay in impulse propagation through the ventricular myocardium. Cardiac specific knockout of other intercalated disc junctional proteins, such as N-cadherin[28], result in more severe ICD disruption and significant conduction slowing through the myocardium.

In conclusion, it has been shown that cardiac-specific loss of CAR results in severe AV node dysfunction. There is no difference in QRS duration or ventricular activation sequence, indicating a junctional escape rhythm that is independent of atrial rhythm. Loss of CAR lowers connexin-45 expression, which may account for the AV block observed, but no change in connexin-43 localization or myocardial conduction velocity. CAR plays an important role maintaining ICD structure and protein localization in the AV node and is required for normal AV conduction.

ENH Knockout Model

Introduction

Enigma homolog protein (ENH) is a PDZ and LIM domain containing protein belonging to the Enigma subfamily, along with cypher (ZASP in humans) and enigma.[107] ENH is highly expressed in cardiac muscle and co-localized with α-actinin at the Z lines.[108] The physiological role of ENH is not fully understood, but it

is thought to act as an anchoring protein in complexes containing kinases and their target proteins. In neurons, ENH binds to both protein kinase C (PKC) and its substrate, N-type calcium channel, and the presence of ENH increases PKC modulation of channel kinetics.[109] Similarly, ENH forms a macromolecular complex binding with protein kinase D1 (PKD1) and its substrate, L-type voltage-gated calcium channel, in cardiomyocytes, and is required for PKD1 modulation of the calcium channel kinetics.[110] Additionally, ENH sequesters the transcription factor Id2 to the cytoplasm, reducing Id2 function in the nucleus.[111] Id2 is expressed in the cardiac conduction system and is involved in a signaling pathway with Tbx5 and Nkx2-5 required for conduction system development, structure, and function.[112]

Cypher, a co-member of the enigma subfamily, is highly homologous to ENH and is also localized at the Z lines in cardiomyocytes. Several studies have been conducted to investigate the role of cypher in cardiac development, structure, and function. Global knockout of cypher results in a severe congenital cardiomyopathy with disorganized Z lines and death soon after birth.[17] Cardiac-specific knockout of cypher in the developing and adult mouse results in the development of a severe dilated cardiomyopathy, associated with disrupted cardiomyocyte ultrastructure, decreased cardiac function, and early death.[18] Clinically, mutations in ZASP (the human ortholog of cypher) were found in patients with dilated cardiomyopathy and left ventricular non-compaction.[113]

ENH Knockout Model

In order to investigate the role of ENH on cardiac structure and function, a murine model lacking ENH was created. These ENH null mice (ENH KO) were viable and did not display an obvious pathological phenotype. Further investigation revealed the development of a mild dilated cardiomyopathy at 3 months in ENH KO hearts, associated with diminished hemodynamic function and disrupted Z lines. ECG recordings revealed a prolonged QS and QJ complex in the ENH KO mice compared to control littermates *in vivo*. To further investigate the effect of ENH ablation on cardiac electrophysiology, optical mapping methods were implemented to observe activation patterns and ventricular action potential propagation in the isolated heart.

Experimental Methods

Isolated Heart Preparation

Optical mapping was performed on isolated hearts from 1-month-old (n=5, WT group; n=5, ENH KO group) and 3-month-old (n=7, WT group; n=5, KO group) mice. All animal protocols were approved by the UCSD Institutional Animal Care and Use Committee. Mice were heparinized and sacrificed by cervical dislocation and the heart was rapidly excised and arrested. The aorta was cannulated and the heart was Langendorff perfused with a heated, oxygenated modified Krebs-Henseleit solution (24.9 mM $NaHCO_3$, 1.2 mM KH_2PO_4, 11.1 mM dextrose, 1.2 mM $MgSO_4$, 118 mM NaCl, and 2.5 mM $CaCl_2$). The heart was submerged in heated perfusate in an optical bath chamber, and a volume-conducted ECG was monitored and recorded throughout the experiment. The heart was paced on the left atria and left ventricular base with a

platinum, unipolar electrode at a cycle length of 150 ms and constant current (x1.5 threshold) using a digital stimulator (DS800; World Precision Instruments).

Optical Mapping

The heart was allowed to equilibrate for 15 minutes after cannulation. The voltage-sensitive dye di-4-ANEPPS (1 ml bolus, 26 μM) was injected into the perfusion line and the fluorescent probe was excited with 470 nm wavelength LED lamps. In order to record action potential propagation over the entire ventricular epicardial surface simultaneously, two high speed CMOS cameras (MiCAM Ultima-L dual camera system; SciMedia) were aligned to image the anterior and posterior epicardial surfaces. Fluorescence was collected with two custom built tandem lens setups (each with two 1x planapo objectives; Leica Microsystems), filtered with a 615 nm wavelength bandpass filter, and focused on the CMOS chip. Digital 14-bit images were recorded at 1,000 frames per second with a spatial resolution of 100 x 100 pixels over a 1 x 1 cm^2 area. No mechanical restraint or chemical intervention was applied to eliminate motion artifact.

Using custom software, activation at each pixel was identified at the maximum rate of change of fluorescence to create maps of activation over the epicardial surface. Global epicardial activation time was calculated as the total time required for anterior and posterior epicardium to activate. During ventricular pacing, apparent epicardial conduction velocity vector fields were calculated as the reciprocal gradient of the activation time fields as described by Bayly, et al.[40]

Results

Activation Time and Sequence During Atrio-Ventricular Conduction

ENH KO and control hearts displayed normal intrinsic rhythm as assessed by analysis of the volume conducted ECG. Optical mapping revealed normal activation sequence of ventricular epicardium during atrio-ventricular conduction (either during intrinsic rhythm or atrial pacing) in the ENH KO hearts compared with control hearts (Figure 3.10A). On the anterior surface, there are clear breakthrough sites on the left and right ventricular epicardia.

However, ENH KO hearts displayed significant delayed global ventricular activation times compared with control hearts during intrinsic rhythm and atrial pacing at a constant cycle length (Figure 3.10B and 3.10C). This delay was observed in hearts from mice at both one month of age (intrinsic: ENH KO, 5.75 ± 0.67 ms vs. control, 4.54 ± 0.75 ms, $P < 0.05$; atrial pacing: ENH KO, 6.29 ± 0.63 ms vs. control, 4.46 ± 0.25 ms, $P < 0.005$) and three months of age (intrinsic: ENH KO, 5.95 ± 1.16 ms vs. control, 4.09 ± 0.65 ms, $P < 0.05$; atrial pacing: ENH KO, 5.93 ± 1.18 ms vs. control, 4.08 ± 0.49 ms, $P < 0.05$). This is in agreement with a prolonged QS complex observed *in vivo*.

Myocardial Conduction Velocity During Ventricular Pacing

Action potential propagation was recorded on the anterior surface during epicardial pacing from the anterior base of the left ventricle (Figure 3.11A and 3.11B). There is no significant difference in apparent epicardial conduction velocity in ENH KO hearts compared to control hearts from one month (ENH KO, 595 ± 39 mm/s vs. control,

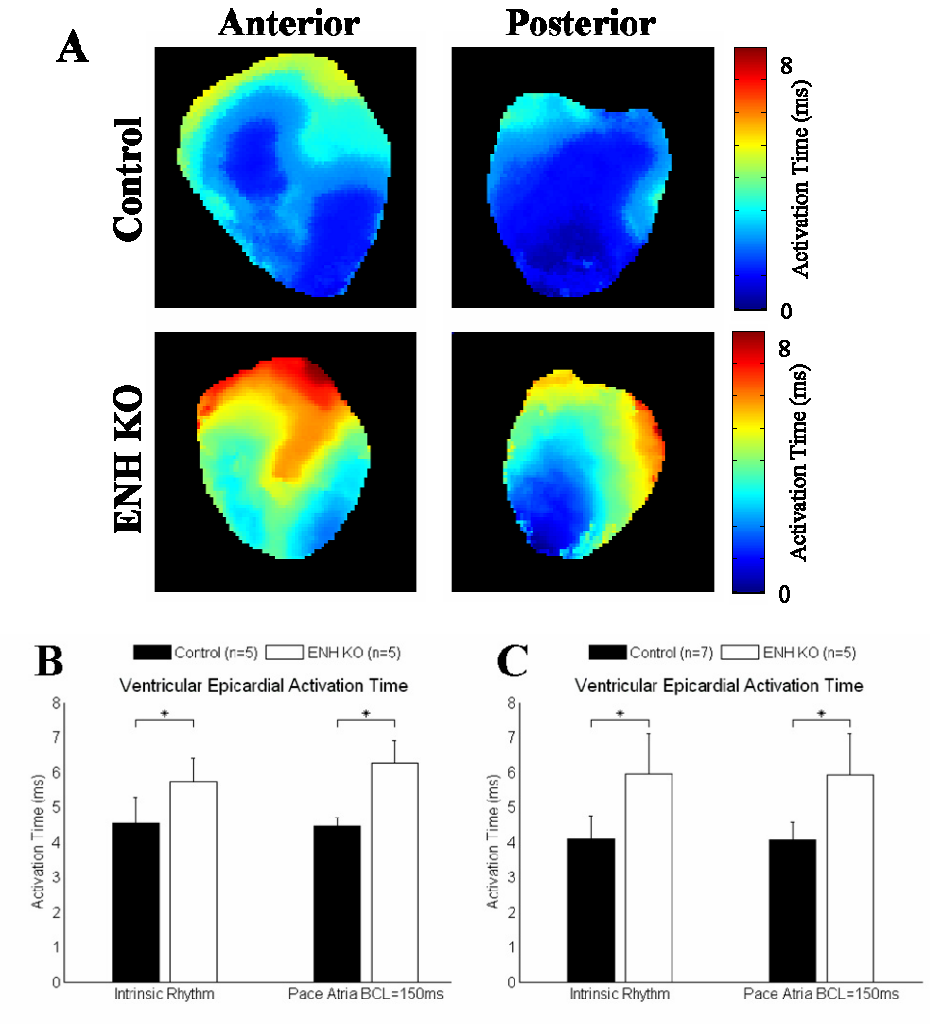

Figure 3.10: (A) Sample ventricular activation maps during atrial pacing at a cycle length of 150 ms. Hearts were from one month old mice. Epicardial activation was significantly delayed in ENH KO hearts compared to control hearts at one month of age (B) and three months of age (C). However, activation patterns on the anterior and posterior surface do not appear different (A). In the anterior view, there are two clear breakthrough sites at the left and right ventricles.

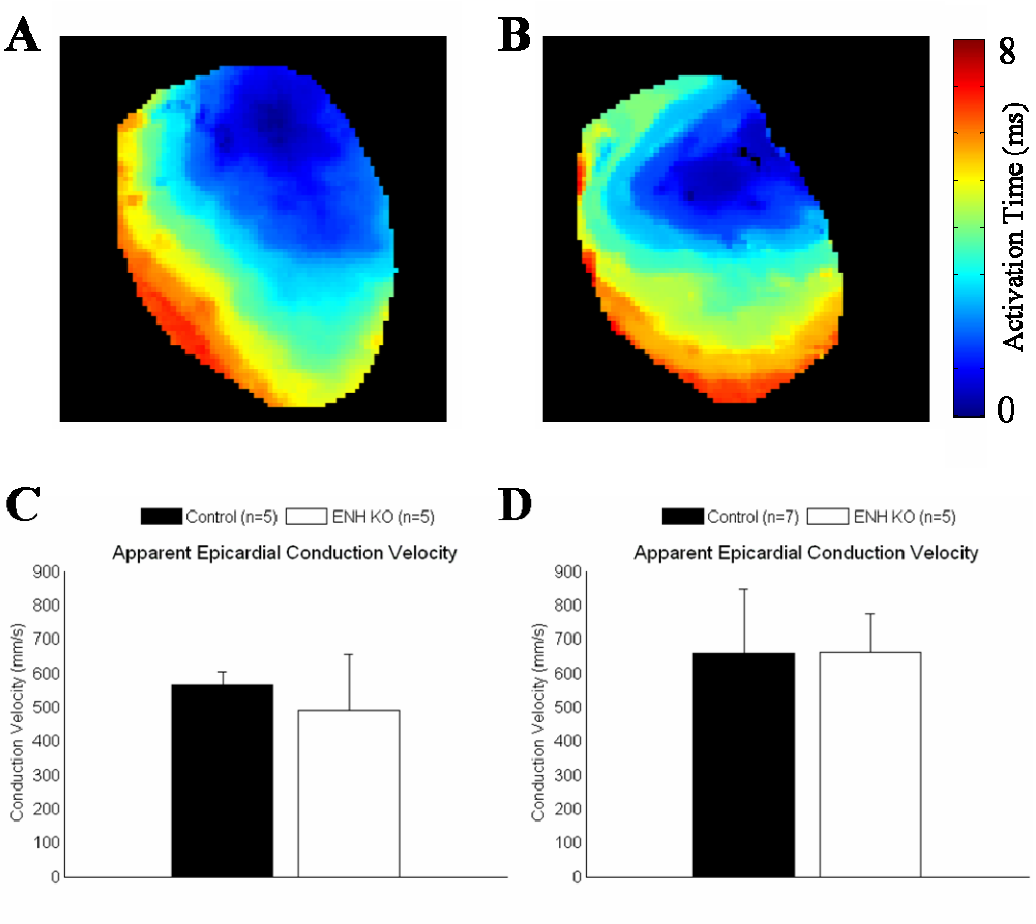

Figure 3.11: Sample activation maps of impulse propagation during ventricular pacing in control (A) and ENH KO (B) one month old hearts. There is no difference in apparent epicardial conduction velocity in ENH KO and control hearts from mice at one month (C) and three months (D) of age.

490 ± 164 mm/s) and three month (ENH KO, 661 ± 115 mm/s vs. control, 659 ± 189 mm/s) old mice. This indicates that there is no significant difference in conductivities or excitability of the ventricular myocardium. Therefore, the observed delay in activation time during atrio-ventricular conduction is likely due to slowed conduction in the conduction system rather than delayed conduction through the ventricular wall to the epicardium.

Discussion

ENH is a member of the enigma subfamily of PDZ and LIM domain containing proteins and is localized to the Z lines of cardiomyocytes in the adult heart.[108] The highly homologous protein, cypher, is required for maintenance of Z line structure and knockout of cypher in the heart resulted in development of a severe cardiomyopathy and early death.[17, 18] During the development of this heart failure, cardiac-specific knockout hearts displayed disrupted AV conduction,[18] but it is unclear if this is directly due to the ablation of cypher. Functional defects of the conduction system, including AV block, have been shown to develop in patients suffering from dilated cardiomyopathy.[114]

ENH deficient mice develop a milder cardiomyopathy at three months of age, which is also associated with disrupted Z line structure and diminished hemodynamic function. ECG analysis showed a prolonged QS and QJ interval in the ENH KO heart compared to control littermates. Optical mapping of global ventricular activation revealed a significant delay in epicardial activation during intrinsic rhythm. To ensure this wasn't due to a difference in intrinsic RR interval, activation times were also

measured during atrial pacing at a constant cycle length and still revealed delayed epicardial activation. This delay is in agreement with the ECG observation of delayed ventricular activation.

The patterns of activation sequence did not appear different in ENH KO hearts and the measured myocardial conduction velocity during ventricular pacing was not different compared to control hearts. These results indicate no gross abnormality of the conduction system, such as complete bundle branch block. However, the delayed activation is not due to delayed impulse propagation through the ventricular wall, but rather likely due to slowed conduction through the specialized conduction system. To ensure that this delayed activation is not a secondary effect of the observed cardiomyopathy, optical mapping was performed on animals at one month of age, prior to development of other pathological symptoms.

ENH has been shown to interact with the transcription factor Id2 and sequesters Id2 in the cytoplasm.[111] Id2 is a negative regulator of protein expression[115] and is highly upregulated during cardiac differentiation.[116] In the cardiac conduction system, Id2 interacts with Tbx5 and Nkx2-5 in a molecular pathway which is necessary for conduction system development.[112] Id2 deficient mice displayed a prolonged QRS duration, and an RsR' wave morphology consistent with left bundle branch block. By sequestering Id2 to the cytoplasm, ENH alters Id2 activity in the nucleus and may prevent development of the fully functional cardiac conduction system.

In conclusion, ENH ablation results in development of a mild dilated cardiomyopathy with disorganized Z lines and decreased cardiac function. ENH KO mice also display delayed ventricular depolarization prior to the development of cardiac

dysfunction. This may be a result of ENH's role in Id2 intracellular distribution and transcription repression function in the nucleus.

Conclusions

Cardiomyocytes are specialized contractile cells with a highly organized intracellular architecture. Intact cytoskeletal structures, and cell-cell and cell-matrix junctions, are required to maintain cardiac mechanical and electrical function. Disruption of the cytoskeletal structure by targeted genetic modification can provide insights into the physiological role of cytoskeletal proteins and create models of clinically observed cardiomyopathies. Here, we have used optical mapping techniques to study the cardiac electrical function of murine models with targeted ablation of four cytoskeletal proteins. Loss of these proteins results in electrophysiological alterations through different mechanisms.

Vinculin and desmoplakin are two structural proteins which are important in anchoring the cytoskeleton to the membrane at cell-cell junctions in the intercalated disc. Cardiac-specific ablation of each of these proteins resulted in disrupted ICD structure, spontaneous arrhythmias, and cardiac dysfunction. Each of these models displayed heterogeneous remodeling of the myocardium, resulting in a proarrhythmic substrate. cVclKO hearts displayed a heterogeneous redistribution of gap junctions, and cDpKO hearts exhibited heterogeneous myocyte loss and fibrofatty replacement of the myocardium. These structural modifications resulted in distributed changes in electrical properties that disrupted action potential propagation through the myocardium.

Additionally, these mice display severe ventricular arrhythmias, resulting in sudden cardiac death in young cVclKO mice.

CAR is thought to serve as a cell-cell adhesion molecule also located at the intercalated disc. CAR deficient hearts display a slight disturbance of the intercalated disc structure, but no apparent disruption of impulse conduction through the functional myocardium. CAR-cKO hearts display normal epicardial activation sequences, but exhibit severe AV conduction defects. In the AV node CAR forms a protein complex with the conduction system gap junctional protein connexin-45. Loss of CAR reduces connexin-45 expression and localization is likely responsible for the AV conduction defects observed.

ENH is important in maintaining the structure of the Z line of the cardiomyocytes, but plays a role in cellular signaling and regulation of gene expression as well. ENH knockout mice develop a mild dilated cardiomyopathy with disrupted Z lines and diminished cardiac function. However, even prior to any pathological symptoms, ENH KO hearts display delayed ventricular activation due to slowed impulse propagation through the conduction system. The role of ENH in the development of this delayed depolarization is hypothesized to be due to its role in the compartmentalization of Id2, a transcription factor that plays an important role in development of the cardiac conduction system.

These four models demonstrate varied effects of cytoskeletal defects on the electrical function of the heart. These proteins play important structural and signaling roles in the cardiomyocyte. In the development cardiac disease, disruption of the

primary cytoskeletal structures can lead to electrophysiological remodeling that can result in increased incidence of ventricular arrhythmias and diminished cardiac function.

The data and figures in the cardiac-specific vinculin knockout section of this chapter are, in part, from the following published work: A. E. Zemljic-Harpf, J. C. Miller, S. A. Henderson, A. T. Wright, A. M. Manso, L. Elsherif, N. D. Dalton, A. K. Thor, G. A. Perkins, A. D. McCulloch, and R. S. Ross, Cardiac-myocyte-specific excision of the vinculin gene disrupts cellular junctions, causing sudden death or dilated cardiomyopathy, *Mol Cell Biol*, vol. 27, pp. 7522-37, 2007. Printed with permission from the American Society of Microbiology and Copyright Clearance Center. The dissertation author was the primary researcher and author of the work presented here, and the co-authors listed in this publication directed and supervised the research that forms the basis of this chapter, or were primary researchers of material not presented here.

The data and figures from cardiac-specific CAR knockout section of this chapter are, in part, from the following published work: B. K. Lim, D. Xiong, A. Dorner, T. J. Youn, A. Yung, T. I. Liu, Y. Gu, N. D. Dalton, A. T. Wright, S. M. Evans, J. Chen, K. L. Peterson, A. D. McCulloch, T. Yajima, and K. U. Knowlton, "Coxsackievirus and adenovirus receptor (CAR) mediates atrioventricular-node function and connexin 45 localization in the murine heart," *J Clin Invest*, vol. 118, pp. 2758-70, 2008. Printed with permission from the American Society for Clinical Investigation and Copyright Clearance Center. The dissertation author was the primary researcher and author of the work presented here, and the co-authors listed in this publication directed and

supervised the research that forms the basis of this chapter, or were primary researchers of material not presented here.

Chapter 4: The Effect of Stretch and Caveolae Unfolding on Conduction Velocity

Introduction

Effect of Stretch on Cardiac Conduction

Mechanical contraction of the heart is coordinated by electrical activity through coordinated calcium ion fluxes and regulation of cytoplasmic calcium concentration, a well known and studied mechanism termed excitation contraction coupling (ECC). However, there is clear evidence of the reverse relationship, in which mechanical perturbations of the myocardium directly affect cardiac electrophysiology. Studies have linked volume overload or increased myocardial strain with triggered and reentrant ventricular arrhythmias.[30] Altered conduction velocity and refractoriness of the myocardium can promote and sustain reentry.[33]

Experimental observations on the acute effects of myocardial strain on conduction velocity have varied widely with experimental preparation, mechanical loading conditions, and measurement techniques. Early investigators measured one dimensional conduction velocity between two electrodes in myocardial strips or specialized ventricular structures during one dimensional stretch. These studies generally showed an increase in conduction velocity with stretch,[43, 44] often followed by a decrease with additional stretch.[41, 42, 45] However, some preparations

displayed a decrease[46] or no change[45, 46] of conduction velocity with stretch. Several whole heart studies revealed delayed ventricular activation with increased ventricular pressure.[47, 49]

In the volume-loaded left ventricle of isolated rabbit hearts, Reiter, *et al.* observed no change in fiber or cross-fiber conduction velocities with graded increase in ventricular load measured with an extracellular electrode array.[52] Conversely, studies in the isolated rabbit atria displayed decreased spatial conduction velocity[53, 54] as well as increased dispersion of conduction velocity, altered direction of propagation, and increased occurrence of local conduction block[54] during myocardial stretch. Using optical mapping techniques, our group has observed a 16% decrease in conduction velocity when intraventricular pressure was raised from 0 to 30 mmHg.[55, 57] Conduction velocity returned to baseline when load was removed.

Stretch induced changes in cardiac electrophysiology have traditionally been attributed to stretch activated channels (SACs). Increased mechanical load can alter resting membrane potential, which can slow conduction due to a decrease in excitability.[59] However, our group has found conduction slowing during ventricular filling was not attenuated in the presence of the SAC blockers gadolinium[57] or streptomycin.[55] Alternatively, stretch may result in changes in tissue and cell geometry, changing path of conduction or altering distributed electrical properties of the myocardium. Rosen *et al.*[45] observed that stretch caused significant membrane unfolding, decreased cell diameter, and slightly increased packing of the extracellular space. Unfolding of ‘slack’ membrane and integration of caveolae to the surface sarcolemma has also been observed in the loaded intact rabbit ventricle.[63] Recent

data indicate that increased membrane tension results in an increase in capacitance.[64] Myocardial stretch might also alter conduction through changes in intercellular coupling. It has been demonstrated that connexin hemichannel permeability is sensitive to both shear strain[65] and membrane stretch,[66] so mechanical forces at cell-cell junctions might directly affect gap junction conductance.

Mills *et al.* implemented a bidomain model analysis of the membrane potential response to a non-excitatory stimulus to investigate changes in these myocardial electrical properties during ventricular volume loading.[57] The results suggested that wall stretch resulted in a 21% increase in cross-fiber space constant, indicating reduced intercellular resistance that would increase conduction velocity, and a 56% increase in membrane capacitance, which would slow conduction. Computational simulations implementing these counteracting changes were consistent with experimental findings of an approximately 15% slowing of conduction during ventricular loading.

Development of our new tandem lens optical mapping system provides an experimental platform to conduct similar studies in a more controlled experimental preparation to investigate the cellular mechanisms responsible for these changes. In particular, this system has been implemented to observe the effect of stretch on conduction velocity in the freely beating mouse heart. Initial studies have been conducted to investigate the role of caveolae and membrane unfolding in this effect. Additionally, preliminary work has been conducted to observe the effect of stretch on conduction velocity in cardiomyocyte monolayers cultured on flexible membranes.

Caveolae in the Heart

Caveolae are small, flask-shaped invaginations of the plasma membrane (50-100 nm in diameter) that are found in most cell types in the heart.[117] These membrane microdomains are enriched in cholesterol and sphingolipids, as well as the structural proteins, caveolins.[118] Caveolae are highly organized lipid rafts that play a role in signal transduction by compartmentalizing signaling proteins, including G-proteins and G-protein coupled receptors.[119] Additionally, they are thought to be involved in cholesterol homeostasis, and the structure and function of caveolae are dependent on cholesterol levels.[120] Finally, many cardiac ion channels localize in caveolae and their kinetics may be altered directly by their surrounding lipid microenvironment, or their proximity to signaling protein complexes.[121]

The caveolin family of proteins consists of three known isoforms; caveolin-1, caveolin-2, and caveolin-3.[117] Caveolin-1 and caveolin-2 are coexpressed in most cells in the heart, including fibroblasts and endothelial cells. Caveolin-1 is required for the formation of invaginated caveolae in these cells.[122] Caveolin-2 is colocalized with caveolin-1, but is not necessary for formation of these structures.[123] Expression of caveolin-3 is specific to muscle cells, and is required for the formation of caveolae in cardiomyocytes.[124] Caveolar structure can also be altered by cholesterol depletion by chemical intervention with compounds such as methyl-beta-cyclodextrin (MβCD).[120] Additionally, mechanical intervention can alter the shape of caveolae. Kohl, et. al. showed that an increase in ventricular pressure resulted in opening of cardiomyocyte caveolae and membrane unfolding in the isolated rabbit heart.[63]

Caveolin-3 KO Mouse Model

Clinically, mutations in caveolin-3 have been associated with muscular degeneration.[125] To investigate the physiological and pathological role of caveolae in skeletal and cardiac muscle, caveolin-3 deficient murine models have been developed and studied.[124, 126, 127] These mice are viable and do not develop apparent clinical symptoms through 30 weeks of age.[126] They lack invaginated caveolae in skeletal muscle fibers and cardiomyocytes. Closer examination of skeletal muscle lacking caveolin-3 expression revealed abnormal organization of the T-tubule system and muscle degeneration.[126, 127] These mice also develop a mild but progressive cardiomyopathy after two months of age.[124] By four months, caveolin-3 deficient mice develop wall thickening, ventricular dilation, reduced fractional shortening, cardiomyocyte hypertrophy, and interstitial fibrosis.

The goal of this work is to investigate the effects of pressure loading on conduction velocity in the freely beating mouse heart and investigate the role of caveolae unfolding in conduction changes associated with load. Additionally, preliminary investigations have been conducted to also investigate changes in conduction velocity with stretch in cardiomyocyte monolayers.

Experimental Methods

Ventricular Loading of the Isolated Mouse Heart

Isolated Heart Preparation

All animal protocols were approved by the UCSD Institutional Animal Care and Use Committee. Mice were heparinized by intraperitoneal injection, sedated with isoflurane, and sacrificed by cervical dislocation. The heart was excised and the aorta rapidly cannulated and retrogradely perfused with warmed and oxygenated modified Krebs-Henseleit solution (24.9 mM $NaHCO_3$, 1.2 mM KH_2PO_4, 11.1 mM dextrose, 1.2 mM $MgSO_4$, 118 mM NaCl, 2.6 mM $CaCl_2$, 4.7 mM KCl). The heart was submerged in a heated optical bath chamber and paced on the left ventricular epicardium at twice diastolic threshold with a unipolar platinum electrode and a digital stimulator (DS8000, World Precision Instruments). A volume conducted ECG was recorded throughout the experiment.

A cannula was inserted into the left ventricle through the pulmonary vein and mitral valve and tied off with suture around the left atrium. The left ventricle was pressure loaded with warmed oxygenated perfusate through the LV cannula by raising the perfusate reservoir. LV pressure was monitored with a fluid filled pressure transducer and recorded throughout the experiment.

Optical Mapping

The voltage-sensitive dye di-4-ANEPPS (1mM bolus, 25 μM) was injected into the perfusion line to stain the myocardium. The heart is aligned to image the LV

epicardium. The ventricular epicardium was illuminated by a 470 nm wavelength LED cluster (LEDtronics). Fluorescence was collected with a custom built tandem lens optical setup (three 1x planapo lenses, Leica) and recorded at two wavelengths. The objective lens collected and collimated fluorescence emission and the light was split with a dichroic mirror at 600 nm. Fluorescence was filtered at 615 nm and 540 nm, and focused onto the sensors of two CMOS cameras (MiCAM Ultima, SciMedia) aligned to record the same field of view. Digital 14-bit images were recorded at 1,000 frames per second with a spatial resolution of 100 x 100 pixels over a 1 x 1 cm^2 area. No mechanical restraint or chemical intervention was applied to eliminate motion artifact.

Experimental Protocol

Once the heart was cannulated, it was perfused and allowed to equilibrate for 15 minutes. End diastolic pressure (EDP) of the LV was regulated by adjusting the height of the reservoir of perfusate attached to the LV cannula. The unloaded state was defined at an EDP of 0 mmHg, and EDP was raised to 30 mmHg in the loaded state. The myocardium was mechanically preconditioned prior to image acquisition. The heart was paced on the mid LV epicardium at a cycle length of 150 ms. Data was acquired in the unloaded state, in the loaded state, and again in the unloaded state. A 1 minute stabilization period was permitted after each load state change prior to data acquisition.

Data Analysis

Images were imported into Matlab and processed using custom written software. A combination of Lucas-Kanade optical flow motion tracking and ratiometry were implemented to minimize motion artifact. The signal was cleaned with a phase shift spatial filter and median temporal filter,[74] and activation was defined at the maximum derivative of the signal during depolarization. This resulted in spatial activation maps for every action potential recorded, and conduction velocity vector fields were calculated from local gradients of activation time.[40] Conduction velocities measured in the loaded state were normalized with respect to the unloaded state.

Stretch of Cardiomyocyte Monolayer

Cardiomyocytes were isolated from 1 to 2 day old Sprague-Dawley rats and seeded on a fibronectin coated grooved silicone membrane mounted in an anisotropic cell stretcher.[128] On this membrane, cells aligned along the grooves to create a longitudinal and transverse orientation of the culture. Cells were cultured for 5 to 6 days with media changes every 2 to 3 days.

Cultures were stained with 30 μM of the potentiometric dye di-8-ANEPPS mixed with 20% Pluronic F-127 in Tyrode's solution. The culture was gently shaken for 15 minutes, and then maintained at room temperature for an additional 25 minutes. The staining solution was removed and replaced by dye-free medium before imaging the cardiomyocyte monolayer. The camera was configured in a vertical position on a focus drive to image the culture from above. Two 1x lenses were implemented to image a field of view of 10 mm x 10 mm. The cells were excited with a high intensity

LED (Luxeon) and fluorescence was collected with the tandem lens optical system, filtered at >610 nm, and focused onto the sensor of the CMOS camera recording 500 frames per second.

The cells were paced with a bipolar line electrode at a constant voltage 1.5x threshold. Action potential propagation was recorded in both the transverse and longitudinal directions through the unstretched monolayer. The cells were stretched, and action potential conduction was measured again. Signals were analyzed as described above to measure conduction velocity in the unstretched and stretched culture.

Results

The Effect of Increased Load on Conduction Velocity in Mouse Heart

To study the effect of increased pressure load on apparent epicardial conduction velocity, optical mapping experiments were performed on the hearts of 6 control, C57/Black mice. Conduction velocity was measured in the direction of fastest (CV_{max}) and slowest (CV_{min}) conduction in the unloaded and loaded states. Mean initial conduction velocity magnitudes were a CV_{max} of 594.7 ± 27.0 mm/s, and a CV_{min} of 329.7 ± 19.0 mm/s. Conduction velocities in the loaded and final unloaded states were normalized with respect to the initial unloaded values of each heart. When left ventricular end diastolic pressure was increased to 30 mmHg, CV_{max} and CV_{min} decreased by 11.7 ± 4.4% and 11.7 ± 4.2%, respectively ($P < 0.05$ for both, Figure 5.1). After EDP was returned to 0 mmHg, CV_{max} and CV_{min} returned to 101.0 ± 1.3% and

100.6 ± 1.3% of initial values. This conduction slowing is similar to that observed in the volume loaded rabbit ventricle.[55]

The Role of Caveolae in Load Induced Conduction Slowing

To investigate the role of caveolae in load induced conduction slowing, preliminary experiments were performed on two experimental models lacking the invaginated lipid rafts: (1) Methyl-β-cyclodextrin (MβCD) depletes cholesterol from the plasma membrane and opens caveolae (n=2); (2) Caveolin-3 deficient hearts (Cav3KO) do not form invaginated caveolae in cardiomyocytes (n=3).

Neither intervention with MβCD nor Cav3 deficiency appeared to alter baseline conduction velocities compared to control hearts (CV_{max} = 605.9 ± 12.4 mm/s and CV_{min} = 340.3 ± 0.5 mm/s in MβCD treated hearts; CV_{max} = 579.7 ± 8.0 mm/s and CV_{min} = 377.8 ± 20.9 mm/s in Cav3KO hearts). When loaded, CV_{max} and CV_{min} only decreased by 2.6 ± 6.3% and 5.2 ± 1.1%, respectfully, in the MβCD treated hearts. In the Cav3KO hearts, CV_{max} decreased by 6.5 ± 6.9%, and CV_{min} decreased by 0.8 ± 5.9% when EDP was raised to 30 mmHg (Figure 5.1C and 5.1D).

The Effect of Stretch on Conduction Velocity in an Anisotropic Monolayer

To investigate the effect of stretch on conduction velocity in the anisotropic cardiomyocyte monolayer, preliminary studies were performed in monolayers cultured on flexible membranes mounted in a biaxal stretching device. Cultured cardiomyoctes aligned along grooves in the membranes displayed clearly anisotropic propagation. In the unstretched state, conduction velocity was 108 mm/s in the longitudinal direction

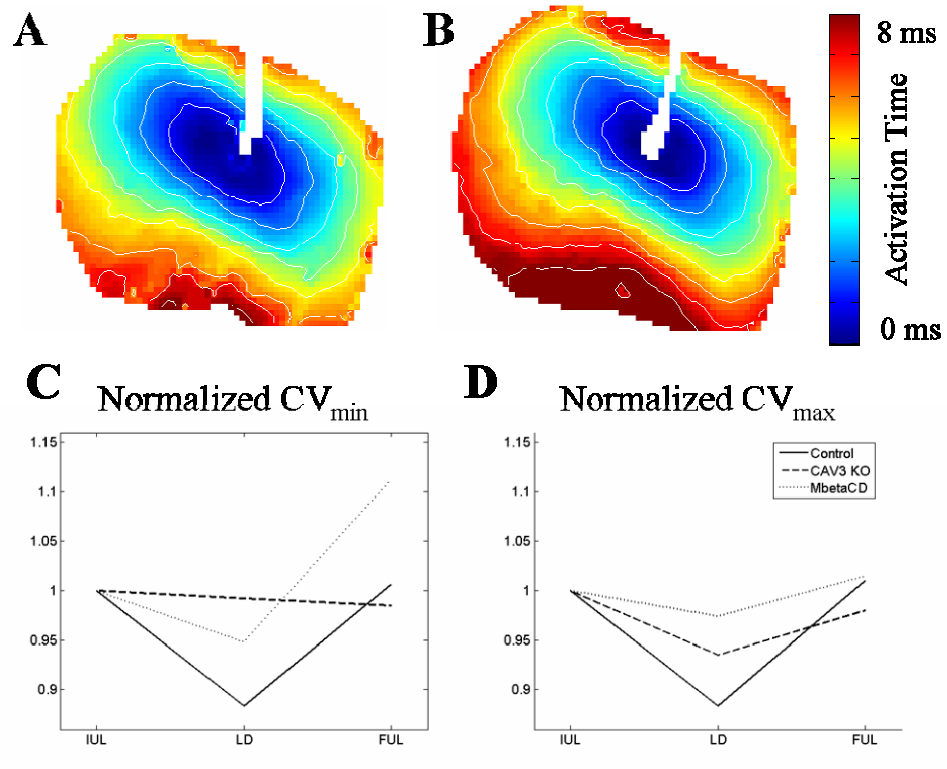

Figure 4.1: Conduction velocity decreases with ventricular loading. Sample activation maps in the unloaded (A) and loaded (B) states showed delayed activation in the loaded ventricle. Increased ventricular pressure resulted in a 12% decrease in conduction velocity in the direction of slowest (C) and fastest (D) conduction in the control heart. Caveolae deficient hearts displayed an attenuated decrease in CV with load.

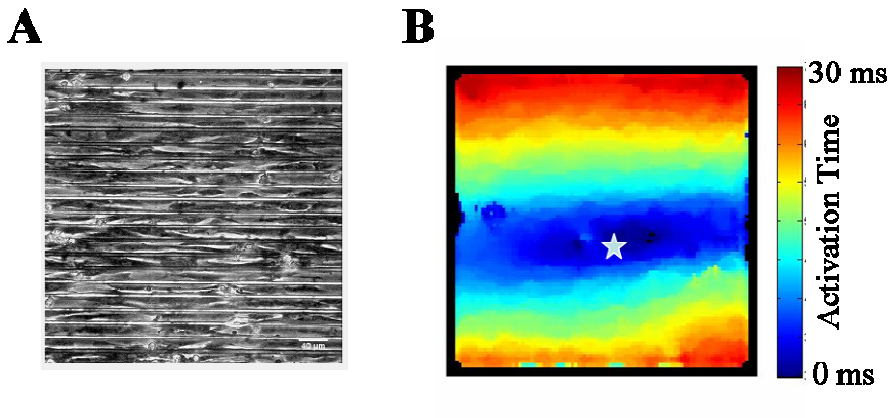

Figure 4.2: Anisotropic cardiomyocyte cultures display anisotropic conduction. (A) Cardiomyocytes cultured on grooved silicone membranes align along the grooves in an anisotropic manner. (B) Activation map of action potential propagation during point pacing (at white star) reveals anisotropic conduction. Propagation is much faster in the longitudinal direction than in the transverse direction.

and 46 mm/s in the transverse direction in cultures paced with bipolar line electrodes. Stretch resulted in a 21% decrease in transverse conduction velocity, but longitudinal conduction velocity was observed to increase by 40%.

Discussion

Mechanoelectric coupling is a physiologic cardiac phenomenon in which mechanical perturbation of the myocardium results in altered electrophysiology. Several studies investigating the effect of stretch on myocardial conduction velocity have revealed varying results. Our group has previously observed conduction slowing in the isolated rabbit heart during ventricular volume loading.[55, 57, 75] To further investigate the underlying mechanisms responsible for stretch-induced changes in conduction velocity, the freely beating murine heart and anisotropic cardiomyocyte monolayers present two new experimental platforms.

The optical mapping system described in Chapter 2 is able to record action potential propagation in the freely beating heart and measure the effects of increased pressure load on ventricular conduction velocity. A 12% reduction in conduction velocity was observed with a 30 mmHg increase in left ventricular pressure. These results are similar to those observed in the isolated rabbit heart,[55] in which a fluid-filled balloon was inserted into the ventricle to apply load to the ventricular myocardium. This may alter stress distributions on the endocardial surface of the ventricle that do not replicate a physiological increase in end diastolic pressure. In the mouse heart, pressure loading with a cannula in the ventricle results in a more

physiological load distribution. Additionally, recordings in the rabbit heart were taken during perfusion of the mechanoelectric uncoupler 2,3-butanedione monoxime (BDM). These uncouplers have been shown to alter calcium handling[129] and ion channel kinetics.[130, 131] Ratiometry and motion correction allow for imaging of the feely beating heart.

Stretch-activated channels are widely considered the primary cause of stretch-induced changes in electrical activity. However, conduction slowing was not attenuated in the presence of stretch-activated channel blockers in the rabbit heart.[55, 57, 75] Mills, *et al.* found that the conduction slowing was associated with an increase in membrane capacitance and myocardial space constant. The underlying cellular mechanisms of these changes are unclear. The evolution of genetic engineering has resulted in thousands of genetically modified mouse models that have become pivotal in cardiac research.[132] Optical mapping of the isolated murine heart provides a powerful tool to investigate the role of individual proteins in electrophysiological function. To investigate the role of caveolae unfolding during increased load, a genetically modified mouse model lacking caveolae in the cardiomyocytes can be studied. Preliminary results in this chapter indicate that lack of caveolar structure might prevent conduction slowing associated with increased load.

Cardiomyocyte monolayers also represent a useful model in many aspects of cardiac research, including hypertrophic signaling pathways,[128] arrhythmia dynamics,[133] and mechanoelectric coupling.[58] Cellular alignment and distribution can be controlled using micropatterning or microfabrication techniques. These cultures can also be more purely composed of cardiomyocytes, limiting observed phenomenon

to these functional myocytes. Genetic transfection can be used to alter gene expression in these cultures as well. The ability to measure action potential propagation in a stretched cardiomyocyte monolayer provides another useful model to investigate underlying cellular mechanisms.

The text and figures of this chapter, in part, will be submitted for publication. The dissertation author was the primary researcher and author of the work presented here, and any co-authors of this publication directed and supervised the research that forms the basis for this chapter.

Chapter 5: Conclusions

Efficient cardiac function is highly dependent on rapid and coordinated cardiac conduction. Clinically, ventricular arrhythmias are associated with cardiomyopathies exhibiting disruption of cardiomyocyte cytoarchitecture or irregular myocardial mechanics. Advances in experimental techniques have led to novel research tools to analyze alterations in cardiac conduction in various cardiac preparations. Additionally, advances in genetic engineering have provided animal models of heart disease, and targeted gene manipulation can give insights into the functional role of proteins in the heart. The goal of this dissertation was to implement novel electrophysiological experimental techniques to investigate the effects of cytoskeletal disruption and altered mechanical load on ventricular conduction.

Optical mapping is a non-contact method used to optically recording action potential propagation through a network of electrically active cells. In cardiac research, optical mapping has been used from the subcellular scale to *in vivo* whole organ imaging. These techniques have been implemented in analysis of arrhythmia dynamics, intercellular coupling, and for electrophysiological phenotyping of murine models of arrhythmic cardiomyopathies. In this work, a new optical mapping system was

designed and constructed to record electrical activity in several experimental models, including the freely beating isolated heart and in cardiomyocyte monolayers.

Cardiomyocytes have a highly organized cytoskeletal architecture designed to produce maximal contractile force and transmit these forces to their environment. Protein complexes at cell-cell and cell-matrix junctions secure the contractile elements to the sarcolemmal and are the mechanical link transmitting forces between cells. Mutations in many cytoskeletal proteins have been associated with disrupted cardiomyocyte structure and the development of cardiomyopathies, clinically. Targeted genetic ablation can disrupt these structures in mouse models. In this work, the effect of targeted ablation of four such proteins revealed development of altered cardiac conduction. Each model displayed a different form of irregular conduction, with different apparent mechanisms responsible for these changes. Vinculin and desmoplakin are structural proteins localized at the intercalated discs to maintain cell-cell junctions. Knockout models lacking these proteins in the heart resulted in disruption of ICD structure and heterogeneous electrical remodeling of the ventricular myocardium that lead to an increased incidence of arrhythmias. CAR is also located at the ICD in adult myocardium to serve as a junctional linker. Knockout of CAR did not alter conduction through the functional myocardium, but it resulted in decrease expression of connexins in the specialized conduction system, leading to severe AV node dysfunction. Alternatively, ablation of the structural protein ENH appears to slow conduction through the His bundles due to its role sequestering the transcription factor Id2. Cardiomyocyte skeletal proteins are pivotal in maintaining mechanical stability of

the heart, but also directly affect cardiac conduction through a number of different cellular mechanisms.

Arrhythmias have been associated with increases in chamber pressure and altered myocardial wall mechanics. Experimentally, stretch has been shown to alter conduction through myocardial samples. In this work, optical mapping techniques were developed to investigate the effect of stretch on conduction velocity in two new cardiac preparations; the freely beating isolated mouse heart and cardiomyocyte cultures. In the isolated mouse heart, ventricular conduction slowing was observed with increased ventricular pressure, similar to results observed in the volume loaded rabbit ventricle. This model can be used to investigate the role of individual proteins with available genetically modified murine models. Preliminary results show that caveolae unfolding may play a role in the alterations in effective membrane capacitance responsible for the observed conduction slowing. Optical mapping techniques used in conjunction with cell stretchers provide an *in vitro* model to study mechanoelectric effects on conduction in a well controlled system. These experimental models provide exciting new platforms to investigate the underlying cellular mechanisms responsible for stretch-induced changes in cardiac conduction.

References

[1] L. Cox, L. Umans, F. Cornelis, D. Huylebroeck, and A. Zwijsen, "A broken heart: a stretch too far: an overview of mouse models with mutations in stretch-sensor components," *Int J Cardiol*, vol. 131, pp. 33-44, 2008.

[2] M. E. Janssen, E. Kim, H. Liu, L. M. Fujimoto, A. Bobkov, N. Volkmann, and D. Hanein, "Three-dimensional structure of vinculin bound to actin filaments," *Mol Cell*, vol. 21, pp. 271-81, 2006.

[3] W. W. Sharp, D. G. Simpson, T. K. Borg, A. M. Samarel, and L. Terracio, "Mechanical forces regulate focal adhesion and costamere assembly in cardiac myocytes," *Am J Physiol*, vol. 273, pp. H546-56, 1997.

[4] E. E. Weiss, M. Kroemker, A. H. Rudiger, B. M. Jockusch, and M. Rudiger, "Vinculin is part of the cadherin-catenin junctional complex: complex formation between alpha-catenin and vinculin," *J Cell Biol*, vol. 141, pp. 755-64, 1998.

[5] M. M. Kreuzberg, K. Willecke, and F. F. Bukauskas, "Connexin-mediated cardiac impulse propagation: connexin 30.2 slows atrioventricular conduction in mouse heart," *Trends Cardiovasc Med*, vol. 16, pp. 266-72, 2006.

[6] S. Dhein, *Cardiac Gap Junctions*. New York: Karger, 1998.

[7] T. Kashimura, M. Kodama, Y. Hotta, J. Hosoya, K. Yoshida, T. Ozawa, R. Watanabe, Y. Okura, K. Kato, H. Hanawa, R. Kuwano, and Y. Aizawa, "Spatiotemporal changes of coxsackievirus and adenovirus receptor in rat hearts during postnatal development and in cultured cardiomyocytes of neonatal rat," *Virchows Arch*, vol. 444, pp. 283-92, 2004.

[8] J. M. Bergelson, J. A. Cunningham, G. Droguett, E. A. Kurt-Jones, A. Krithivas, J. S. Hong, M. S. Horwitz, R. L. Crowell, and R. W. Finberg, "Isolation of a common receptor for Coxsackie B viruses and adenoviruses 2 and 5," *Science*, vol. 275, pp. 1320-3, 1997.

[9] M. J. van Raaij, E. Chouin, H. van der Zandt, J. M. Bergelson, and S. Cusack, "Dimeric structure of the coxsackievirus and adenovirus receptor D1 domain at 1.7 A resolution," *Structure*, vol. 8, pp. 1147-55, 2000.

[10] L. E. Stephens, A. E. Sutherland, I. V. Klimanskaya, A. Andrieux, J. Meneses, R. A. Pedersen, and C. H. Damsky, "Deletion of beta 1 integrins in mice results in inner cell mass failure and peri-implantation lethality," *Genes Dev*, vol. 9, pp. 1883-95, 1995.

[11] W. Xu, H. Baribault, and E. D. Adamson, "Vinculin knockout results in heart and brain defects during embryonic development," *Development*, vol. 125, pp. 327-37, 1998.

[12] S. J. Monkley, X. H. Zhou, S. J. Kinston, S. M. Giblett, L. Hemmings, H. Priddle, J. E. Brown, C. A. Pritchard, D. R. Critchley, and R. Fassler, "Disruption of the talin gene arrests mouse development at the gastrulation stage," *Dev Dyn*, vol. 219, pp. 560-74, 2000.

[13] A. E. Zemljic-Harpf, S. Ponrartana, R. T. Avalos, M. C. Jordan, K. P. Roos, N. D. Dalton, V. Q. Phan, E. D. Adamson, and R. S. Ross, "Heterozygous inactivation of the vinculin gene predisposes to stress-induced cardiomyopathy," *Am J Pathol*, vol. 165, pp. 1033-44, 2004.

[14] S. Y. Shai, A. E. Harpf, C. J. Babbitt, M. C. Jordan, M. C. Fishbein, J. Chen, M. Omura, T. A. Leil, K. D. Becker, M. Jiang, D. J. Smith, S. R. Cherry, J. C. Loftus, and R. S. Ross, "Cardiac myocyte-specific excision of the beta1 integrin gene results in myocardial fibrosis and cardiac failure," *Circ Res*, vol. 90, pp. 458-64, 2002.

[15] M. Gotthardt, R. E. Hammer, N. Hubner, J. Monti, C. C. Witt, M. McNabb, J. A. Richardson, H. Granzier, S. Labeit, and J. Herz, "Conditional expression of mutant M-line titins results in cardiomyopathy with altered sarcomere structure," *J Biol Chem*, vol. 278, pp. 6059-65, 2003.

[16] S. Arber, J. J. Hunter, J. Ross, Jr., M. Hongo, G. Sansig, J. Borg, J. C. Perriard, K. R. Chien, and P. Caroni, "MLP-deficient mice exhibit a disruption of cardiac cytoarchitectural organization, dilated cardiomyopathy, and heart failure," *Cell*, vol. 88, pp. 393-403, 1997.

[17] Q. Zhou, P. H. Chu, C. Huang, C. F. Cheng, M. E. Martone, G. Knoll, G. D. Shelton, S. Evans, and J. Chen, "Ablation of Cypher, a PDZ-LIM domain Z-line protein, causes a severe form of congenital myopathy," *J Cell Biol*, vol. 155, pp. 605-12, 2001.

[18] M. Zheng, H. Cheng, X. Li, J. Zhang, L. Cui, K. Ouyang, L. Han, T. Zhao, Y. Gu, N. D. Dalton, M. L. Bang, K. L. Peterson, and J. Chen, "Cardiac-specific ablation of Cypher leads to a severe form of dilated cardiomyopathy with premature death," *Hum Mol Genet*, vol. 18, pp. 701-13, 2009.

[19] A. G. Reaume, P. A. de Sousa, S. Kulkarni, B. L. Langille, D. Zhu, T. C. Davies, S. C. Juneja, G. M. Kidder, and J. Rossant, "Cardiac malformation in neonatal mice lacking connexin43," *Science*, vol. 267, pp. 1831-4, 1995.

[20] P. A. Guerrero, R. B. Schuessler, L. M. Davis, E. C. Beyer, C. M. Johnson, K. A. Yamada, and J. E. Saffitz, "Slow ventricular conduction in mice heterozygous for a connexin43 null mutation," *J Clin Invest*, vol. 99, pp. 1991-8, 1997.

[21] G. E. Morley, D. Vaidya, F. H. Samie, C. Lo, M. Delmar, and J. Jalife, "Characterization of conduction in the ventricles of normal and heterozygous Cx43 knockout mice using optical mapping [see comments]," *J Cardiovasc Electrophysiol*, vol. 10, pp. 1361-75, 1999.

[22] D. E. Gutstein, G. E. Morley, H. Tamaddon, D. Vaidya, M. D. Schneider, J. Chen, K. R. Chien, H. Stuhlmann, and G. I. Fishman, "Conduction Slowing and Sudden Arrhythmic Death in Mice With Cardiac- Restricted Inactivation of Connexin43," *Circ Res*, vol. 88, pp. 333-339., 2001.

[23] D. E. Gutstein, F. Y. Liu, M. B. Meyers, A. Choo, and G. I. Fishman, "The organization of adherens junctions and desmosomes at the cardiac intercalated disc is independent of gap junctions," *J Cell Sci*, vol. 116, pp. 875-85, 2003.

[24] G. L. Radice, H. Rayburn, H. Matsunami, K. A. Knudsen, M. Takeichi, and R. O. Hynes, "Developmental defects in mouse embryos lacking N-cadherin," *Dev Biol*, vol. 181, pp. 64-78, 1997.

[25] C. Bierkamp, K. J. McLaughlin, H. Schwarz, O. Huber, and R. Kemler, "Embryonic heart and skin defects in mice lacking plakoglobin," *Dev Biol*, vol. 180, pp. 780-5, 1996.

[26] P. Ruiz, V. Brinkmann, B. Ledermann, M. Behrend, C. Grund, C. Thalhammer, F. Vogel, C. Birchmeier, U. Gunthert, W. W. Franke, and W. Birchmeier, "Targeted mutation of plakoglobin in mice reveals essential functions of desmosomes in the embryonic heart," *J Cell Biol*, vol. 135, pp. 215-25, 1996.

[27] I. Kostetskii, J. Li, Y. Xiong, R. Zhou, V. A. Ferrari, V. V. Patel, J. D. Molkentin, and G. L. Radice, "Induced deletion of the N-cadherin gene in the heart leads to dissolution of the intercalated disc structure," *Circ Res*, vol. 96, pp. 346-54, 2005.

[28] J. Li, V. V. Patel, I. Kostetskii, Y. Xiong, A. F. Chu, J. T. Jacobson, C. Yu, G. E. Morley, J. D. Molkentin, and G. L. Radice, "Cardiac-specific loss of N-cadherin leads to alteration in connexins with conduction slowing and arrhythmogenesis," *Circ Res*, vol. 97, pp. 474-81, 2005.

[29] P. Kirchhof, L. Fabritz, M. Zwiener, H. Witt, M. Schafers, S. Zellerhoff, M. Paul, T. Athai, K. H. Hiller, H. A. Baba, G. Breithardt, P. Ruiz, T. Wichter, and B. Levkau, "Age- and training-dependent development of arrhythmogenic right ventricular cardiomyopathy in heterozygous plakoglobin-deficient mice," *Circulation*, vol. 114, pp. 1799-806, 2006.

[30] W. G. Stevenson and L. W. Stevenson, "Prevention of sudden death in heart failure," *J Cardiovasc Electrophysiol*, vol. 12, pp. 112-4, 2001.

[31] P. Taggart and P. M. Sutton, "Cardiac mechano-electric feedback in man: clinical relevance," *Prog Biophys Mol Biol*, vol. 71, pp. 139-54, 1999.

[32] C. S. Kuo, K. Munakata, C. P. Reddy, and B. Surawicz, "Characteristics and possible mechanism of ventricular arrhythmia dependent on the dispersion of action potential durations," *Circulation*, vol. 67, pp. 1356-67, 1983.

[33] F. Ravelli, "Mechano-electric feedback and atrial fibrillation," *Prog Biophys Mol Biol*, vol. 82, pp. 137-49, 2003.

[34] J. M. Kootsey, "Electrical Propagation in Distributed Cardiac Tissue," in *Theory of Heart: Biomechanics, Biophysics, and Nonlinear Dynamics of Cardiac Function*, L. Glass, P. Hunter, and A. D. McCulloch, Eds. New York: Springer-Verlag, 1991, pp. 391-403.

[35] D. M. Roden, J. R. Balser, A. L. George, Jr., and M. E. Anderson, "Cardiac ion channels," *Annu Rev Physiol*, vol. 64, pp. 431-75, 2002.

[36] S. Rohr, J. P. Kucera, and A. G. Kleber, "Slow conduction in cardiac tissue, I: effects of a reduction of excitability versus a reduction of electrical coupling on microconduction," *Circ Res*, vol. 83, pp. 781-94, 1998.

[37] A. Nygren and W. R. Giles, "Mathematical simulation of slowing of cardiac conduction velocity by elevated extracellular [K+] in a human atrial strand," *Ann Biomed Eng*, vol. 28, pp. 951-7, 2000.

[38] C. Cabo, A. M. Pertsov, W. T. Baxter, J. M. Davidenko, R. A. Gray, and J. Jalife, "Wave-front curvature as a cause of slow conduction and block in isolated cardiac muscle," *Circ Res*, vol. 75, pp. 1014-28, 1994.

[39] D. A. Hooks, K. A. Tomlinson, S. G. Marsden, I. J. LeGrice, B. H. Smaill, A. J. Pullan, and P. J. Hunter, "Cardiac microstructure: implications for electrical propagation and defibrillation in the heart," *Circ Res*, vol. 91, pp. 331-8, 2002.

[40] P. V. Bayly, B. H. KenKnight, J. M. Rogers, R. E. Hillsley, R. E. Ideker, and W. M. Smith, "Estimation of conduction velocity vector fields from epicardial mapping data," *IEEE Trans Biomed Eng*, vol. 45, pp. 563-71, 1998.

[41] Z. J. Penefsky and B. F. Hoffman, "Effects of stretch on mechanical and electrical properties of cardiac muscle," *Am J Physiol*, vol. 204, pp. 433-438, 1963.

[42] F. B. Sachse, B. W. Steadman, B. B. JH, B. B. Punske, and B. Taccardi, "Conduction velocity in myocardium modulated by strain: measurement instrumentation and initial results," *Conf Proc IEEE Eng Med Biol Soc*, vol. 5, pp. 3593-6, 2004.

[43] K. A. Deck, "[Changes in the Resting Potential and the Cable Properties of Purkinje Fibers During Stretch]," *Pflugers Arch Gesamte Physiol Menschen Tiere*, vol. 280, pp. 131-40, 1964.

[44] G. Dominguez and H. A. Fozzard, "Effect of stretch on conduction velocity and cable properties of cardiac Purkinje fibers," *Am J Physiol*, vol. 237, pp. C119-24, 1979.

[45] M. R. Rosen, M. J. Legato, and R. M. Weiss, "Developmental changes in impulse conduction in the canine heart," *Am J Physiol*, vol. 240, pp. H546-54, 1981.

[46] J. F. Spear and E. N. Moore, "Stretch-induced excitation and conduction disturbances in the isolated rat myocardium," *J Electrocardiol*, vol. 5, pp. 15-24, 1972.

[47] D. A. Sideris, S. T. Toumanidis, K. Kostopoulos, A. Pittaras, G. S. Spyropoulos, E. B. Kostis, and S. D. Moulopoulos, "Effect of acute ventricular pressure changes on QRS duration," *J Electrocardiol*, vol. 27, pp. 199-202, 1994.

[48] F. Solti, T. Vecsey, V. Kekesi, and A. Juhasz-Nagy, "The effect of atrial dilatation on the genesis of atrial arrhythmias," *Cardiovasc Res*, vol. 23, pp. 882-6, 1989.

[49] M. Zabel, S. Portnoy, and M. R. Franz, "Effect of sustained load on dispersion of ventricular repolarization and conduction time in the isolated intact rabbit heart," *J Cardiovasc Electrophysiol*, vol. 7, pp. 9-16., 1996.

[50] W. X. Zhu, S. B. Johnson, R. Brandt, J. Burnett, and D. L. Packer, "Impact of volume loading and load reduction on ventricular refractoriness and conduction properties in canine congestive heart failure," *J Am Coll Cardiol*, vol. 30, pp. 825-33, 1997.

[51] P. Tavi, M. Laine, and M. Weckström, "Effect of gadolinium on stretch-induced changes in contraction and intracellularly recorded action- and afterpotentials of rat isolated atrium," *British Journal of Pharmacology*, vol. 118, pp. 407-13, 1996.

[52] M. J. Reiter, M. Landers, Z. Zetelaki, C. J. Kirchhof, and M. A. Allessie, "Electrophysiological effects of acute dilatation in the isolated rabbit heart: cycle length-dependent effects on ventricular refractoriness and conduction velocity," *Circulation*, vol. 96, pp. 4050-6., 1997.

[53] F. J. Chorro, S. Egea, L. Mainar, J. Canoves, J. Sanchis, E. Llavador, V. Lopez-Merino, and L. Such, "[Acute changes in wavelength of the process of auricular activation induced by stretching. Experimental study]," *Rev Esp Cardiol*, vol. 51, pp. 874-83, 1998.

[54] S. C. Eijsbouts, M. Majidi, M. van Zandvoort, and M. A. Allessie, "Effects of acute atrial dilation on heterogeneity in conduction in the isolated rabbit heart," *J Cardiovasc Electrophysiol*, vol. 14, pp. 269-78, 2003.

[55] D. Sung, R. W. Mills, J. Schettler, S. M. Narayan, J. H. Omens, and A. D. McCulloch, "Ventricular filling slows epicardial conduction and increases action potential duration in an optical mapping study of the isolated rabbit heart," *J Cardiovasc Electrophysiol*, vol. 14, pp. 739-49, 2003.

[56] D. Sung, J. H. Omens, and A. D. McCulloch, "Model-based analysis of optically mapped epicardial activation patterns and conduction velocity," *Ann Biomed Eng*, vol. 28, pp. 1085-92, 2000.

[57] R. W. Mills, S. M. Narayan, and A. D. McCulloch, "Mechanisms of conduction slowing during myocardial stretch by ventricular volume loading in the rabbit," *Am J Physiol Heart Circ Physiol*, vol. 295, pp. H1270-H1278, 2008.

[58] Y. Zhang, R. B. Sekar, A. D. McCulloch, and L. Tung, "Cell cultures as models of cardiac mechanoelectric feedback," *Prog Biophys Mol Biol*, vol. 97, pp. 367-82, 2008.

[59] M. R. Franz, "Mechano-electrical feedback in ventricular myocardium," *Cardiovasc Res*, vol. 32, pp. 15-24, 1996.

[60] T. G. McNary, K. Sohn, B. Taccardi, and F. B. Sachse, "Experimental and computational studies of strain-conduction velocity relationships in cardiac tissue," *Prog Biophys Mol Biol*, vol. 97, pp. 383-400, 2008.

[61] S. C. Calaghan, A. Belus, and E. White, "Do stretch-induced changes in intracellular calcium modify the electrical activity of cardiac muscle?," *Prog Biophys Mol Biol*, vol. 82, pp. 81-95, 2003.

[62] L. Eckardt, P. Kirchhof, G. Monnig, G. Breithardt, M. Borggrefe, and W. Haverkamp, "Modification of stretch-induced shortening of repolarization by streptomycin in the isolated rabbit heart," *J Cardiovasc Pharmacol*, vol. 36, pp. 711-21., 2000.

[63] P. Kohl, P. J. Cooper, and H. Holloway, "Effects of acute ventricular volume manipulation on in situ cardiomyocyte cell membrane configuration," *Prog Biophys Mol Biol*, vol. 82, pp. 221-7, 2003.

[64] T. M. Suchyna, S. R. Besch, and F. Sachs, "Dynamic regulation of mechanosensitive channels: capacitance used to monitor patch tension in real time," *Physical Biology*, vol. 1, pp. 1-18, 2004.

[65] P. P. Cherian, A. J. Siller-Jackson, S. Gu, X. Wang, L. F. Bonewald, E. Sprague, and J. X. Jiang, "Mechanical strain opens connexin 43 hemichannels in osteocytes: a novel mechanism for the release of prostaglandin," *Mol Biol Cell*, vol. 16, pp. 3100-6, 2005.

[66] L. Bao, F. Sachs, and G. Dahl, "Connexins are mechanosensitive," *Am J Physiol Cell Physiol*, vol. 287, pp. C1389-95, 2004.

[67] S. P. Thomas, J. P. Kucera, L. Bircher-Lehmann, Y. Rudy, J. E. Saffitz, and A. G. Kleber, "Impulse propagation in synthetic strands of neonatal cardiac myocytes with genetically reduced levels of connexin43," *Circ Res*, vol. 92, pp. 1209-16, 2003.

[68] M. Kondo, V. Nesterenko, and C. Antzelevitch, "Cellular basis for the monophasic action potential. Which electrode is the recording electrode?," *Cardiovascular Research*, vol. 63, pp. 635-644, 2004.

[69] A. V. Sahakian, M. S. Peterson, S. Shkurovich, M. Hamer, T. Votapka, T. Ji, and S. Swiryn, "A simultaneous multichannel monophasic action potential electrode array for in vivo epicardial repolarization mapping," *IEEE Trans Biomed Eng*, vol. 48, pp. 345-53, 2001.

[70] K. Imfeld, S. Neukom, A. Maccione, Y. Bornat, S. Martinoia, P. A. Farine, M. Koudelka-Hep, and L. Berdondini, "Large-scale, high-resolution data acquisition system for extracellular recording of electrophysiological activity," *IEEE Trans Biomed Eng*, vol. 55, pp. 2064-73, 2008.

[71] G. Salama and M. Morad, "Merocyanine 540 as an optical probe of transmembrane electrical activity in the heart," *Science*, vol. 191, pp. 485-7, 1976.

[72] E. Entcheva, S. N. Lu, R. H. Troppman, V. Sharma, and L. Tung, "Contact fluorescence imaging of reentry in monolayers of cultured neonatal rat ventricular myocytes," *J Cardiovasc Electrophysiol*, vol. 11, pp. 665-76, 2000.

[73] E. H. Ratzlaff and A. Grinvald, "A tandem-lens epifluorescence macroscope: hundred-fold brightness advantage for wide-field imaging," *J Neurosci Methods*, vol. 36, pp. 127-37, 1991.

[74] D. Sung, J. Somayajula-Jagai, P. Cosman, R. Mills, and A. D. McCulloch, "Phase shifting prior to spatial filtering enhances optical recordings of cardiac action potential propagation," *Ann Biomed Eng*, vol. 29, pp. 854-61., 2001.

[75] R. W. Mills, "Mechanisms of slow conductions during ventricular volume loading," 2006, pp. xiii, 97.

[76] S. Kettlewell, N. L. Walker, S. M. Cobbe, F. L. Burton, and G. L. Smith, "The electrophysiological and mechanical effects of 2,3-butane-dione monoxime and cytochalasin-D in the Langendorff perfused rabbit heart," *Exp Physiol*, vol. 89, pp. 163-72, 2004.

[77] L. C. Baker, R. Wolk, B.-R. Choi, S. Watkins, P. Plan, A. Shah, and G. Salama, "Effects of mechanical uncouplers, diacetyl monoxime, and cytochalasin-D on the electrophysiology of perfused mouse hearts," *Am J Physiol Heart Circ Physiol*, vol. 287, pp. H1771-1779, 2004.

[78] S. B. Knisley, R. K. Justice, W. Kong, and P. L. Johnson, "Ratiometry of transmembrane voltage-sensitive fluorescent dye emission in hearts," *Am J Physiol Heart Circ Physiol*, vol. 279, pp. H1421-33, 2000.

[79] M. Inagaki, I. Hidaka, T. Aiba, T. Tatewaki, K. Sunagawa, and M. Sugimachi, "High resolution optical mapping of cardiac action potentials in freely beating rabbit hearts," *Conf Proc IEEE Eng Med Biol Soc*, vol. 5, pp. 3578-80, 2004.

[80] G. K. Rohde, B. M. Dawant, and S. F. Lin, "Correction of motion artifact in cardiac optical mapping using image registration," *IEEE Trans Biomed Eng*, vol. 52, pp. 338-41, 2005.

[81] S. Iravanian, Y. Nabutovsky, C. R. Kong, S. Saha, N. Bursac, and L. Tung, "Functional reentry in cultured monolayers of neonatal rat cardiac cells," *Am J Physiol Heart Circ Physiol*, vol. 285, pp. H449-56, 2003.

[82] N. Bursac, K. K. Parker, S. Iravanian, and L. Tung, "Cardiomyocyte cultures with controlled macroscopic anisotropy: a model for functional electrophysiological studies of cardiac muscle," *Circ Res*, vol. 91, pp. e45-54, 2002.

[83] B. Geiger, K. T. Tokuyasu, A. H. Dutton, and S. J. Singer, "Vinculin, an intracellular protein localized at specialized sites where microfilament bundles terminate at cell membranes," *Proc Natl Acad Sci U S A*, vol. 77, pp. 4127-31, 1980.

[84] E. Zamir and B. Geiger, "Molecular complexity and dynamics of cell-matrix adhesions," *J Cell Sci*, vol. 114, pp. 3583-90, 2001.

[85] E. J. Birks, J. L. Hall, P. J. Barton, S. Grindle, N. Latif, J. P. Hardy, J. E. Rider, N. R. Banner, A. Khaghani, L. W. Miller, and M. H. Yacoub, "Gene profiling changes in cytoskeletal proteins during clinical recovery after left ventricular-assist device support," *Circulation*, vol. 112, pp. I57-64, 2005.

[86] T. M. Olson, S. Illenberger, N. Y. Kishimoto, S. Huttelmaier, M. T. Keating, and B. M. Jockusch, "Metavinculin mutations alter actin interaction in dilated cardiomyopathy," *Circulation*, vol. 105, pp. 431-7, 2002.

[87] A. E. Zemljic-Harpf, J. C. Miller, S. A. Henderson, A. T. Wright, A. M. Manso, L. Elsherif, N. D. Dalton, A. K. Thor, G. A. Perkins, A. D. McCulloch, and R. S. Ross, "Cardiac-myocyte-specific excision of the vinculin gene disrupts cellular junctions, causing sudden death or dilated cardiomyopathy," *Mol Cell Biol*, vol. 27, pp. 7522-37, 2007.

[88] D. E. Gutstein, G. E. Morley, D. Vaidya, F. Liu, F. L. Chen, H. Stuhlmann, and G. I. Fishman, "Heterogeneous expression of gap junction channels in the heart leads to conduction defects and ventricular dysfunction," *Circulation*, vol. 104, pp. 1194-9., 2001.

[89] M. R. Franz, R. Cima, D. Wang, D. Profitt, and R. Kurz, "Electrophysiological effects of myocardial stretch and mechanical determinants of stretch-activated arrhythmias [published erratum appears in Circulation 1992 Nov;86(5):1663]," *Circulation*, vol. 86, pp. 968-78, 1992.

[90] M. Noorman, M. A. van der Heyden, T. A. van Veen, M. G. Cox, R. N. Hauer, J. M. de Bakker, and H. V. van Rijen, "Cardiac cell-cell junctions in health and disease: Electrical versus mechanical coupling," *J Mol Cell Cardiol*, vol. 47, pp. 23-31, 2009.

[91] J. E. Saffitz, A. Asimaki, and H. Huang, "Arrhythmogenic right ventricular cardiomyopathy: new insights into disease mechanisms and diagnosis," *J Investig Med*, vol. 57, pp. 861-4, 2009.

[92] N. Protonotarios and A. Tsatsopoulou, "Naxos disease and Carvajal syndrome: cardiocutaneous disorders that highlight the pathogenesis and broaden the spectrum of arrhythmogenic right ventricular cardiomyopathy," *Cardiovasc Pathol*, vol. 13, pp. 185-94, 2004.

[93] S. Sen-Chowdhry, P. Syrris, and W. J. McKenna, "Genetics of right ventricular cardiomyopathy," *J Cardiovasc Electrophysiol*, vol. 16, pp. 927-35, 2005.

[94] A. Asimaki, H. Tandri, H. Huang, M. K. Halushka, S. Gautam, C. Basso, G. Thiene, A. Tsatsopoulou, N. Protonotarios, W. J. McKenna, H. Calkins, and J. E. Saffitz, "A new diagnostic test for arrhythmogenic right ventricular cardiomyopathy," *N Engl J Med*, vol. 360, pp. 1075-84, 2009.

[95] K. S. Grossmann, C. Grund, J. Huelsken, M. Behrend, B. Erdmann, W. W. Franke, and W. Birchmeier, "Requirement of plakophilin 2 for heart morphogenesis and cardiac junction formation," *J Cell Biol*, vol. 167, pp. 149-60, 2004.

[96] S. Pieperhoff and W. W. Franke, "The area composita of adhering junctions connecting heart muscle cells of vertebrates. VI. Different precursor structures in non-mammalian species," *Eur J Cell Biol*, vol. 87, pp. 413-30, 2008.

[97] H. Tada, N. Aihara, T. Ohe, C. Yutani, S. Hamada, H. Miyanuma, M. Takamiya, and S. Kamakura, "Arrhythmogenic right ventricular cardiomyopathy underlies syndrome of right bundle branch block, ST-segment elevation, and sudden death," *Am J Cardiol*, vol. 81, pp. 519-22, 1998.

[98] T. Honda, H. Saitoh, M. Masuko, T. Katagiri-Abe, K. Tominaga, I. Kozakai, K. Kobayashi, T. Kumanishi, Y. G. Watanabe, S. Odani, and R. Kuwano, "The coxsackievirus-adenovirus receptor protein as a cell adhesion molecule in the developing mouse brain," *Brain Res Mol Brain Res*, vol. 77, pp. 19-28, 2000.

[99] M. Ito, M. Kodama, M. Masuko, M. Yamaura, K. Fuse, Y. Uesugi, S. Hirono, Y. Okura, K. Kato, Y. Hotta, T. Honda, R. Kuwano, and Y. Aizawa, "Expression of coxsackievirus and adenovirus receptor in hearts of rats with experimental autoimmune myocarditis," *Circ Res*, vol. 86, pp. 275-80, 2000.

[100] D. R. Asher, A. M. Cerny, S. R. Weiler, J. W. Horner, M. L. Keeler, M. A. Neptune, S. N. Jones, R. T. Bronson, R. A. Depinho, and R. W. Finberg, "Coxsackievirus and adenovirus receptor is essential for cardiomyocyte development," *Genesis*, vol. 42, pp. 77-85, 2005.

[101] A. A. Dorner, F. Wegmann, S. Butz, K. Wolburg-Buchholz, H. Wolburg, A. Mack, I. Nasdala, B. August, J. Westermann, F. G. Rathjen, and D. Vestweber, "Coxsackievirus-adenovirus receptor (CAR) is essential for early embryonic cardiac development," *J Cell Sci*, vol. 118, pp. 3509-21, 2005.

[102] J. W. Chen, B. Zhou, Q. C. Yu, S. J. Shin, K. Jiao, M. D. Schneider, H. S. Baldwin, and J. M. Bergelson, "Cardiomyocyte-specific deletion of the coxsackievirus and adenovirus receptor results in hyperplasia of the embryonic left ventricle and abnormalities of sinuatrial valves," *Circ Res*, vol. 98, pp. 923-30, 2006.

[103] C. A. Shaw, P. C. Holland, M. Sinnreich, C. Allen, K. Sollerbrant, G. Karpati, and J. Nalbantoglu, "Isoform-specific expression of the Coxsackie and adenovirus receptor (CAR) in neuromuscular junction and cardiac intercalated discs," *BMC Cell Biol*, vol. 5, pp. 42, 2004.

[104] C. J. Cohen, J. T. Shieh, R. J. Pickles, T. Okegawa, J. T. Hsieh, and J. M. Bergelson, "The coxsackievirus and adenovirus receptor is a transmembrane component of the tight junction," *Proc Natl Acad Sci U S A*, vol. 98, pp. 15191-6, 2001.

[105] B. K. Lim, D. Xiong, A. Dorner, T. J. Youn, A. Yung, T. I. Liu, Y. Gu, N. D. Dalton, A. T. Wright, S. M. Evans, J. Chen, K. L. Peterson, A. D. McCulloch, T. Yajima, and K. U. Knowlton, "Coxsackievirus and adenovirus receptor (CAR) mediates atrioventricular-node function and connexin 45 localization in the murine heart," *J Clin Invest*, vol. 118, pp. 2758-70, 2008.

[106] U. Lisewski, Y. Shi, U. Wrackmeyer, R. Fischer, C. Chen, A. Schirdewan, R. Juttner, F. Rathjen, W. Poller, M. H. Radke, and M. Gotthardt, "The tight junction protein CAR regulates cardiac conduction and cell-cell communication," *J Exp Med*, vol. 205, pp. 2369-79, 2008.

[107] S. Kuroda, C. Tokunaga, Y. Kiyohara, O. Higuchi, H. Konishi, K. Mizuno, G. N. Gill, and U. Kikkawa, "Protein-protein interaction of zinc finger LIM domains with protein kinase C," *J Biol Chem*, vol. 271, pp. 31029-32, 1996.

[108] N. Nakagawa, M. Hoshijima, M. Oyasu, N. Saito, K. Tanizawa, and S. Kuroda, "ENH, containing PDZ and LIM domains, heart/skeletal muscle-specific protein, associates with cytoskeletal proteins through the PDZ domain," *Biochem Biophys Res Commun*, vol. 272, pp. 505-12, 2000.

[109] Y. Maeno-Hikichi, S. Chang, K. Matsumura, M. Lai, H. Lin, N. Nakagawa, S. Kuroda, and J. F. Zhang, "A PKC epsilon-ENH-channel complex specifically modulates N-type Ca2+ channels," *Nat Neurosci*, vol. 6, pp. 468-75, 2003.

[110] A. D. Maturana, S. Walchli, M. Iwata, S. Ryser, J. Van Lint, M. Hoshijima, W. Schlegel, Y. Ikeda, K. Tanizawa, and S. Kuroda, "Enigma homolog 1 scaffolds protein kinase D1 to regulate the activity of the cardiac L-type voltage-gated calcium channel," *Cardiovasc Res*, vol. 78, pp. 458-65, 2008.

[111] A. Lasorella and A. Iavarone, "The protein ENH is a cytoplasmic sequestration factor for Id2 in normal and tumor cells from the nervous system," *Proc Natl Acad Sci U S A*, vol. 103, pp. 4976-81, 2006.

[112] I. P. Moskowitz, J. B. Kim, M. L. Moore, C. M. Wolf, M. A. Peterson, J. Shendure, M. A. Nobrega, Y. Yokota, C. Berul, S. Izumo, J. G. Seidman, and C. E. Seidman, "A molecular pathway including Id2, Tbx5, and Nkx2-5 required for cardiac conduction system development," *Cell*, vol. 129, pp. 1365-76, 2007.

[113] M. Vatta, B. Mohapatra, S. Jimenez, X. Sanchez, G. Faulkner, Z. Perles, G. Sinagra, J. H. Lin, T. M. Vu, Q. Zhou, K. R. Bowles, A. Di Lenarda, L. Schimmenti, M. Fox, M. A. Chrisco, R. T. Murphy, W. McKenna, P. Elliott, N. E. Bowles, J. Chen, G. Valle, and J. A. Towbin, "Mutations in Cypher/ZASP in patients with dilated cardiomyopathy and left ventricular non-compaction," *J Am Coll Cardiol*, vol. 42, pp. 2014-27, 2003.

[114] J. L. Jefferies and J. A. Towbin, "Dilated cardiomyopathy," *Lancet*, vol. 375, pp. 752-62, 2010.

[115] R. Benezra, R. L. Davis, D. Lockshon, D. L. Turner, and H. Weintraub, "The protein Id: a negative regulator of helix-loop-helix DNA binding proteins," *Cell*, vol. 61, pp. 49-59, 1990.

[116] J. Y. Lim, W. H. Kim, J. Kim, and S. I. Park, "Induction of Id2 expression by cardiac transcription factors GATA4 and Nkx2.5," *J Cell Biochem*, vol. 103, pp. 182-94, 2008.

[117] T. M. Williams and M. P. Lisanti, "The Caveolin genes: from cell biology to medicine," *Ann Med*, vol. 36, pp. 584-95, 2004.

[118] T. V. Kurzchalia and R. G. Parton, "Membrane microdomains and caveolae," *Curr Opin Cell Biol*, vol. 11, pp. 424-31, 1999.

[119] P. A. Insel, B. P. Head, R. S. Ostrom, H. H. Patel, J. S. Swaney, C. M. Tang, and D. M. Roth, "Caveolae and lipid rafts: G protein-coupled receptor signaling microdomains in cardiac myocytes," *Ann N Y Acad Sci*, vol. 1047, pp. 166-72, 2005.

[120] E. J. Smart and R. G. Anderson, "Alterations in membrane cholesterol that affect structure and function of caveolae," *Methods Enzymol*, vol. 353, pp. 131-9, 2002.

[121] R. C. Balijepalli and T. J. Kamp, "Caveolae, ion channels and cardiac arrhythmias," *Prog Biophys Mol Biol*, vol. 98, pp. 149-60, 2008.

[122] B. Razani, J. A. Engelman, X. B. Wang, W. Schubert, X. L. Zhang, C. B. Marks, F. Macaluso, R. G. Russell, M. Li, R. G. Pestell, D. Di Vizio, H. Hou, Jr., B. Kneitz, G. Lagaud, G. J. Christ, W. Edelmann, and M. P. Lisanti, "Caveolin-1 null mice are viable but show evidence of hyperproliferative and vascular abnormalities," *J Biol Chem*, vol. 276, pp. 38121-38, 2001.

[123] B. Razani, X. B. Wang, J. A. Engelman, M. Battista, G. Lagaud, X. L. Zhang, B. Kneitz, H. Hou, Jr., G. J. Christ, W. Edelmann, and M. P. Lisanti, "Caveolin-2-deficient mice show evidence of severe pulmonary dysfunction without disruption of caveolae," *Mol Cell Biol*, vol. 22, pp. 2329-44, 2002.

[124] S. E. Woodman, D. S. Park, A. W. Cohen, M. W. Cheung, M. Chandra, J. Shirani, B. Tang, L. A. Jelicks, R. N. Kitsis, G. J. Christ, S. M. Factor, H. B. Tanowitz, and M. P. Lisanti, "Caveolin-3 knock-out mice develop a progressive cardiomyopathy and show hyperactivation of the p42/44 MAPK cascade," *J Biol Chem*, vol. 277, pp. 38988-97, 2002.

[125] C. Minetti, F. Sotgia, C. Bruno, P. Scartezzini, P. Broda, M. Bado, E. Masetti, M. Mazzocco, A. Egeo, M. A. Donati, D. Volonte, F. Galbiati, G. Cordone, F. D. Bricarelli, M. P. Lisanti, and F. Zara, "Mutations in the caveolin-3 gene cause autosomal dominant limb-girdle muscular dystrophy," *Nat Genet*, vol. 18, pp. 365-8, 1998.

[126] Y. Hagiwara, T. Sasaoka, K. Araishi, M. Imamura, H. Yorifuji, I. Nonaka, E. Ozawa, and T. Kikuchi, "Caveolin-3 deficiency causes muscle degeneration in mice," *Hum Mol Genet*, vol. 9, pp. 3047-54, 2000.

[127] F. Galbiati, J. A. Engelman, D. Volonte, X. L. Zhang, C. Minetti, M. Li, H. Hou, Jr., B. Kneitz, W. Edelmann, and M. P. Lisanti, "Caveolin-3 null mice show a loss of caveolae, changes in the microdomain distribution of the dystrophin-glycoprotein complex, and t-tubule abnormalities," *J Biol Chem*, vol. 276, pp. 21425-33, 2001.

[128] S. M. Gopalan, C. Flaim, S. N. Bhatia, M. Hoshijima, R. Knoell, K. R. Chien, J. H. Omens, and A. D. McCulloch, "Anisotropic stretch-induced hypertrophy in neonatal ventricular myocytes micropatterned on deformable elastomers," *Biotechnol Bioeng*, vol. 81, pp. 578-87, 2003.

[129] W. Adams, A. W. Trafford, and D. A. Eisner, "2,3-Butanedione monoxime (BDM) decreases sarcoplasmic reticulum Ca content by stimulating Ca release in isolated rat ventricular myocytes," *Pflugers Arch*, vol. 436, pp. 776-81, 1998.

[130] A. Coulombe, I. A. Lefevre, E. Deroubaix, D. Thuringer, and E. Coraboeuf, "Effect of 2,3-butanedione 2-monoxime on slow inward and transient outward currents in rat ventricular myocytes," *J Mol Cell Cardiol*, vol. 22, pp. 921-32., 1990.

[131] Y. Watanabe, T. Iwamoto, I. Matsuoka, S. Ohkubo, T. Ono, T. Watano, M. Shigekawa, and J. Kimura, "Inhibitory effect of 2,3-butanedione monoxime (BDM) on Na(+)/Ca(2+) exchange current in guinea-pig cardiac ventricular myocytes," *Br J Pharmacol*, vol. 132, pp. 1317-25, 2001.

[132] J. D. Molkentin and J. Robbins, "With great power comes great responsibility: using mouse genetics to study cardiac hypertrophy and failure," *J Mol Cell Cardiol*, vol. 46, pp. 130-6, 2009.

[133] L. Tung and J. Cysyk, "Imaging fibrillation/defibrillation in a dish," *J Electrocardiol*, vol. 40, pp. S62-5, 2007.